



UNIVERSITY OF PERUGIA

Doctorate in "Ingegneria dell'Informazione"
Cycle XVI

DEPARTMENT OF ELECTRONIC AND
INFORMATION ENGINEERING

ANALYSIS OF MULTIUSER COMMUNICATION
SYSTEMS WITH TRANSMITTER- AND
RECEIVER-INDUCED DISTORTIONS

Luca Rugini

Advisor:
Prof. Saverio Cacopardi

Coordinator:
Prof. Michele La Cava

Co-Advisor:
Dr. Paolo Banelli

A DISSERTATION SUBMITTED FOR THE DEGREE OF
DOCTOR OF PHILOSOPHY

October 2003

To my family

ACKNOWLEDGMENTS

First, I would like to thank Prof. Saverio Cacopardi for having made possible my research activity in cooperation with the Telecommunications Group of our department. A particular thank to Dr. Paolo Banelli for his continuous guide and interest about my studies. Some parts of this thesis would not have been possible without his suggestions.

In addition, I thank Dr. Giuseppe Baruffa for his help concerning technical and non-technical issues. Many thanks to all the people of the Telecommunications Group, especially to Dr. Dario Di Sorte, Dr. Mauro Femminella, Ing. Leonardo Piacentini, and Ing. Matteo Berioli.

Last, but not least, I would like to thank my parents, Nazzareno and Marisa, and my brother, Marco, for their continuous encouragement during these years.

LIST OF CONTRIBUTIONS

Part of the material presented in this thesis has been either published or submitted for publication in technical journals and in proceedings of international conferences. Since these papers are not explicitly cited in the text, we report the list of contributions herein.

- L. Rugini, P. Banelli, and S. Cacopardi, “Theoretical analysis and performance of the decorrelating detector for DS-CDMA signals in nonlinear fading channels,” to appear in *IEEE Trans. Wireless Commun.*, first issue 2004.
- P. Banelli and L. Rugini, “BER performance degradation of MC-DS-CDMA systems jointly affected by transmitter HPA and receiver CFO in frequency selective fading channels,” accepted in *Proc. IEEE Int. Symp. Control Commun. Signal Processing 2004*, Sept. 2003.
- L. Rugini, P. Banelli, and G. B. Giannakis, “MMSE-based local ML detection of linearly precoded OFDM signals,” submitted to *IEEE Int. Conf. Commun. 2004*, Sept. 2003.
- L. Rugini, P. Banelli, and S. Cacopardi, “Probability of error of OFDM systems with carrier frequency offset in frequency-selective fading channels,” submitted to *IEEE Int. Conf. Commun. 2004*, Sept. 2003.
- L. Rugini and P. Banelli, “Impact of frequency synchronization errors and intermodulation distortion on the performance of multicarrier DS-CDMA systems,” submitted to *EURASIP J. Appl. Signal Processing*, Aug. 2003.
- L. Rugini and P. Banelli, “BER of OFDM systems impaired by carrier frequency offset in multipath fading channels,” submitted to *IEEE Trans. Wireless Commun.*, Apr. 2003.
- L. Rugini, P. Banelli, and S. Cacopardi, “SER performance of linear multiuser detectors for DS-CDMA downlink with transmitter nonlinear distortions,” submitted to *IEEE Trans. Veh. Technol.*, Mar. 2003.
- L. Rugini and P. Banelli, “Symbol error probability of linearly modulated signals affected by Gaussian interference in Rayleigh fading channels,” submitted to *IEEE Trans. Commun.*, Jan. 2003.

- L. Rugini, P. Banelli, and S. Cacopardi, “Regularized MMSE multiuser detection using covariance matrix tapering,” in *Proc. IEEE Int. Conf. Commun.*, May 2003.
- P. Banelli, L. Rugini, and S. Cacopardi, “Optimum output power back-off in nonlinear channels for OFDM based WLAN,” in *Proc. IEEE Int. Symp. Signal Processing Inform. Technol.*, Dec. 2002.
- L. Rugini, P. Banelli, and S. Cacopardi, “Effects of high-power amplification on linear multiuser detectors performance in DS-CDMA frequency-selective fading channels,” in *Proc. IEEE Global Telecommun. Conf.*, Nov. 2002.
- L. Rugini, P. Banelli, and S. Cacopardi, “Performance analysis of the decorrelating multiuser detector for nonlinear amplified DS-CDMA signals,” in *Proc. IEEE Int. Conf. Commun.*, Apr./May 2002.
- L. Rugini, P. Banelli, and S. Cacopardi, “An analytical upper bound on MMSE performance using approximated MMSE multiuser detector in flat Rayleigh fading channels,” in *Proc. European Wireless*, Feb. 2002.
- P. Banelli, S. Cacopardi, and L. Rugini, “Improved performance of MMSE multiuser receivers for asynchronous CDMA: preliminary results,” in *Proc. IEEE Int. Conf. Commun.*, June 2001.
- P. Banelli, S. Cacopardi, and L. Rugini, “Estimation errors sensitivity of MMSE multiuser receivers in DS-CDMA,” in *Proc. COST 262 Workshop Multiuser Detection in Spread Spectrum Communications*, Jan. 2001.

MATHEMATICAL NOTATION

$ a $	absolute value of a
$\arg(a)$	phase of a
$\operatorname{Re}(a)$	real part of a
$\operatorname{Im}(a)$	imaginary part of a
$\operatorname{sign}(a)$	sign of a
$\operatorname{csgn}(a)$	complex sign of a
$\lceil a \rceil$	smallest integer larger than or equal to a
$\lfloor a \rfloor$	largest integer smaller than or equal to a
$(a)_{\bmod N}$	remainder after integer division of a by N
$E\{a\}$	expectation of random variable a
$f(a) * g(a)$	convolution operator, $f(a) * g(a) = \int_{-\infty}^{+\infty} f(t)g(a-t)dt$
$\operatorname{sinc}(a)$	cardinal sine of a , $\operatorname{sinc}(a) = \lim_{t \rightarrow a} \frac{\sin(\pi t)}{\pi t}$
$Q(a)$	Q-function of a , $Q(a) = \frac{1}{\sqrt{2\pi}} \int_a^{+\infty} e^{-t^2/2} dt$
\mathbf{a}	column vector \mathbf{a} or row vector \mathbf{a}
$\ \mathbf{a}\ $	l_2 -norm of vector \mathbf{a}
\mathbf{A}	matrix \mathbf{A}
\mathbf{A}^*	complex conjugate of matrix \mathbf{A}
\mathbf{A}^T	transpose of matrix \mathbf{A}
\mathbf{A}^H	Hermitian transpose of matrix \mathbf{A}
\mathbf{A}^{-1}	inverse of matrix \mathbf{A}
\mathbf{A}^\dagger	Moore-Penrose pseudoinverse of matrix \mathbf{A}
$\operatorname{tr}(\mathbf{A})$	trace of matrix \mathbf{A}
$\operatorname{rank}(\mathbf{A})$	rank of matrix \mathbf{A}
$\det(\mathbf{A})$	determinant of matrix \mathbf{A}
$\lambda_{\max}(\mathbf{A})$	largest eigenvalue of matrix \mathbf{A}

$\lambda_{\min}(\mathbf{A})$	smallest eigenvalue of matrix \mathbf{A}
$\chi(\mathbf{A})$	condition number of matrix \mathbf{A} , $\chi(\mathbf{A}) = \frac{\lambda_{\max}(\mathbf{A})}{\lambda_{\min}(\mathbf{A})}$
$\mathbf{A} \circ \mathbf{B}$	Hadamard product between matrices \mathbf{A} and \mathbf{B}
$\mathbf{A} \otimes \mathbf{B}$	Kronecker product between matrices \mathbf{A} and \mathbf{B}
$\mathbf{0}_{M \times N}$	$M \times N$ zero matrix
$\mathbf{1}_{M \times N}$	$M \times N$ all-one matrix
\mathbf{I}_N	$N \times N$ identity matrix
$\text{diag}(a_1, \dots, a_N)$	$N \times N$ diagonal matrix with a_n as its (n,n) th entry
$[\mathbf{a}]_n$	n th entry of vector \mathbf{a}
$[\mathbf{A}]_{m,n}$	(m,n) th entry of matrix \mathbf{A}
$[\mathbf{A}]_{:,n}$	n th column of matrix \mathbf{A}
$[\mathbf{A}]_{m,:}$	m th row of matrix \mathbf{A}
$[\mathbf{A}]_{:,m:n}$	columns m up to n of matrix \mathbf{A}
$[\mathbf{A}]_{m:n,:}$	rows m up to n of matrix \mathbf{A}
$[\mathbf{A}]_{m:n,p:q}$	rows m up to n and columns p up to q of matrix \mathbf{A}

LIST OF ACRONYMS

ACI	adjacent channel interference
AMMSE	approximated minimum mean-squared error
AM/AM	amplitude modulation to amplitude modulation
AM/PM	amplitude modulation to phase modulation
AV	auxiliary-vector
AWGN	additive white Gaussian noise
BER	bit-error rate
BPSK	binary phase-shift keying
CFO	carrier frequency offset
CLT	central limit theorem
CMOE	constrained minimum output energy
CMT	covariance matrix tapering
CSI	channel state information
CSM	cross spectral metric
DA	data-aided
DMI	direct matrix inversion
DS-CDMA	direct-sequence code-division multiple-access
EPC-TC	estimated principal component with true channel
EVD	eigenvalue decomposition
FFT	fast Fourier transform
FIR	finite impulse response
HPA	high-power amplifier
IBI	interblock interference
IBO	input back-off
IC	interference cancellation
ICI	intercarrier interference
IFFT	inverse fast Fourier transform
IMD	intermodulation distortion

IMI-EC	ideal matrix inverse with estimated channel
IMMSE	improved minimum mean-squared error
INR	interference-to-noise ratio
IPA	ideally predistorted amplifier
IPC-EC	ideal principal component with estimated channel
ISI	intersymbol interference
KLT	Karhunen-Loève transform
LDD	linear decorrelating detector
LOS	line-of-sight
LS	least squares
LSMI	loaded sample matrix inversion
MAC	medium access control
MAI	multiple-access interference
MAICI	multiple-access intercarrier interference
MC-CDMA	multicarrier code-division multiple-access
MC-DS-CDMA	multicarrier direct-sequence code-division multiple-access
MF	matched filter
ML	maximum-likelihood
MMSE	minimum mean-squared error
MSE	mean-squared error
MSWF	multistage Wiener filter
MUD	multiuser detection
MVDR	minimum variance distortionless response
NLA	nonlinear amplifier
NLD	nonlinear distortion
NLOS	non-line-of-sight
NRMSE	normalized root mean-squared error
OBO	output back-off
OFDM	orthogonal frequency-division multiplexing
OFDMA	orthogonal frequency-division multiple-access
PAPR	peak-to-average power ratio
PAR	peak-to-average ratio
PC	principal component

PD	partial despreading
PDF	probability density function
PSD	power spectral density
PSK	phase-shift keying
QAM	quadrature amplitude modulation
QPSK	quaternary phase-shift keying
SER	symbol-error rate
SINR	signal-to-interference plus noise ratio
SIR	signal-to-interference ratio
SMI	sample matrix inversion
SMI-TC	sample matrix inversion with true channel
SNR	signal-to-noise ratio
SOI	signal of interest
SSPA	solid state power amplifier
TD	total degradation
TSVD	truncated singular value decomposition
TWTA	traveling-wave tube amplifier
WH	Walsh-Hadamard
WLAN	wireless local area network
ZF	zero-forcing

CONTENTS

Acknowledgments	ii
List of Contributions	iii
Mathematical Notation	v
List of Acronyms	vii
Contents	x
1 Introduction	1
2 Receiver Estimation Errors in DS-CDMA Systems	4
2.1 DS-CDMA System Model	5
2.2 Estimation Errors on the MMSE Detector	8
2.2.1 <i>Ideal MMSE Detector</i>	8
2.2.2 <i>Estimated MMSE Detectors</i>	9
2.2.3 <i>Simulation Results</i>	11
2.3 Improved Detectors for Uplink Transmissions	17
2.3.1 <i>PC Detector with Tikhonov Regularization</i>	18
2.3.2 <i>Exploiting the Channel Information of the Other Users</i>	20
2.3.3 <i>Simulation Results</i>	21
2.4 Regularized Detectors for Downlink Transmissions	26
2.4.1 <i>Overview of Reduced-Rank Approaches</i>	27
2.4.2 <i>A Full-Rank Detector Using Covariance Matrix Tapering</i>	28
2.4.3 <i>Simulation Results</i>	31
3 Nonlinear Amplifier Distortions in DS-CDMA Systems	37
3.1 System Model with Nonlinear Amplifiers	39
3.2 Characterization of the Nonlinear Distortions	42
3.3 Performance of Linear Multiuser Detectors	45
3.3.1 <i>SER Performance in AWGN Channels</i>	45
3.3.2 <i>SER Performance in Flat-Fading Channels</i>	49

3.3.3	<i>SER Performance in Frequency-Selective Fading Channels</i>	51
3.3.4	<i>Total Degradation</i>	55
3.4	Validation by Simulation Results	56
4	Frequency Synchronization Errors and Nonlinear Amplifier Distortions in Multicarrier DS-CDMA Systems	70
4.1	Multicarrier DS-CDMA System Model	72
4.2	Performance Analysis in Multicarrier DS-CDMA Systems	79
4.2.1	<i>BER Performance in Flat-Fading Channels</i>	80
4.2.2	<i>BER Performance in Frequency-Selective Fading Channels</i>	86
4.3	Performance Analysis in OFDM Systems	90
4.3.1	<i>BER Performance in Rayleigh Channels</i>	91
4.3.2	<i>BER Performance in Rician Channels</i>	94
4.4	Simulation Results	96
5	Conclusions	110
5.1	Future work	111
	Appendix A	113
	Appendix B	114
	Appendix C	116
	Bibliography	120

1. INTRODUCTION

It is expected that audio, video, data, and multimedia communications will be the main services supported by future wireless communications systems. Indeed, the widespread use of such services over wired links, as it happens with the conventional Internet, leads to forecast a parallel development of the wireless counterpart of Internet [BPHN][GHBK][BZM].

The problems associated with such wireless services are not only of technical nature, but also business-related. As an example, multimedia services require high data rates, that is, a large amount of bandwidth, which is not easy to locate over the frequency spectrum. Indeed, in order to design an international network, it is mandatory to take into account the spectrum constrains of each country. However, the technical issues remain significant, especially if compared to wired systems, where the bandwidth requirements can be fulfilled by the use of fiber optics. As a matter of fact, for wireless systems, the lack of bandwidth drives the research community to the study of new bandwidth-efficient transmission technologies [YaHa][Lim][BPHN][GHBK]. These schemes should be capable to handle the multipath environment that is characteristic of high data-rate communications, as well as the scenario where several users simultaneously access to different applications.

Most of the transmission schemes proposed for next-generation wireless systems are based on spread-spectrum techniques, on multicarrier techniques, or on combinations of both the approaches [PrOj][NePr][YaHa][FaFe]. As an example, the direct-sequence code-division multiple-access (DS-CDMA) technique [PrOj] adopts suitable spreading codes to expand the information on a wide frequency band. The signals of multiple users are allowed to overlap both in frequency and in time domains. In such a situation, the receiver should be able to counteract both the intersymbol and the multiuser interference thanks to a suitable design of the spreading codes [DiJa] or to a multiuser detector that takes into account the

statistics of the interference [Verd]. On the other hand, the orthogonal frequency-division multiplexing (OFDM) technique [NePr][Pand] splits the high-rate stream into many low-rate signals, to be transmitted over parallel subcarriers. These subcarriers are overlapped in the frequency domain, in such a way that the peak of each subcarrier lies on the nulls of the other carriers, thereby increasing the spectral efficiency while maintaining the orthogonality of the data. Thanks to the cyclic prefix, multicarrier techniques are also able to turn a frequency-selective multipath channel into a single-tap frequency-flat channel on each subcarrier [NePr], thus relaxing the complexity requirements of the channel equalizer. Moreover, many multicarrier techniques do not require a contiguous bandwidth. As a consequence of the previous remarks, it is not surprising that many researchers are investigating how to combine these two techniques, in order to collect the advantages of both [FaFe][HaPr].

Although suitable for frequency-selective fading channels, spread-spectrum and multicarrier techniques are sensitive to the imperfect knowledge of the parameters that are necessary to design the receiver. Just to show few examples, if the multipath channel estimation is not accurate, the bit-error rate (BER) performance degrades significantly [BeKa][ChHo]. Another source of degradation, which could be non-negligible in future packet networks, is the small size of the transmitted data blocks, because in this case the receiver cannot obtain reliable estimates of the received signal statistics. Moreover, multicarrier techniques are particularly sensitive to an imperfect frequency synchronization at the receiver side [PBM]. In addition, in practical cases, the nonlinearity behavior of the transmitter produces considerable performance degradation [NePr]. Hence, a complete BER analysis of such communication systems should also include such phenomena.

In this thesis, we investigate the effects of some of these impairments on the BER performance of single-carrier and multicarrier DS-CDMA systems. The main part of the thesis is devoted to the effects of the nonlinear distortions introduced in the downlink by the transmitter. Analytical and semi-analytical BER expressions are derived for both single-carrier and multicarrier DS-CDMA systems. Different linear receivers and different channel

conditions are considered. For multicarrier systems, the BER analysis includes the effects caused by imperfect frequency synchronization at the receiver side. For single-carrier DS-CDMA systems, the performance degradation due to short data packets is outlined, and some countermeasures are proposed for both uplink and downlink systems.

The thesis is organized as follows. Chapter 2 deals with the effect of short data blocks on the BER performance of single-carrier DS-CDMA systems equipped with a non-ideal minimum mean-squared error receiver. In Chapter 3, we investigate the performance of single-carrier DS-CDMA downlink systems subject to the nonlinear distortions produced by the transmitting amplifier. Chapter 4 extends the BER analysis to multicarrier DS-CDMA systems, taking into account a possible carrier frequency offset between the transmitter and the receiver oscillators. In Chapter 5, we draw some concluding remarks.

2. RECEIVER ESTIMATION ERRORS IN DS-CDMA SYSTEMS

Multisuser detection (MUD) techniques [Verd] have the capability of reducing the multiple-access interference (MAI) in direct-sequence code-division multiple-access (DS-CDMA) systems. Among the multisuser receivers proposed in the literature (see [Verd] and the references therein), the linear minimum mean-squared error (MMSE) detector offers a good trade-off between performance and complexity [HoTs]. Indeed, the linear MMSE receiver jointly minimizes the effects of thermal noise, intersymbol interference (ISI) and MAI on the bit-error rate (BER) performance. Moreover, the MMSE detector, implemented as a Wiener filter at the chip level, is moderately complex because it does not require the knowledge of the interfering users' parameters (spreading codes, channels, and timing) [HoTs]. Specifically, the Wiener MMSE filter is obtained by multiplying the inverse of the covariance matrix of the received signal with the signature waveform vector of the user of interest [Verd][HoTs][Hayk], and therefore the interfering users' parameters are implicitly contained into the covariance matrix of the received signal.

In realistic scenarios, the signature waveform vector and the covariance matrix are not known and they must be estimated. The estimation errors, which depend on the employed estimation techniques, clearly become larger when a small sample set is used for the estimation. Some examples where the detector is obtained by using small data sets include:

- Transmissions of short data blocks;
- Transmissions over slowly time varying channels, where it is convenient to use data blocks within the channel coherence time.

Another advantage of the Wiener MMSE filter is that the chip-rate sampling allows the channel estimation by blind techniques [WaPo]. The main benefit of the blind methods is

the bandwidth saving due to the absence of training sequences, which becomes significant when the data block is short. In this context, batch methods should be preferred with respect to adaptive algorithms, because their convergence is not assured.

In multiuser DS-CDMA environments, the covariance matrix of the received signal is often ill-conditioned, being characterized by a high eigenvalue spread for high values of the signal-to-noise ratio (SNR). As a consequence of the high eigenvalue spread, the matrix inversion contained in the MMSE detector tends to enhance the covariance matrix estimation errors, causing significant performance degradation [Hayk].

Aim of this chapter is to investigate the BER performance degradation due to such estimation errors, by comparing the performance of the estimated MMSE detector with the ideal MMSE one. The sensitivity to the errors caused by a popular channel estimation algorithm and by the covariance matrix estimation is examined both separately and jointly. Moreover, some techniques that reduce the effect of such errors are proposed. For uplink transmissions, a two-step approach that exploits the estimated channels of all the users is proposed. For downlink scenarios, we propose a modified MMSE detector that takes advantage of a regularization technique. Simulation results are used in order to validate the usefulness of the proposed detectors.

2.1. DS-CDMA SYSTEM MODEL

We introduce the system model that will be used throughout this chapter. A DS-CDMA system with K active users is considered. Using a notation similar to [WaPo], the transmitted signal of the k th user is expressed by

$$x_k(t) = A_k \sum_{i=0}^{P-1} b_k[i] s_k(t - iT_s - \tau_k), \quad (1)$$

where P is the number of transmitted symbols within the channel coherence time, T_s is the

symbol duration, A_k , $b_k[i]$, $s_k(t)$, and τ_k are the amplitude, the i th symbol, the spreading waveform, and the asynchronism delay of the user k , respectively. The symbols $\{b_k[i]\}$ are independent and equiprobable random variables drawn from the set $\{\pm 1\}$. The spreading waveform is expressed by

$$s_k(t) = \sum_{j=0}^{N-1} c_k[j] \psi(t - jT_c), \quad (2)$$

where N is the processing gain, $T_c = T_s / N$ is the chip duration, $\psi(t)$ is the chip pulse shaping waveform, assumed rectangular for the sake of simplicity, and $c_k[j] \in \{\pm 1/\sqrt{N}\}$ is the $(j+1)$ th value of the short spreading code assigned to the k th user. The transmitted signal $x_k(t)$ passes through a slowly time varying multipath channel, assumed to be constant during the transmission of the P symbols, and characterized by an impulse response expressed by

$$g_k(\tau) = \sum_{q=1}^{Q_k} \beta_{q,k} \delta(\tau - \tau_{q,k}), \quad (3)$$

where Q_k is the number of paths, $\beta_{q,k}$ and $\tau_{q,k}$ are the complex gain and the propagation delay of the q th path of the k th user channel, respectively, and $\delta(\tau)$ is the Dirac delta function. At the receiver side, denoting with $n(t)$ the additive white Gaussian noise (AWGN), the received signal

$$r(t) = \sum_{k=1}^K \int_{-\infty}^{+\infty} g_k(\tau) x_k(t - \tau) d\tau + n(t) \quad (4)$$

is firstly filtered by a chip-matched filter, and successively sampled at the chip rate $1/T_c$, thus obtaining

$$r_n[l] = \int_{lT_s + nT_c}^{lT_s + (n+1)T_c} r(t) \psi(t - lT_s - nT_c) dt \quad (5)$$

$$= \sum_{k=1}^K \sum_{i=0}^{P-1} b_k[i] h_{n,k}[l-i] + n_n[l], \quad (6)$$

$$h_{n,k}[i] = \sum_{q=1}^{Q_k} \sum_{j=0}^{N-1} \beta_{q,k} A_k c_k[j] R_\psi(iT_s + (n-j)T_c - \tau_{q,k} - \tau_k), \quad (7)$$

$$n_n[l] = \int_{lT_s+nT_c}^{lT_s+(n+1)T_c} n(t)\psi(t-lT_s-nT_c)dt, \quad (8)$$

where $R_\psi(\tau)$ is the autocorrelation function of the chip pulse shaping waveform $\psi(t)$. The sampling instant can be selected to compensate for the asynchronism delay of the user of interest. Alternatively, if the sampling instant is arbitrarily chosen, the average power loss of the useful signal is 1.76 dB [BeAa]. However, the interfering signals suffer from the same power loss.

By setting $\underline{r}[l] = [r_0[l] \cdots r_{N-1}[l]]^T$, $\underline{n}[l] = [n_0[l] \cdots n_{N-1}[l]]^T$, $\underline{b}[l] = [b_1[l] \cdots b_K[l]]^T$, and by defining $\underline{H}[l]$ as the $N \times K$ matrix with elements $[\underline{H}[l]]_{n,k} = h_{n-1,k}[l]$, (6) can be rearranged as

$$\underline{r}[l] = \sum_{i=0}^{P-1} \underline{H}[l-i] \underline{b}[i] + \underline{n}[l]. \quad (9)$$

Taking into account that the K channels have a finite impulse response (FIR), with memory $L = \max_{q,k} \{ \lceil (\tau_{q,k} + \tau_k) / T_s \rceil \}$ symbol intervals, it follows that $\underline{H}[l] = \mathbf{0}_{N \times K}$ when $l \geq L+1$. Assuming that the receiver window spans M symbol intervals, we obtain

$$\mathbf{r}[l] = \mathbf{H}\mathbf{b}[l] + \mathbf{n}[l], \quad (10)$$

where $\mathbf{r}[l] = [\underline{r}[l]^T \cdots \underline{r}[l+M-1]^T]^T$ and $\mathbf{n}[l] = [\underline{n}[l]^T \cdots \underline{n}[l+M-1]^T]^T$ are column vectors of dimension MN , $E\{\mathbf{n}[l]\mathbf{n}[l]^H\} = \sigma^2 \mathbf{I}_{MN}$ is the covariance matrix of the background noise, $\mathbf{b}[l] = [\underline{b}[l-L]^T \cdots \underline{b}[l+M-1]^T]^T$ is a column vector of size $(L+M)K$, and \mathbf{H} is the $MN \times (L+M)K$ block Toeplitz channel matrix expressed by

$$\mathbf{H} = \begin{bmatrix} \underline{H}[L] & \cdots & \cdots & \underline{H}[0] & \cdots & \mathbf{0}_{N \times K} \\ & \ddots & & & \ddots & \\ \mathbf{0}_{N \times K} & \underline{H}[L] & \cdots & \cdots & \underline{H}[0] & \end{bmatrix}. \quad (11)$$

2.2. ESTIMATION ERRORS ON THE MMSE DETECTOR

In this section, our aim is to focus on the sources of errors that arise in the linear MMSE detector estimation process. We consider the MMSE detector because of its good performance among the linear receivers [Verd], and also because it is widely employed as a first stage of multistage detectors based on interference cancellation (IC) techniques [Cru1]. The main sources of impairment herein considered are the estimation errors due to the imperfect knowledge of the covariance matrix of the received signal, and the ones caused by a well-known blind channel estimation technique [WaPo]. Although the errors produced by such impairments have already been analyzed in [Xu1] and [Xu2], we will focus on their effect on the BER of the MMSE detector. For the errors caused by imperfect time synchronization, the reader is redirected to [BeAa][Madh1][Madh2][WaPo].

2.2.1. Ideal MMSE Detector

For the adopted binary phase-shift keying (BPSK) modulation, the decision rule of a linear receiver is expressed by

$$\hat{b}_k[l] = \text{sign}(\text{Re}(\mathbf{w}_k^H \mathbf{r}[l])), \quad (12)$$

where \mathbf{w}_k is a column vector that represents the detector of the user k . The detector that minimizes the mean-squared error (MSE) $E\{|b_k[l] - \mathbf{w}_k^H \mathbf{r}[l]|^2\}$ can be obtained as a Wiener filter [Verd][HoTs][Hayk], as expressed by

$$\mathbf{w}_{\text{MMSE},k} = \mathbf{R}^{-1} \mathbf{h}_k, \quad (13)$$

where $\mathbf{R} = E\{\mathbf{r}[l]\mathbf{r}[l]^H\}$ is the $MN \times MN$ covariance matrix of the received signal, and \mathbf{h}_k , obtained as the $(KL+k)$ th column of \mathbf{H} , is the signature waveform (i.e., the channel-affected spreading code) of the user k . The detector in (13) is also known as minimum variance distortionless response (MVDR) filter. By applying the eigenvalue decomposition (EVD) $\mathbf{R} = \mathbf{U}\mathbf{\Lambda}\mathbf{U}^H$, and assuming that the eigenvalues in $\mathbf{\Lambda}$ are arranged in non-increasing order (i.e., $\lambda_1 \geq \lambda_2 \geq \dots \geq \lambda_{MN}$), (13) can equivalently be expressed by [WaPo]

$$\mathbf{w}_{\text{MMSE},k} = \mathbf{U}_S \mathbf{\Lambda}_S^{-1} \mathbf{U}_S^H \mathbf{h}_k = \sum_{i=1}^D \frac{\mathbf{u}_i^H \mathbf{h}_k}{\lambda_i} \mathbf{u}_i, \quad (14)$$

where λ_i and \mathbf{u}_i represent the i th eigenvalue-eigenvector pair, $D = \text{rank}(\mathbf{H})$ is the dimension of the signal subspace, $\mathbf{\Lambda}_S = \text{diag}(\lambda_1, \dots, \lambda_D)$, and $\mathbf{U}_S = [\mathbf{u}_1 \cdots \mathbf{u}_D]$ contains the D eigenvectors that compose the signal subspace. The equivalence between (13) and (14) is a direct consequence of

$$\mathbf{U}_N^H \mathbf{h}_k = \mathbf{0}_{MN-D \times 1}, \quad (15)$$

where $\mathbf{U}_N = [\mathbf{u}_{D+1} \cdots \mathbf{u}_{MN}]$ contains the eigenvectors of the noise subspace. Such an equation is also the basis of subspace-based blind channel estimation techniques [MDCM].

2.2.2. Estimated MMSE Detectors

In practical situations, neither \mathbf{R} nor \mathbf{h}_k is known. Consequently, when \mathbf{R} and \mathbf{h}_k are replaced by their estimated versions $\hat{\mathbf{R}}$ and $\hat{\mathbf{h}}_k$, the system link budget has to take into account the effects of the estimation errors. As far as the covariance matrix estimation is concerned, the maximum-likelihood (ML) estimate of \mathbf{R} is expressed by [Rich]

$$\hat{\mathbf{R}} = \frac{1}{P} \sum_{l=0}^{P-1} \mathbf{r}[l] \mathbf{r}[l]^H, \quad (16)$$

whose EVD $\hat{\mathbf{R}} = \hat{\mathbf{U}} \hat{\mathbf{\Lambda}} \hat{\mathbf{U}}^H$ produces the ML estimate of the eigenvalues and eigenvectors of \mathbf{R} [BeAa]. In many practical situations, the value of P has to be kept small, leading to non-negligible covariance matrix estimation errors [Xu1]. As an example, when $P < MN$, $\hat{\mathbf{R}}$ is not full rank and therefore not invertible. As a rule of thumb, we can assume that the covariance matrix estimation errors are small when $P > 6MN$ [Carl]. However, when the system is not fully loaded, the matrix \mathbf{H} can be tall, with $D = \text{rank}(\mathbf{H})$ strictly lower than MN . In such a situation, the covariance matrix \mathbf{R} is often ill-conditioned, especially when the SNR is high. Therefore, the matrix inversion contained in the MMSE detector amplifies the small covariance matrix estimation errors, according to the eigenvalue spread χ (or condition number) of \mathbf{R} [Hayk][HoJo1], which is the ratio between the maximum and the

minimum eigenvalue of \mathbf{R} .

It is worth noting that a high eigenvalue spread of \mathbf{R} produces also an amplification of the possible signature waveform mismatch $\Delta \mathbf{h}_k = \hat{\mathbf{h}}_k - \mathbf{h}_k$ [Madh1][Hayk]. Moreover, it should be pointed out that the problem of a small P is exacerbated when multiple antennas are used at the receiver side, since the dimension of \mathbf{R} increases by a factor equal to the number of the receiving antennas [GSSP].

The channel vector \mathbf{h}_k can be estimated either by the aid of training sequences [MHM] or by blind techniques [WaPo][ToPe]. In this thesis, we mainly focus on the subspace-based blind channel estimation technique proposed in [WaPo]. Indeed, in the short data block situation, the training symbols of data-aided (DA) channel estimation techniques consume an high fraction of the transmitted block. The subspace-based blind channel estimation techniques use the EVD of (16) to estimate the eigenvectors of the noise subspace. Consequently, when only the estimated version $\hat{\mathbf{U}}_N$ is available, an estimate $\hat{\mathbf{h}}_k$ of the true channel \mathbf{h}_k can be obtained by solving (15) in the least squares (LS) sense, making use of the code sequence $\{c_k[j]\}$ of the user of interest [WaPo].

Since the covariance matrix inverse is estimated by inverting (16), the receiver expressions (13) and (14) become

$$\hat{\mathbf{w}}_{\text{SMI},k} = \hat{\mathbf{R}}^{-1} \hat{\mathbf{h}}_k = \sum_{i=1}^{MN} \frac{\hat{\mathbf{u}}_i^H \hat{\mathbf{h}}_k}{\hat{\lambda}_i} \hat{\mathbf{u}}_i, \quad (17)$$

$$\hat{\mathbf{w}}_{\text{PC},k} = \hat{\mathbf{U}}_S \hat{\mathbf{\Lambda}}_S^{-1} \hat{\mathbf{U}}_S^H \hat{\mathbf{h}}_k = \sum_{i=1}^D \frac{\hat{\mathbf{u}}_i^H \hat{\mathbf{h}}_k}{\hat{\lambda}_i} \hat{\mathbf{u}}_i, \quad (18)$$

respectively. The receiver in (17) is known as sample matrix inversion (SMI) or direct matrix inversion (DMI) detector, while the one in (18) is commonly referred as principal component (PC) or Karhunen-Loève transform (KLT) detector. It is noteworthy that the relation $\hat{\mathbf{U}}_N^H \hat{\mathbf{h}}_k = \mathbf{0}_{MN-D \times 1}$ is not satisfied, because the estimated channels do not lie completely in the estimated signal subspace. Therefore, the receivers (17) and (18) are in general different.

In order to isolate the effects of the covariance and channel estimation on the BER performance, we also introduce the so-called partially-estimated receivers, where the covariance matrix estimation is coupled with the ideal channel knowledge, and vice versa, the exact covariance matrix is coupled with the estimated channel. As a consequence, we define the ideal matrix inverse receiver with estimated channel (IMI-EC) as

$$\hat{\mathbf{w}}_{\text{IMI-EC},k} = \mathbf{R}^{-1} \hat{\mathbf{h}}_k, \quad (19)$$

and the SMI receiver with true channel (SMI-TC) as

$$\hat{\mathbf{w}}_{\text{SMI-TC},k} = \hat{\mathbf{R}}^{-1} \mathbf{h}_k. \quad (20)$$

In addition, we define

$$\hat{\mathbf{w}}_{\text{IPC-EC},k} = \mathbf{U}_S \mathbf{\Lambda}_S^{-1} \mathbf{U}_S^H \hat{\mathbf{h}}_k, \quad (21)$$

and

$$\hat{\mathbf{w}}_{\text{EPC-TC},k} = \hat{\mathbf{U}}_S \hat{\mathbf{\Lambda}}_S^{-1} \hat{\mathbf{U}}_S^H \mathbf{h}_k, \quad (22)$$

as the ideal PC receiver with estimated channel (IPC-EC), and the estimated PC receiver with true channel (EPC-TC).

2.2.3. *Simulation Results*

We make use of simulation results to compare the BER performance of the ideal MMSE receiver, the estimated MMSE receivers (SMI in (17) and PC in (18)), and the partially-estimated MMSE receivers (19)-(22). Gold sequences [DiJa] of length $N = 31$ have been chosen for the short spreading codes $\{c_k[j]\}$. The chip rate has been fixed to $1/T_c = 8.192$ Mega chips per second, and consequently the bit rate of each user is approximately equal to 264 Kb per second. The channel model is compliant with the pedestrian B channel defined in [ETSI]. The chosen chip rate $1/T_c$ and the processing gain N lead to a maximum delay spread that is slightly longer than one symbol duration. The uplink situation is considered, with asynchronism delays $\{\tau_k\}$ uniformly distributed in

$[0, T_s)$. The asynchronism delays and the maximum delay spreads of all the users are assumed known at the base station, and hence the maximum channel order L is assumed known. The smoothing factor M , which is also the dimension in symbol intervals of the observation window at the receiver side, has been selected by taking into account the identifiability conditions [WaPo]

$$M \geq \left\lceil \frac{KL}{N-K} \right\rceil, \quad (23)$$

$$(N-K)M^2 + (N-2K)LM \geq KL^2 + N(L+1). \quad (24)$$

Lets now assume that the covariance matrix \mathbf{R} is estimated by using $P = 300$ bits, with a consequent estimation window of $\Delta T = PT_s \approx 1.1$ ms. For a mobile transmitter with speed $V \leq 30$ Km/h and a carrier frequency $f = 2$ GHz, the Clarke autocorrelation function [Skla] assumes the value $J_0(2\pi f \Delta T V / c) \geq 0.96$, where $J_0(\cdot)$ is the zero-order Bessel function of the first kind, and c is the speed of light. Therefore, the channels of the mobile users can be considered constant, as supposed in this thesis.

The SNR, defined as $\text{SNR} = A_1^2 / \sigma^2$, is the one of the user 1, which is assumed to be the user of interest. The MAI level is defined as $\text{MAI} = A_2^2 / A_1^2$, where it is assumed that all the interfering signals have the same power. The normalized root MSE (NRMSE) is defined by $\text{NRMSE} = N_{ch}^{-1/2} \left(\sum_{i=1}^{N_{ch}} \|\hat{\mathbf{h}}_1^{(i)} - \mathbf{h}_1^{(i)}\|^2 / \|\mathbf{h}_1^{(i)}\|^2 \right)^{1/2}$, where $\mathbf{h}_1^{(i)}$ denotes the i th signature waveform realization of user 1, and $N_{ch} = 300$ is the number of independent simulations. The unknown complex scalar factor of the blind channel estimation algorithm [BeAa] is compensated for by assuming the knowledge of the phase of the maximum magnitude coefficient of \mathbf{h}_k . In near-far scenarios, the figures show the BER of the weakest user (i.e., user 1).

Fig. 1 shows that the channel estimation algorithm is near-far resistant, because the simulated NRMSE does not depend on the amount of MAI for a given number K of users. Moreover, Fig. 1 and Fig. 2 evidence that the channel estimation performance is highly influenced by the number of active users, and by the averaging factor P , respectively.

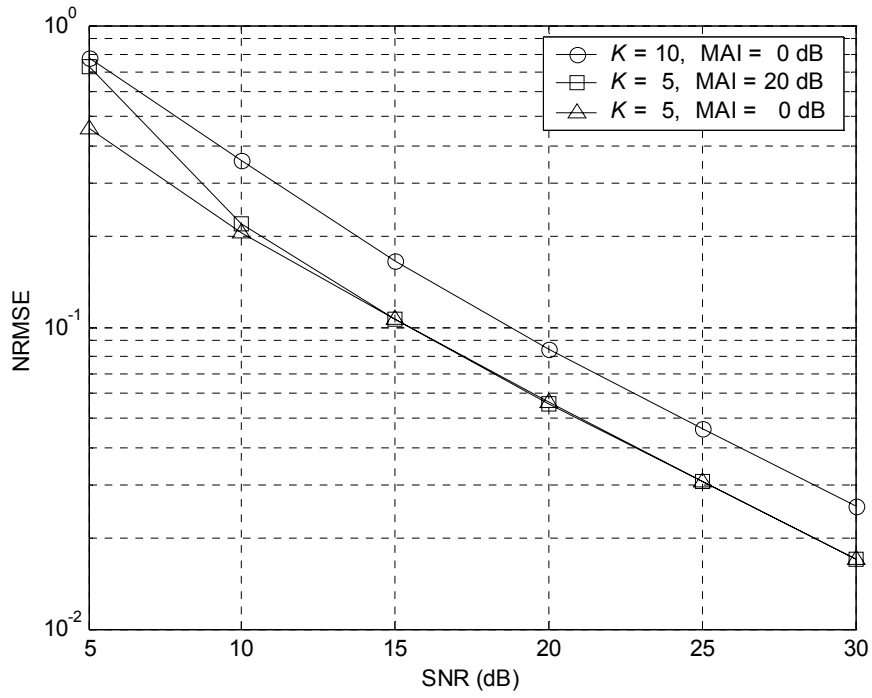


Fig. 1. Performance of the channel estimation algorithm ($P = 300$).

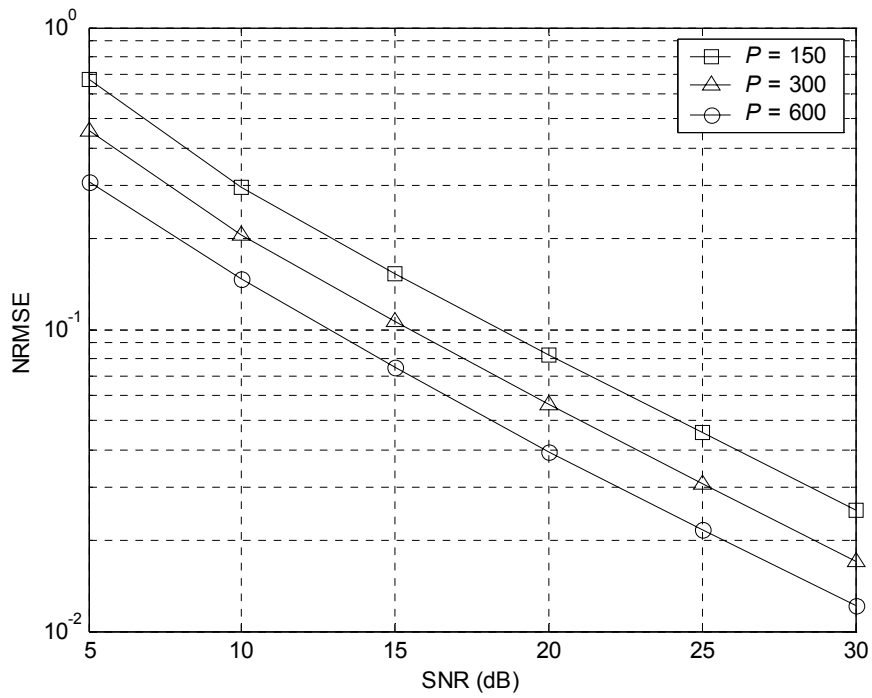


Fig. 2. Performance of the channel estimation algorithm ($K = 5, \text{ MAI} = 0 \text{ dB}$).

Fig. 3 and Fig. 4 compare the BER performance of the ideal, estimated, and partially-estimated PC detectors, in a scenario with power control and in a near-far situation, respectively. In Fig. 5, a similar comparison is performed by considering the SMI detectors. In the following, we point out some observations.

- All the figures highlight the high SNR penalty of the fully estimated MMSE receivers, which are the PC and the SMI, with respect to the ideal MMSE. Such penalty tends to increase for increasing SNR, since the estimation errors of the covariance matrix inverse are higher at high SNR.
- In scenarios with perfect power control (Fig. 3), the two partially-estimated PC receivers (21) and (22) show BER performance characterized by a different behavior. Indeed, at low SNR, where the channel estimation errors are higher, the IPC-EC detector (21) has a significant BER degradation with respect to the EPC-TC detector (22). On the contrary, for increasing SNR, the IPC-EC detector significantly outperforms the EPC-TC one. Indeed, when the SNR increases, the channel estimate improves (see Fig. 1), while, due to the increased eigenvalue spread of $\mathbf{U}_s \mathbf{\Lambda}_s \mathbf{U}_s^H$, the estimation errors are highly amplified by the inversion operation, causing a BER floor whose value depends on the averaging factor P . Obviously, the BER of the fully estimated PC detector (18) is imposed by the performance of the two partially-estimated ones. Therefore an improved detector should have a better inverse matrix estimation at high SNR and a better channel estimation at low SNR.
- In strong near-far situations, the IPC-EC receiver outperforms the EPC-TC one also at low SNR, because the channel estimation algorithm exploits the higher power of the interfering signals.
- As shown in Fig. 5, the receivers that use the full matrix inverse have a higher BER degradation with respect to the ones of Fig 4, which use the signal subspace only. Indeed, when $i > D$, the quantities $\mathbf{u}_i^H \hat{\mathbf{h}}_k$, $\hat{\mathbf{u}}_i^H \mathbf{h}_k$, and $\hat{\mathbf{u}}_i^H \hat{\mathbf{h}}_k$, are not negligible with respect to λ_i , $\hat{\lambda}_i$, and $\hat{\lambda}_i$, respectively. It can also be noted that, at high SNR, the SMI detector with estimated channel outperforms the partially-estimated detectors (19) and

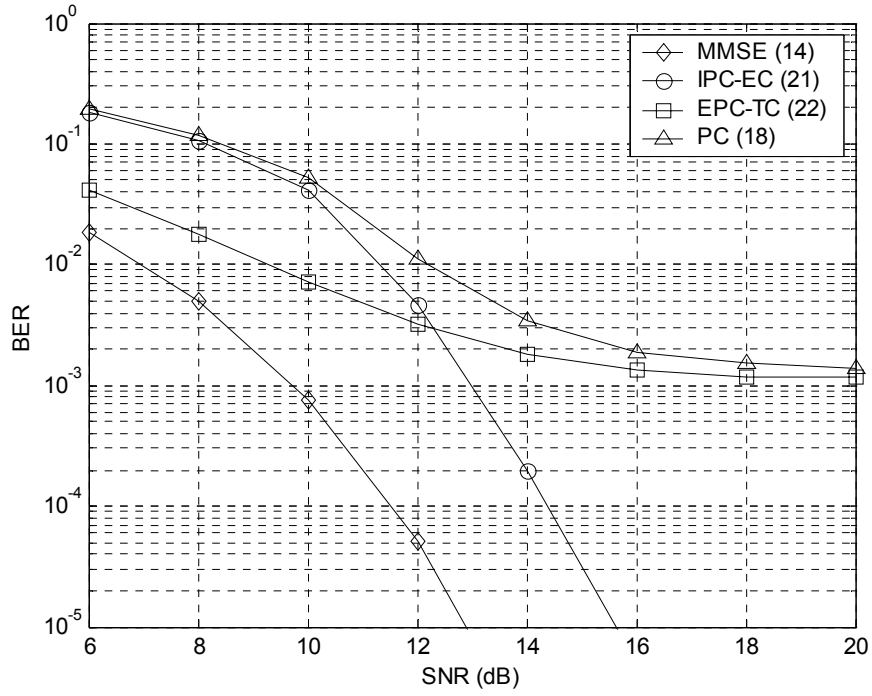


Fig. 3. BER comparison among the PC-type detectors ($K = 5$, $\text{MAI} = 0$ dB, $P = 150$).

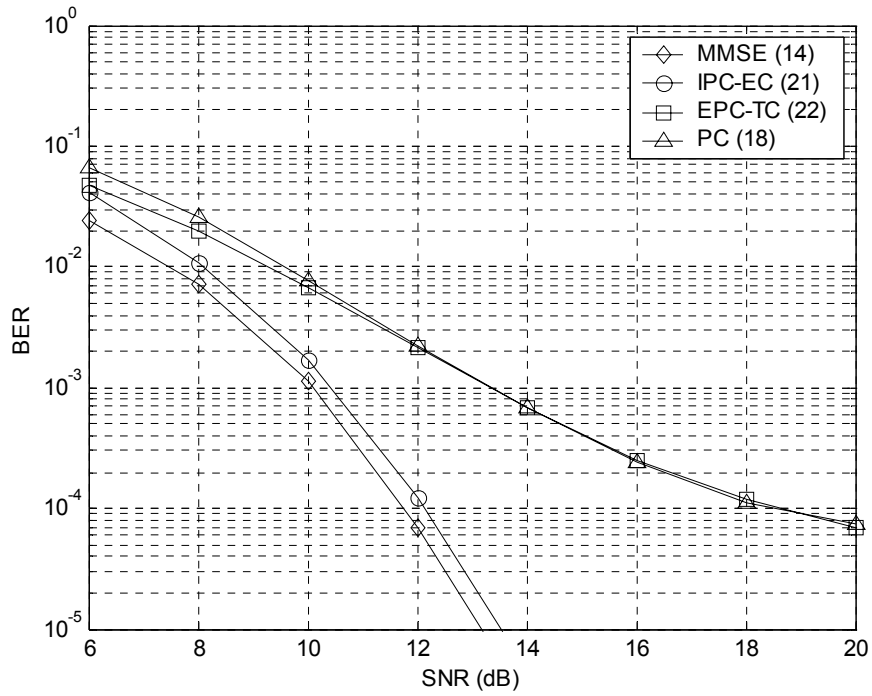


Fig. 4. BER comparison among the PC-type detectors ($K = 5$, $\text{MAI} = 20$ dB, $P = 300$).

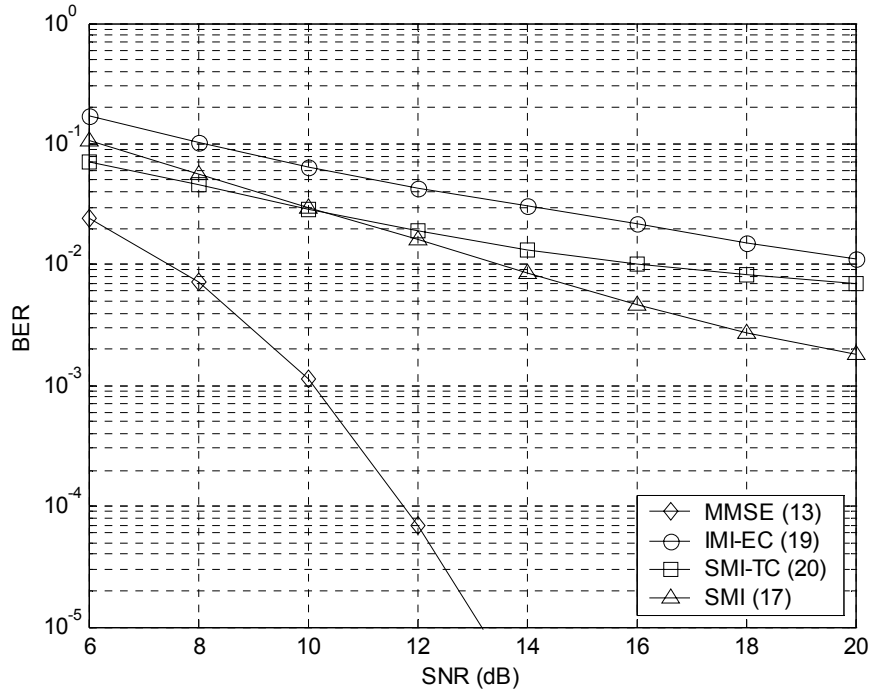


Fig. 5. BER comparison among the SMI-type detectors ($K = 5$, MAI = 20 dB, $P = 300$).

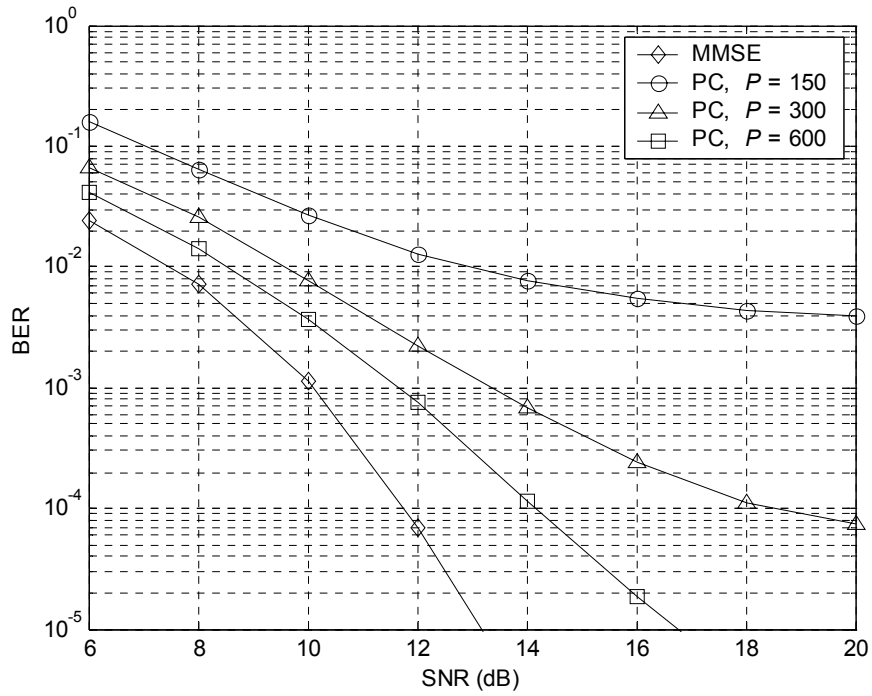


Fig. 6. Effect of P on the BER of the PC detector ($K = 5$, MAI = 20 dB).

(20), provided that P is not too low. This behavior may be explained by the quasi-orthogonality relation $\hat{\mathbf{U}}_N^H \hat{\mathbf{h}}_k \approx \mathbf{0}_{MN-D \times 1}$ caused by the channel estimation algorithm, i.e., $\|\hat{\mathbf{U}}_N^H \hat{\mathbf{h}}_k\| \leq \|\mathbf{U}_N^H \hat{\mathbf{h}}_k\|$, and $\|\hat{\mathbf{U}}_N^H \hat{\mathbf{h}}_k\| \leq \|\hat{\mathbf{U}}_N^H \mathbf{h}_k\|$.

Fig. 6 illustrates that the BER floor is highly dependent on the averaging factor P . Moreover, when P is sufficiently high, the BER approaches the one of the ideal MMSE detector. However, the performance can be unacceptable when some practical constraints (e.g., user mobility) impose a low value of P .

2.3. IMPROVED DETECTORS FOR UPLINK TRANSMISSIONS

The results of the previous section have highlighted that, differently from the MSE of the channel estimate, the BER of the estimated MMSE detectors cannot be reduced by increasing the SNR, because of the covariance matrix estimation errors. The effects of such errors can be reduced in different ways. A first option is to obtain a new covariance matrix estimate by exploiting the estimated channels of all the users, provided that these channel estimates are quite accurate. However, this method requires the knowledge of channels, timing, and spreading codes of all the users, and therefore it is feasible in the uplink only.

A second approach relies on regularization techniques [Hans], which improve the conditioning by conveniently modifying the covariance matrix. A related alternative is based on reduced-rank techniques [HoTs], which project the received signal onto a lower-dimensional subspace, thereby resulting in a covariance matrix (of the projected received signal) with smaller eigenvalue spread. Anyway, certain reduced-rank techniques are sometimes classified as regularization methods [Hans]. The regularization techniques, either full-rank or reduced-rank, can be exploited also in the downlink.

In this section, we will consider both the approaches, focusing on the uplink scenario.

2.3.1. PC Detector with Tikhonov Regularization

By defining the error committed on the i th eigenvalue as $\Delta\lambda_i = \hat{\lambda}_i - \lambda_i$, and the error on the corresponding eigenvector as $\Delta\mathbf{u}_i = \hat{\mathbf{u}}_i - \mathbf{u}_i$, (18) can be rewritten as

$$\hat{\mathbf{w}}_{\text{PC},k} = \sum_{i=1}^D \frac{(\mathbf{u}_i + \Delta\mathbf{u}_i)^H (\mathbf{h}_k + \Delta\mathbf{h}_k)}{\lambda_i + \Delta\lambda_i} (\mathbf{u}_i + \Delta\mathbf{u}_i) = \mathbf{w}_{\text{MMSE},k} + \mathbf{e}_{0,k} + \mathbf{e}_{1,k} + \mathbf{e}_{2,k}, \quad (25)$$

where

$$\mathbf{e}_{0,k} = -\sum_{i=1}^D \frac{\Delta\lambda_i}{\lambda_i + \Delta\lambda_i} \frac{\mathbf{u}_i^H \mathbf{h}_k}{\lambda_i} \mathbf{u}_i, \quad (26)$$

$$\mathbf{e}_{1,k} = \sum_{i=1}^D \frac{\Delta\mathbf{u}_i^H (\mathbf{h}_k + \Delta\mathbf{h}_k) + \mathbf{u}_i^H \Delta\mathbf{h}_k}{\lambda_i + \Delta\lambda_i} \mathbf{u}_i, \quad (27)$$

$$\mathbf{e}_{2,k} = \sum_{i=1}^D \frac{(\mathbf{u}_i + \Delta\mathbf{u}_i)^H (\mathbf{h}_k + \Delta\mathbf{h}_k)}{\lambda_i + \Delta\lambda_i} \Delta\mathbf{u}_i. \quad (28)$$

An approach for reducing the norm of $\hat{\mathbf{w}}_{\text{PC},k} - \mathbf{w}_{\text{MMSE},k} = \mathbf{e}_{0,k} + \mathbf{e}_{1,k} + \mathbf{e}_{2,k}$ is to add a positive number ν to the eigenvalues of the signal subspace. Such an approach is a particular form of Tikhonov regularization [Hans]. When the regularization is applied to all the eigenvalues, it holds true that $\mathbf{U}(\mathbf{\Lambda} + \nu\mathbf{I}_{MN})\mathbf{U}^H = \mathbf{R} + \nu\mathbf{I}_{MN}$, which corresponds to the constrained minimum output energy (CMOE) receiver of [HMV][Madh1], as expressed by

$$\hat{\mathbf{w}}_{\text{CMOE},k} = (\hat{\mathbf{R}} + \nu\mathbf{I}_{MN})^{-1} \hat{\mathbf{h}}_k = \sum_{i=1}^{MN} \frac{\hat{\mathbf{u}}_i^H \hat{\mathbf{h}}_k}{\hat{\lambda}_i + \nu} \hat{\mathbf{u}}_i. \quad (29)$$

Such a DS-CDMA receiver has been obtained by incorporating into the MSE minimization a constraint on the norm of the detector vector. In this case, the regularization parameter ν is also the Lagrange multiplier involved in the minimization. In the array processing literature, this detector is known as diagonal loaded SMI (LSMI) [Carl].

When the regularization is applied to the signal subspace, the receiver can be expressed as

$$\hat{\mathbf{w}}_{\text{PC-CMOE},k} = \hat{\mathbf{U}}_S (\hat{\mathbf{\Lambda}}_S + \nu\mathbf{I}_D)^{-1} \hat{\mathbf{U}}_S^H \hat{\mathbf{h}}_k = \sum_{i=1}^D \frac{\hat{\mathbf{u}}_i^H \hat{\mathbf{h}}_k}{\hat{\lambda}_i + \nu} \hat{\mathbf{u}}_i \quad (30)$$

$$= \mathbf{w}_{\text{MMSE},k} + \tilde{\mathbf{e}}_{0,k} + \tilde{\mathbf{e}}_{1,k} + \tilde{\mathbf{e}}_{2,k}, \quad (31)$$

$$\tilde{\mathbf{e}}_{0,k} = -\sum_{i=1}^D \frac{\Delta\lambda_i + \nu}{\lambda_i + \Delta\lambda_i + \nu} \frac{\mathbf{u}_i^H \mathbf{h}_k}{\lambda_i} \mathbf{u}_i, \quad (32)$$

$$\tilde{\mathbf{e}}_{1,k} = \sum_{i=1}^D \frac{\Delta\mathbf{u}_i^H (\mathbf{h}_k + \Delta\mathbf{h}_k) + \mathbf{u}_i^H \Delta\mathbf{h}_k}{\lambda_i + \Delta\lambda_i + \nu} \mathbf{u}_i, \quad (33)$$

$$\tilde{\mathbf{e}}_{2,k} = \sum_{i=1}^D \frac{(\mathbf{u}_i + \Delta\mathbf{u}_i)^H (\mathbf{h}_k + \Delta\mathbf{h}_k)}{\lambda_i + \Delta\lambda_i + \nu} \Delta\mathbf{u}_i. \quad (34)$$

By (33) and (34), it is evident that an increase of ν produces a decrease of the error $\|\tilde{\mathbf{e}}_{1,k} + \tilde{\mathbf{e}}_{2,k}\|$. However, at the same time, $\tilde{\mathbf{e}}_{0,k}$ approaches $-\mathbf{w}_{\text{MMSE},k}$, thus suppressing the useful component of the PC-CMOE receiver. As a consequence, when the estimation errors are small, $\|\mathbf{e}_{1,k} + \mathbf{e}_{2,k}\|$ is already small, and hence the parameter ν has a negative effect, because it tends to suppress the useful component. On the contrary, if such errors are considerably high, we can obtain a satisfactory reduction of $\|\tilde{\mathbf{e}}_{1,k} + \tilde{\mathbf{e}}_{2,k}\|$ without an excessive diminution of $\|\mathbf{w}_{\text{MMSE},k} + \tilde{\mathbf{e}}_{0,k}\|$, provided that the value of ν is not too large.

In the following, we outline some remarks.

- The parameter ν enables the reduction of the eigenvalue spread from the value $\chi = \lambda_1 / \lambda_D$ to the value $\chi = (\lambda_1 + \nu) / (\lambda_D + \nu)$, with a consequent reduction of the variance of the estimation error on the detector. However, such a variance reduction is accompanied with an increase of bias, because the matrix $\hat{\mathbf{U}}_S (\hat{\mathbf{\Lambda}}_S + \nu \mathbf{I}_D)^{-1} \hat{\mathbf{U}}_S^H$ in (30) can be interpreted as a biased estimate of \mathbf{R}^{-1} .
- Since $\lambda_i = \sigma^2$ for $i = D+1, \dots, MN$, when $\nu \gg \sigma^2$ the PC-CMOE receiver is practically equivalent to the CMOE receiver, because $\hat{\mathbf{U}}_N^H \hat{\mathbf{h}}_k \approx \mathbf{0}_{MN-D \times 1}$.
- When $\nu \rightarrow +\infty$, both the CMOE and the PC-CMOE receivers tend to a scaled version of the RAKE receiver, which is expressed by

$$\hat{\mathbf{w}}_{\text{RAKE},k} = \hat{\mathbf{h}}_k. \quad (35)$$

Indeed, since $\nu \gg \lambda_i$, we have $\hat{\mathbf{U}} (\hat{\mathbf{\Lambda}} + \nu \mathbf{I}_{MN})^{-1} \hat{\mathbf{U}}^H \hat{\mathbf{h}}_k \approx \hat{\mathbf{U}} (\nu \mathbf{I}_{MN})^{-1} \hat{\mathbf{U}}^H \hat{\mathbf{h}}_k \approx \nu^{-1} \hat{\mathbf{h}}_k$. As a

consequence, if ν is too high, the PC-CMOE receiver loses its interference mitigation capability.

The proposed receiver is therefore a CMOE-type receiver. However, in [HMV] the norm constraint has been introduced to take into account the signature waveform mismatch $\Delta\mathbf{h}_k$, whose norm decreases for increasing SNR. On the contrary, in our case, the main errors are $\Delta\mathbf{u}_i$ and $\Delta\lambda_i$, because the drawback originates from the inversion of the covariance matrix. As shown in Section 2.2, this error exists when $\Delta\mathbf{h}_k = \mathbf{0}_{MN \times 1}$ too.

Nevertheless, as in [Madh2], the main difficulty is the choice of ν , because the optimum value should depend not only on the system ill-conditioning, but also on the amount of estimation errors (i.e., on the parameter P and on the algorithm used for channel estimation). Some suboptimal choices of ν can be found in [Madh2] and in [Hans].

2.3.2. Exploiting the Channel Information of the Other Users

A second estimate of the matrix \mathbf{R} , alternative to the sample covariance matrix expressed by (16), can be obtained by exploiting the fact that the data of different users are uncorrelated, as expressed by $E\{\mathbf{b}[l]\mathbf{b}[l]^H\} = \mathbf{I}_{(M+L)K}$. Since the noise term is white, by (10), the covariance matrix of the received signal can be expressed by

$$\mathbf{R} = E\{\mathbf{r}[l]\mathbf{r}[l]^H\} = \mathbf{H}\mathbf{H}^H + \sigma^2\mathbf{I}_{MN}. \quad (36)$$

Therefore, it is possible to obtain an alternative estimate of \mathbf{R} by means of

$$\tilde{\mathbf{R}} = \hat{\mathbf{H}}\hat{\mathbf{H}}^H + \hat{\sigma}^2\mathbf{I}_{MN}, \quad (37)$$

with $\hat{\mathbf{H}}$ obtained by solving (15) in the LS sense, exploiting the knowledge of the spreading sequences of all the users. The above technique was suggested by observing that the norm of $\Delta\mathbf{h}_k$ can be very low, and it decreases when the SNR increases (see Fig. 1 and Fig. 2). Consequently, $\tilde{\mathbf{R}}$ should be an accurate estimate of \mathbf{R} . This new receiver, which will be called improved MMSE (IMMSE) detector, can be expressed by

$$\hat{\mathbf{w}}_{\text{IMMSE},k} = \tilde{\mathbf{R}}^{-1}\hat{\mathbf{h}}_k. \quad (38)$$

In the following, we draw some comments.

- In order to form $\hat{\mathbf{H}}$, the IMMSE receiver needs the estimated signature waveforms of all the users. However, since we are considering the uplink scenario, this seems a reasonable assumption, because the base station, which knows the spreading codes of all the K active users, has to detect the data of all the users, and consequently has to estimate all the K channels in any case.
- The IMMSE detector (38) requires the inversion of the new covariance matrix estimate $\tilde{\mathbf{R}}$. Therefore, the computational complexity of the receiver design is roughly doubled with respect to the SMI and the PC receivers. However, only one additional matrix inversion is necessary. The same matrix $\tilde{\mathbf{R}}^{-1}$ can then be used to detect the data of all the users.
- The noise power σ^2 can be estimated by making use of the eigenvalues of the noise subspace, as expressed by

$$\hat{\sigma}^2 = \frac{1}{MN - D} \sum_{i=D+1}^{MN} \hat{\lambda}_i. \quad (39)$$

Although we have assumed the noise term $\mathbf{n}[l]$ in (10) as white, the proposed approach can also be used when the noise is colored. Indeed, the base station can estimate the noise covariance matrix $\mathbf{N} = E\{\mathbf{n}[l]\mathbf{n}[l]^H\}$ when no user is active, e.g., before the start of the data transmission. As shown in [MDCM], the subspace-based channel estimation algorithm can be easily modified to take into account the colored noise. Hence, in this case, (37) can be replaced by

$$\tilde{\mathbf{R}} = \hat{\mathbf{H}}\hat{\mathbf{H}}^H + \hat{\mathbf{N}}, \quad (40)$$

and the IMMSE receiver can still be obtained as in (38).

2.3.3. Simulation Results

In this section, we provide some simulation results to validate the effectiveness of the proposed approaches. The simulation scenario is the same of Section 2.2.3.

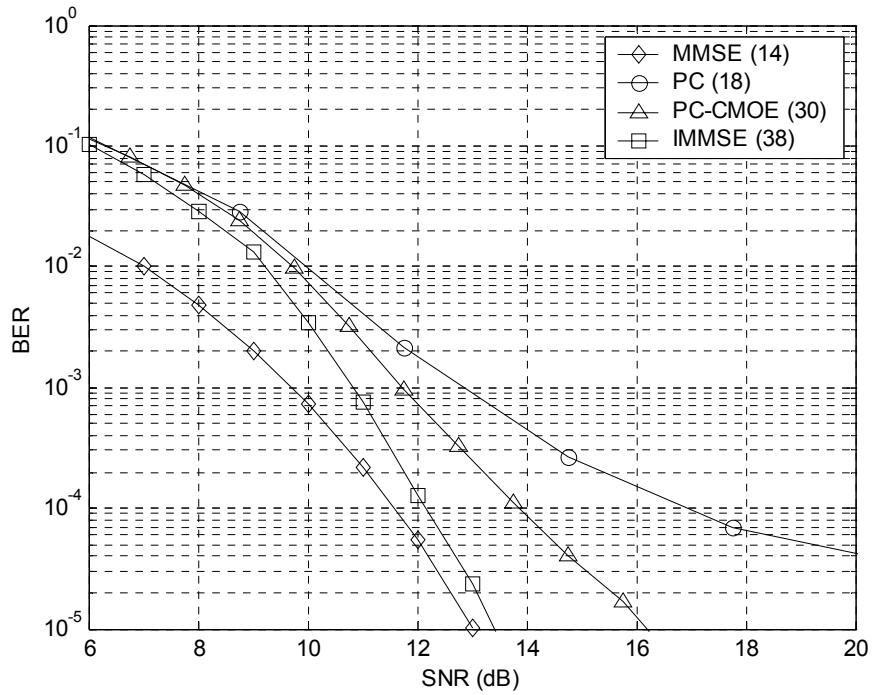


Fig. 7. BER comparison among the MMSE detectors ($K = 5$, $\text{MAI} = 0$ dB, $P = 300$).

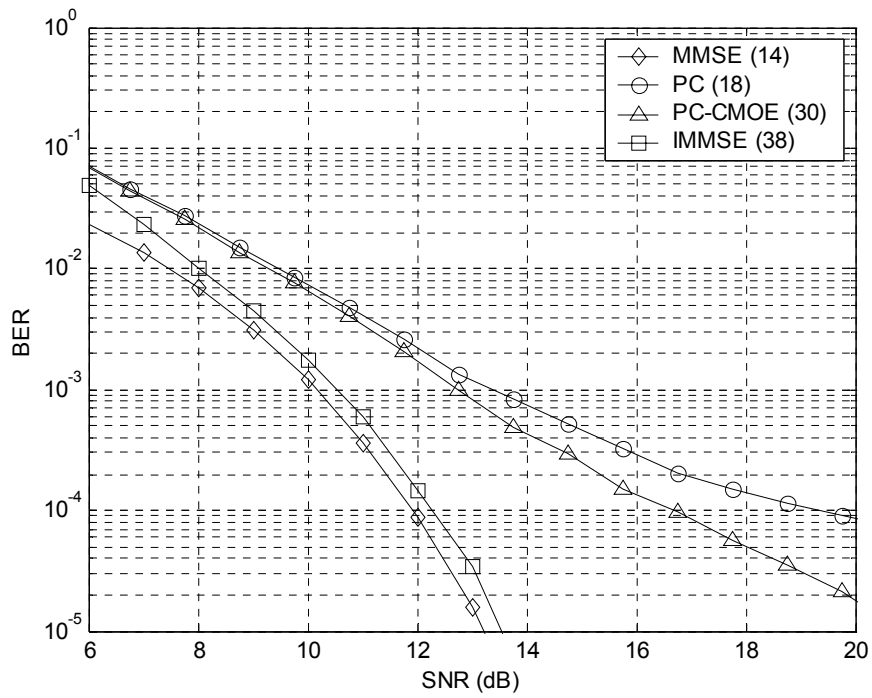


Fig. 8. BER comparison among the MMSE detectors ($K = 5$, $\text{MAI} = 20$ dB, $P = 300$).

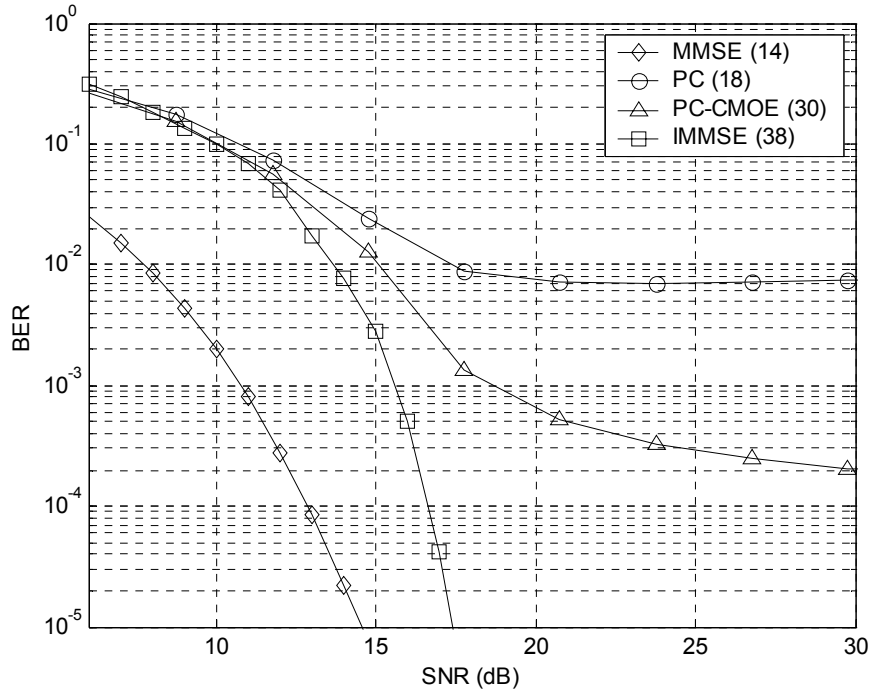


Fig. 9. BER comparison among the MMSE detectors ($K = 10$, MAI = 0 dB, $P = 300$).

Fig. 7, Fig. 8, and Fig. 9 show the BER performance of the proposed detectors in three different scenarios. As expected, all the three figures highlight the high SNR penalty of the estimated MMSE receiver, which is denoted with PC, with respect to the ideal MMSE. As far as the PC-CMOE receiver is concerned, we have chosen the value of ν that minimizes the BER for each SNR. In all the scenarios, the PC-CMOE receiver exhibits a SNR gain with respect to the estimated MMSE receiver. This gain increases for high SNR values. However, also the SNR penalty with respect to the ideal MMSE receiver increases. The first fact is caused by the eigenvalue spread reduction obtained by the regularization parameter ν , while the second one depends on the biasing effect introduced by ν .

On the contrary, the IMMSE receiver, which significantly outperforms the PC-CMOE detector, presents a BER performance that approaches the ideal one when the SNR increases. Indeed, for increasing SNR, the estimation errors of the covariance matrix in (37) decrease, because the channel matrix $\hat{\mathbf{H}}$ is accurately estimated, as shown in Fig. 1 and in

Fig. 2. This fact is confirmed by the smaller performance gain at low SNR, where the channel estimate is not very accurate.

By direct comparison of Fig. 7 and Fig. 8, it is noteworthy that, at low SNR, the BER in the near-far condition (MAI = 20 dB) outperforms the one in the power control situation (MAI = 0 dB). This fact is particularly evident for the IMMSE receiver, which exploits the higher power of the other users in the channel estimation step. Moreover, it should be pointed out that the PC-CMOE receiver is not effective in near-far situations (Fig. 8) as in ideal power control situations (Fig. 7). This fact does not depend on the channel estimation, but on the covariance matrix eigenvalue spread, which is higher in the near-far situation.

Fig. 10 and Fig. 11 show the BER performance of the PC-CMOE receiver as a function of the regularization parameter. For graphical convenience, we have compressed the values of the abscissa axis by means of an arctangent-logarithmic function. It is shown the existence of a unique optimum value, which depends on the scenario (number of users, MAI level, SNR, and signal powers).

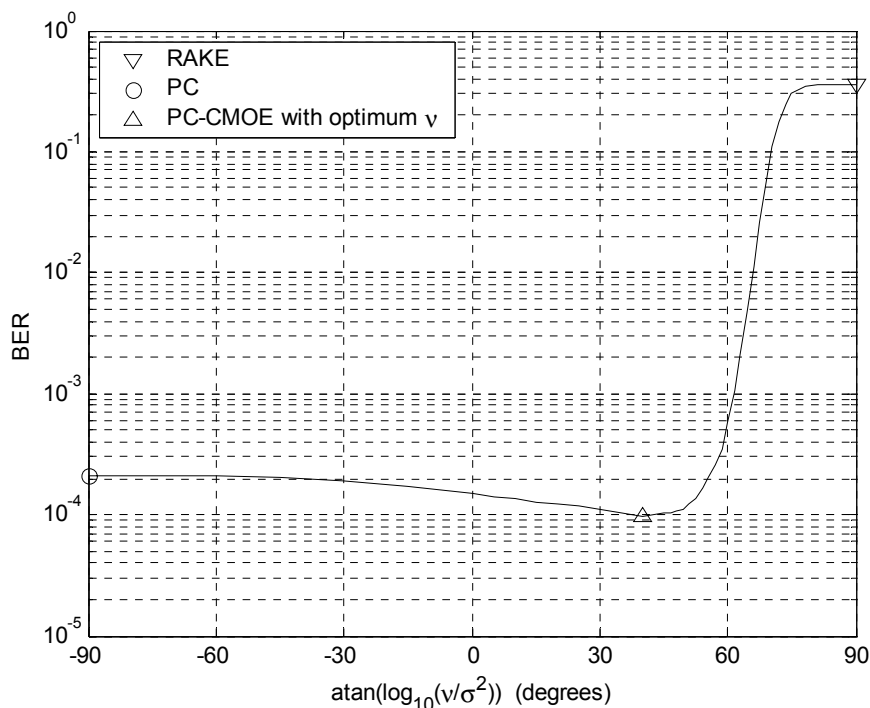


Fig. 10. BER of the PC-CMOE versus v ($K = 5$, MAI = 20 dB, SNR = 16.76 dB).

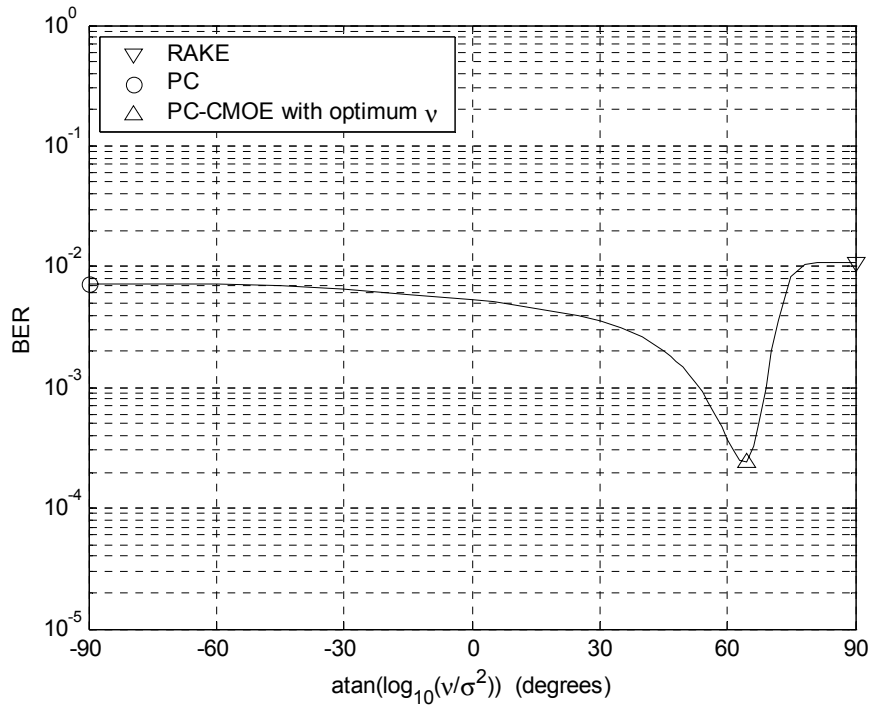


Fig. 11. BER of the PC-CMOE versus ν ($K = 10$, MAI = 0 dB, SNR = 26.76 dB).

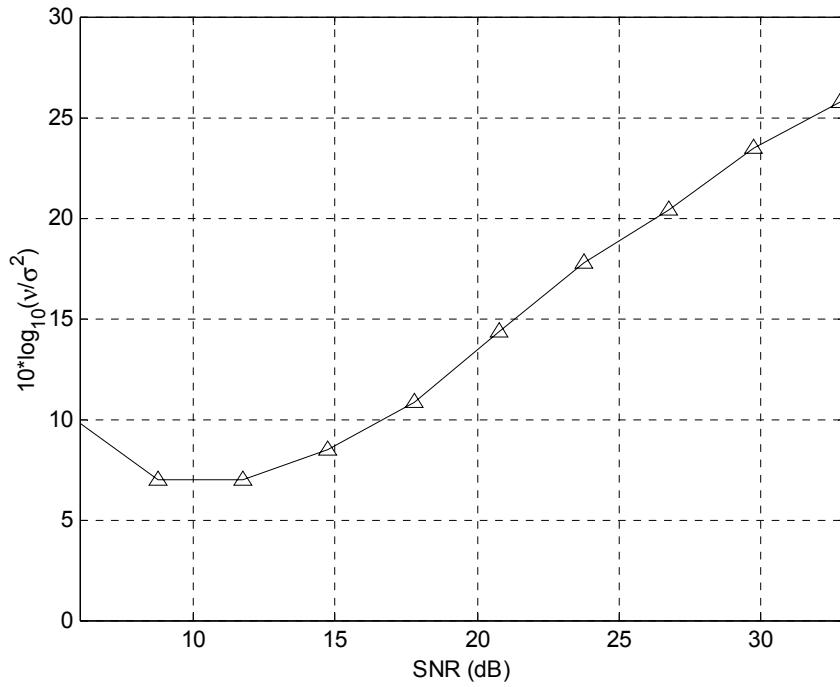


Fig. 12. Optimal value of ν as a function of the SNR ($K = 10$, MAI = 0 dB).

Fig. 12 shows the behavior of the optimum parameter ν as a function of the SNR. The linear dependence at high SNR is not surprising, because, for a fixed noise power σ^2 , an SNR increase corresponds to an increase of the signal subspace eigenvalues. Consequently, the correction should scale in a similar manner. On the contrary, when the SNR is low, the parameter ν has to compensate for the channel estimation errors too, and therefore the linear dependence is no longer satisfied.

2.4. REGULARIZED DETECTORS FOR DOWNLINK TRANSMISSIONS

As previously anticipated by the CMOE detector, regularization techniques [Hans] deal with ill-conditioned problems by substituting the matrix \mathbf{R} with a matrix characterized by a smaller eigenvalue spread. Consequently, the variance of the estimation errors decreases, at the cost of introducing some bias in the detector estimate. The goal of these techniques is to find a good trade-off between bias and variance, constructing the regularized matrix by judiciously modifying $\hat{\mathbf{R}}$. Among the eigenvalue spread reduction techniques, we can distinguish between full-rank regularization techniques, where the inverse covariance matrix \mathbf{R}^{-1} is approximated by a matrix with full rank MN , and reduced-rank approaches, where the inverse covariance matrix is approximated by a matrix with rank r lower than MN .

Most of the techniques proposed in the DS-CDMA literature fall in this second category. The main reason is that the projection of the received signal onto a lower-dimensional subspace speeds up the convergence of adaptive algorithms, because the number of parameters to be updated is smaller with respect to the full-rank case. However, since we are dealing with short data blocks, the application of adaptive algorithms seems inopportune, because the limited time may not be enough to guarantee the convergence of the algorithm. Therefore, when batch approaches are employed, also the full-rank regularization techniques should be considered, because a higher subspace dimension leads to an increased number of degrees of freedom, which can potentially be exploited to improve the

performance.

We want to point out that the distinction between full-rank and reduced-rank regularization methods is not always sharp. As an example, the CMOE detector, which exploits the full-rank Tikhonov regularization technique, is very similar to the PC-CMOE receiver, which is a rank- D approach. On the contrary, the performance of the PC-CMOE receiver is very different from that of the PC detector, which is a rank- D detector too.

In the following, we overview some low-rank techniques proposed for DS-CDMA systems. In Section 2.4.2, we discuss a novel full-rank method based on the covariance matrix tapering (CMT) technique.

2.4.1. Overview of Reduced-Rank Approaches

A first possibility to obtain a regularized detector consists in applying the EVD to \mathbf{R} and in neglecting the eigenvectors associated with the $MN-r$ smallest eigenvalues. Using this kind of regularization, usually referred as truncated singular value decomposition (TSVD) [Hans], the reduced-rank detector of the user k can be expressed as

$$\hat{\mathbf{w}}_{\text{TSVD},k} = \hat{\mathbf{U}}_r \hat{\mathbf{\Lambda}}_r^{-1} \hat{\mathbf{U}}_r^H \hat{\mathbf{h}}_k, \quad (41)$$

where \mathbf{U}_r contains only the r selected eigenvectors. If r is equal to D , the detector is constrained to lie in the signal subspace, and therefore it coincides with the PC detector (18). However, a choice $r < D$ could allow better performance in the presence of covariance estimation errors [Hans]. In this way, the eigenvalue spread is reduced from $\chi(\mathbf{R}) = \lambda_1(\mathbf{R})/\sigma^2$ to $\chi(\mathbf{U}_r \mathbf{\Lambda}_r \mathbf{U}_r^H) = \lambda_1(\mathbf{R})/\lambda_r(\mathbf{R})$, where $\lambda_r(\mathbf{R}) > \sigma^2$ is the r th largest eigenvalue of \mathbf{R} . A similar approach is proposed in [CGA], where, according to the cross spectral metric (CSM) [GoRe], the r eigenvectors are chosen in order to minimize the MSE.

A regularizing effect can also be obtained by constraining the detector to lie in the r -dimensional Krylov subspace $\mathbf{K}_r(\mathbf{R}, \mathbf{h}_k) = \text{span}\{\mathbf{h}_k, \mathbf{R}\mathbf{h}_k, \dots, \mathbf{R}^{r-1}\mathbf{h}_k\}$ [GoVa] associated with \mathbf{R} and \mathbf{h}_k , because the obtained detector can be considered as an approximation of the

TSVD detector [Hans]. The multistage Wiener filter (MSWF) [HoGo], which is the MMSE detector constrained to the Krylov subspace, is obtained by exploiting an orthonormal basis $\mathbf{V}_{r,k}$ of $\mathbf{K}_r(\mathbf{R}, \mathbf{h}_k)$, as expressed by

$$\hat{\mathbf{w}}_{\text{MSWF},k} = \hat{\mathbf{V}}_{r,k} (\hat{\mathbf{V}}_{r,k}^H \hat{\mathbf{R}} \hat{\mathbf{V}}_{r,k})^{-1} \hat{\mathbf{V}}_{r,k}^H \hat{\mathbf{h}}_k. \quad (42)$$

A related technique is the auxiliary-vector (AV) algorithm of [KQMB]. In this case, the detector is obtained as the linear combination of non-orthogonal vectors chosen within the subspace $\mathbf{K}_r(\mathbf{B}\mathbf{R}, \mathbf{h}_k)$, where $\mathbf{B} = \mathbf{I}_{MN} - \mathbf{h}_k \mathbf{h}_k^H / \|\mathbf{h}_k\|^2$.

A different reduced-rank method is the partial despreading (PD) approach proposed in [SiMi]. In this case, the detector can be expressed by

$$\hat{\mathbf{w}}_{\text{PD},k} = \hat{\mathbf{P}}_k (\hat{\mathbf{P}}_k^H \hat{\mathbf{R}} \hat{\mathbf{P}}_k)^{-1} \hat{\mathbf{P}}_k^H \hat{\mathbf{h}}_k, \quad (43)$$

where $\hat{\mathbf{P}}_k$ is an $MN \times r$ matrix whose r th column contains only the (MN/r) th subvector of $\hat{\mathbf{h}}_k$ (we have assumed that MN/r is an integer number). Indeed, the effect of $\hat{\mathbf{P}}_k$ is to despread the received signal only partially, applying a Wiener filter after the partial despreading. In this case, in general, we cannot conclude that the eigenvalue spread is reduced. Nevertheless, since the matrix to be inverted in (43) is $r \times r$, the PD approach is able to weaken the estimation errors, because the number P of snapshots, if compared to r , is higher than in the full-rank case, where P has to be compared to MN . Hence, the covariance matrix estimation errors are reduced before the inversion. However, the price paid for such an advantage is the lost of $MN - r$ degrees of freedom.

2.4.2. A Full-Rank Detector Using Covariance Matrix Tapering

In this section, we propose a new multiuser detector based on the CMT approach, which is also known as covariance matrix augmentation. The CMT technique has been originally proposed in [Mail][Zatm][Guer] for robust beamforming in order to widen the nulls of the antenna array pattern. The basic idea of CMT is to multiply the elements of \mathbf{R} with different weights, attenuating those elements far apart from the main diagonal. In mathematical terms, the CMT detector can be expressed as

$$\hat{\mathbf{w}}_{\text{CMT},k} = (\hat{\mathbf{R}} \circ \mathbf{T})^{-1} \hat{\mathbf{h}}_k, \quad (44)$$

where the symbol \circ represents the Hadamard (i.e., element-wise) product [HoJo1] between matrices, and \mathbf{T} is the tapering matrix (real, symmetric, and Toeplitz). In the following, we show that the CMT approach gives rise to an eigenvalue spread $\chi(\mathbf{R} \circ \mathbf{T})$ smaller than $\chi(\mathbf{R})$, thus enabling the bias-variance trade-off.

Theorem 1 (Schur product theorem): If \mathbf{R} and \mathbf{T} are $MN \times MN$ positive semidefinite (p.s.d.) matrices, then $\mathbf{R} \circ \mathbf{T}$ is p.s.d.. Moreover, if \mathbf{R} is positive definite (p.d.) and \mathbf{T} is p.s.d. with no zero entries on the main diagonal, then $\mathbf{R} \circ \mathbf{T}$ is p.d..

Proof: See [HoJo2].

Definition 1: An $MN \times MN$ matrix \mathbf{T} is a correlation matrix if \mathbf{T} is Hermitian p.s.d. with $\mathbf{I}_{MN} \circ \mathbf{T} = \mathbf{I}_{MN}$, i.e., with all ones on the main diagonal.

Theorem 2 (Eigenvalue spread theorem): If \mathbf{R} is an $MN \times MN$ p.d. matrix and \mathbf{T} is an $MN \times MN$ correlation matrix, then

$$\chi(\mathbf{R} \circ \mathbf{T}) \leq \chi(\mathbf{R}). \quad (45)$$

Proof: See Appendix A.

Theorem 2 proves that the CMT certainly is a full-rank regularization technique, but it does not guide us in the design of a suitable tapering matrix. In [Mail] and [Zatm], the tapering matrix is chosen as

$$[\mathbf{T}_{\text{sinc},\alpha}]_{m,n} = \text{sinc}(\alpha |m - n|), \quad (46)$$

where $\alpha > 0$ is the regularization parameter. Anyway, by Theorem 2, any correlation matrix can be selected. For instance, the Tikhonov regularization can be interpreted as a particular way to enhance the main diagonal of \mathbf{R} with respect to the other diagonals. However, since multipath channels introduce significant correlation between nearby chips, also the diagonals close to the main diagonal should be enhanced with respect to the faraway diagonals. Hence, a reasonable choice of \mathbf{T} should produce an attenuation that increases when moving away from the main diagonal. As a consequence, the elements of the tapering matrix should be chosen as

$$[\mathbf{T}]_{m,n} = f(|m-n|), \quad (47)$$

where $f(x)$ is a nonincreasing weighting function of x .

Moreover, it should be pointed out that the sinc-shaped profile of (46) seems to be inappropriate for both high and low values of α . Indeed, for high values of α , the sinc function in (46) has an oscillating behavior, and some weights are negative. On the other hand, for low values of α , the sinc function in (46) is concave. This implies that several diagonals close to the main diagonal are weighted with similar weights, while only few faraway diagonals are attenuated. This philosophy is just the opposite with respect to the one of the Tikhonov regularization.

As a result of the previous remarks, we propose a matrix \mathbf{T} whose function (47) has a second derivative equal to zero (i.e., the diagonals are weighted linearly), as expressed by

$$[\mathbf{T}_{\text{tri},\alpha}]_{m,n} = \text{clip}(1 - \alpha |m-n|), \quad (48)$$

where the clipping function $\text{clip}(x)$ forces the negative values of x to zero in order to guarantee that all the weights fall in the $[0,1]$ set. Furthermore, we also propose a matrix \mathbf{T} whose function (47) is convex, as expressed by

$$[\mathbf{T}_{\text{exp},\alpha}]_{m,n} = e^{-\alpha|m-n|}. \quad (49)$$

In all the cases, the parameter $\alpha > 0$ controls the amount of regularization. As it happens for the CMOE receiver, the CMT receiver is equivalent to the SMI receiver when the regularization parameter is set to zero, while it tends to the RAKE receiver for high values of the regularization parameter. Indeed, if $\alpha = 0$, the tapering matrices defined by (46), (48), and (49) become equal to $\mathbf{T} = \mathbf{1}_{MN \times MN}$, i.e., to the all-one matrix. In this case, no regularization is applied. On the contrary, for increasing α , the tapering matrices defined by (48) and (49) tend to the identity matrix \mathbf{I}_{MN} . In this case, only the elements of the main diagonal of $\hat{\mathbf{R}}$ are selected, and, since these elements are approximately equal, the CMT receiver in (44) is practically a scaled version of the RAKE receiver (35). When such an amount of regularization is applied, the eigenvalue spread $\chi(\mathbf{R} \circ \mathbf{T})$ is roughly equal to 1, but the receiver has lost the interference mitigation capability of the MMSE receiver.

Of course, neither $\alpha = 0$ nor $\alpha \rightarrow +\infty$ is optimal in the short data record case. As it happens for the PC-CMOE receiver, the optimum value of the regularization parameter depends not only on the chosen tapering matrix, but also on the scenario. Obviously, when P increases, the optimum value of α should decrease. Different algorithms for the automatic choice of α can be derived by exploiting the methods employed for other regularization techniques [Hans][KQMB]. These algorithms are still under investigation, and therefore they are not considered in the present thesis.

2.4.3. Simulation Results

In this section, we present some simulation results in order to compare the performance of the different regularized detectors. We consider a downlink situation (MAI = 0 dB) with a base station that transmits data to K active users. Gold sequences of length $N = 31$ have been chosen for the short spreading codes $\{c_k[j]\}$. The amplitudes of the $Q_k = 15$ chip-spaced channel paths are modeled as independent zero-mean complex Gaussian random variables with variance $E\{|\beta_{q,k}|^2\} = 1/Q_k$. Since the channel memory in symbol intervals is $L = 1$, the size of the receiving window has been fixed to $M = 2$ symbol intervals, and therefore the dimension of \mathbf{R} is equal to $MN = 62$.

In the first scenario, we consider $K = 10$ users with equal powers $A_k = A$ and data blocks of length $P = 6MN = 372$. The SNR is defined as $\text{SNR} = A^2 / \sigma^2$. We also assume $\hat{\mathbf{h}}_k = \mathbf{h}_k$. Although the perfect channel knowledge is realistic only in AWGN channels (where \mathbf{h}_k represents the user code), we want to focus on the effects of the covariance matrix estimation errors. Fig. 13 shows the BER of the CMT detector (44) with exponential law (49) as a function of the regularization parameter α . It is evident that there exists an optimum value of $\alpha \approx 0.05$ that minimizes the BER. This optimum value seems to be approximately constant over the SNR. Moreover, it is noteworthy that the CMT detector BER is smaller than the SMI detector BER (obtained by CMT with $\alpha = 0$) for all the values of α in the range $0 < \alpha \leq 0.4$. This fact implies that also a non-optimal choice of α allows improved performance with respect to the SMI.

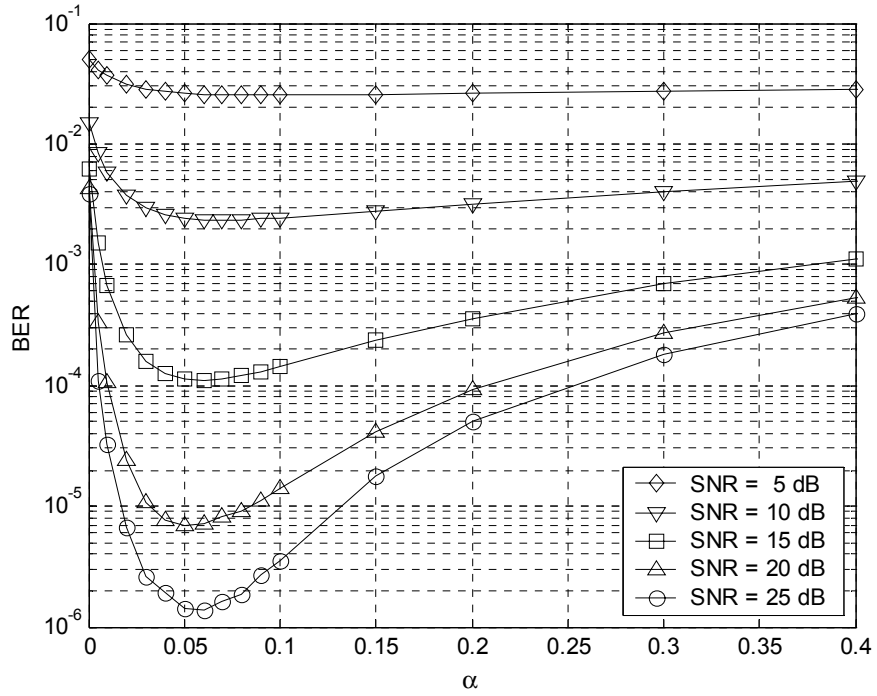


Fig. 13. BER of the CMT detector versus α (exponential profile (49), $K = 10$, $P = 372$).

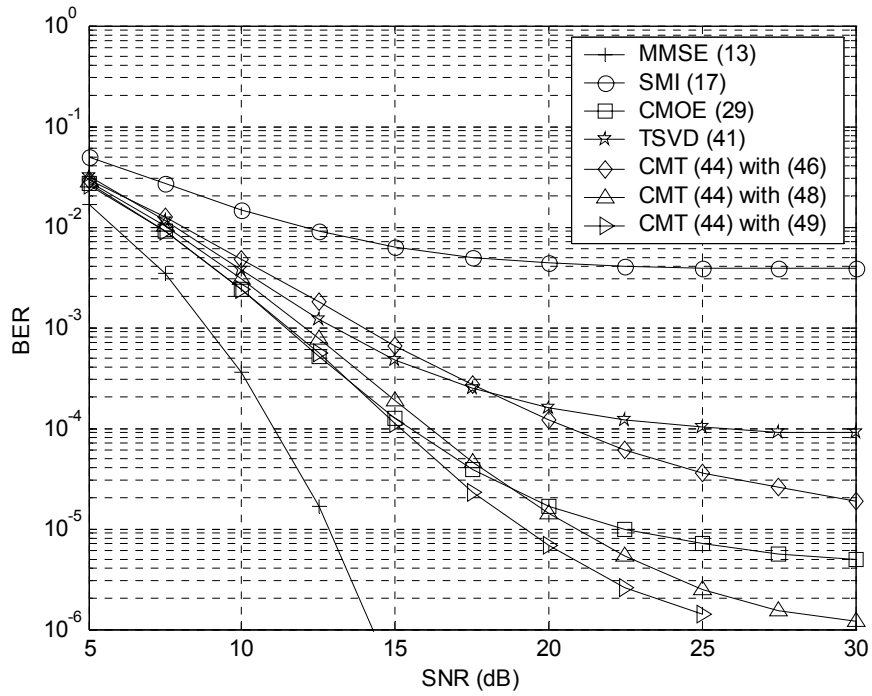


Fig. 14. BER of the regularized detectors (ideal channel, $K = 10$, $P = 372$).

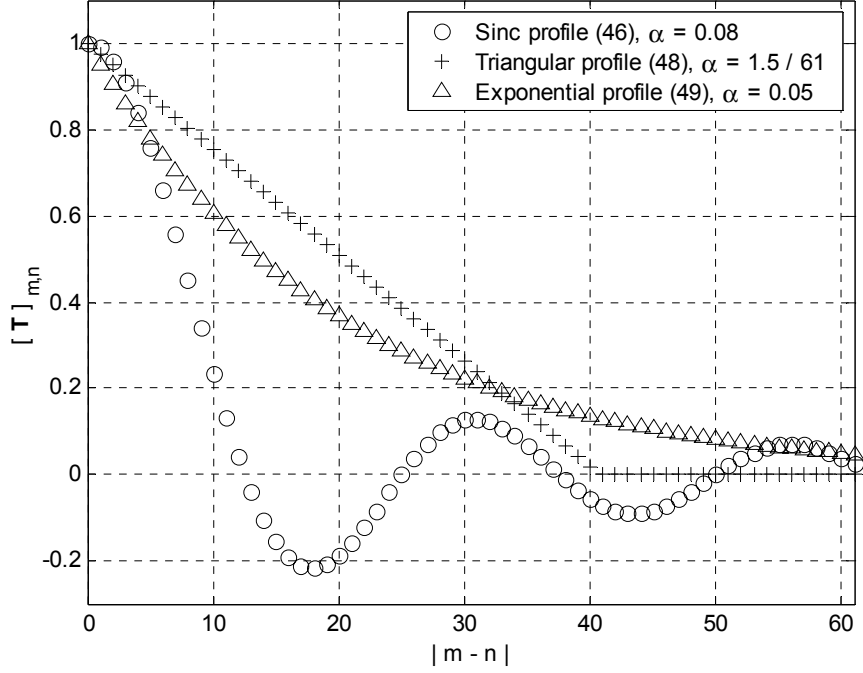


Fig. 15. Optimum profiles of the CMT detectors (ideal channel, $K = 10$, $P = 372$).

Fig. 14 compares the BER of the regularized detectors expressed by (29), (41), and (44). In order to have a fair comparison, we have chosen the regularization parameter that gives the best performance for each detector. Such an optimal regularization parameter is $\nu = 0.01 \text{tr}(\hat{\mathbf{R}})$ for the CMOE receiver (29), $r = D - 6 = 24$ for the TSVD receiver (41), and $\alpha = 0.08$, $\alpha = 1.5/61$, and $\alpha = 0.05$, for the CMT detectors with sinc, triangular, and exponential profile, respectively. It can be observed that the two proposed CMT detectors outperform the CMT detector with the sinc profile (46). Among all the estimated detectors, the CMT with exponential profile (49) gives the best performance when $\text{SNR} > 15$ dB, producing the same BER of the CMOE detector at lower SNR. As a side result, although not shown in the figure, the TSVD detector with optimum rank $r = 24$ outperforms the PC detector, which is equivalent to the TSVD detector with suboptimum rank $D = 30$.

Fig. 15 shows the tapering profiles (46), (48), and (49) for the best α for each CMT detector. It should be noted that all the three optimum profiles highly attenuate the elements

of $\hat{\mathbf{R}}$ that are very far from the main diagonal (i.e., when $|m-n| \geq 45$). Indeed, since the multipath channel does not span a whole symbol interval, the last rows of $\underline{H}[L]$ in (11) are equal to the all-zero matrix, and hence the exact \mathbf{R} contains a zero matrix block in the north-east (and in the south-west) corner.

In the second scenario, we consider $K=5$ equal power users and data blocks of length $P=8MN=496$. In this case, the signature waveform vector is simply estimated using a training sequence [MHM] of length $B=2.5MN=155$. Fig. 16 shows the BER performance of each optimum regularized detector. The optimum regularization parameter is $\nu=0.02 \text{tr}(\hat{\mathbf{R}})$ for the CMOE receiver (29), $r=D-2=13$ for the TSVD receiver (41), and $\alpha=0.1$ for the CMT detector (44) with exponential profile (49). We omitted the CMT detector with triangular profile (48), whose BER for $\alpha=6/61$ is the same of the exponential CMT, and the CMT with sinc profile (46), which performs slightly worse. In this scenario, none of the detectors outperforms the others for all SNRs. At low SNR (SNR < 15 dB) the TSVD detector gives the best performance, while at medium SNR the CMOE detector outperforms the other ones. At high SNR (SNR > 24 dB) the CMT detector slightly outperforms the CMOE detector, but the BER improvement is smaller with respect to the first scenario. This fact is due to the poor channel estimate provided by the DA algorithm of [MHM]. Therefore, in order to achieve high performance, the CMT detector has to be used together with a better channel estimation technique, such as the subspace-based one. Indeed, by applying the method in [WaPo] using small values of P , at high SNR, the covariance matrix estimation errors only are significant, while the signature waveform estimation errors are negligible.

In the third scenario, we assume that the channel is estimated by the subspace-based blind technique. The other parameters are the same of the first scenario, i.e., $K=10$ and $P=6MN=372$. Fig. 17 compares the BER of the different CMT detectors. In this case, due to the accurate channel estimation, the optimum regularization parameters of the CMT detectors are the same than in the first scenario. It can be observed that the two proposed CMT detectors outperform the one with the sinc profile (46) employed for beamforming.

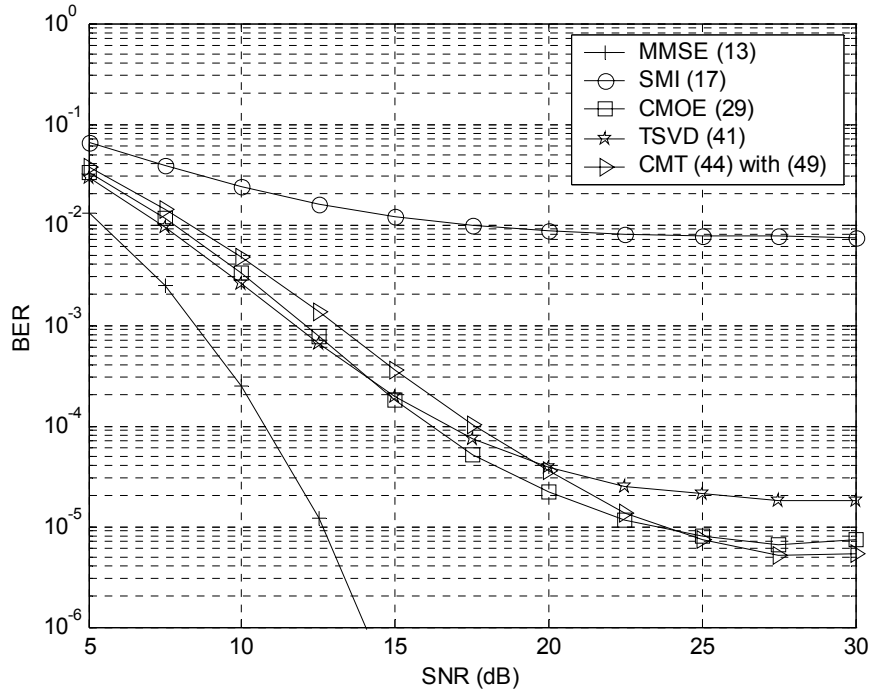


Fig. 16. BER of the regularized detectors (DA channel estimation, $K = 5$, $P = 496$).

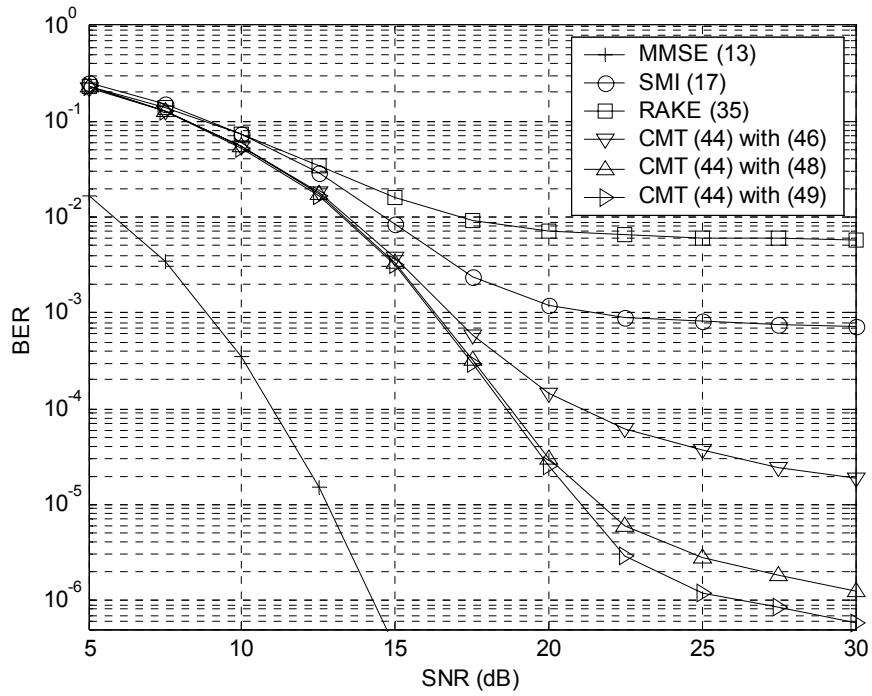


Fig. 17. BER of the regularized detectors (blind channel estimation, $K = 10$, $P = 372$).

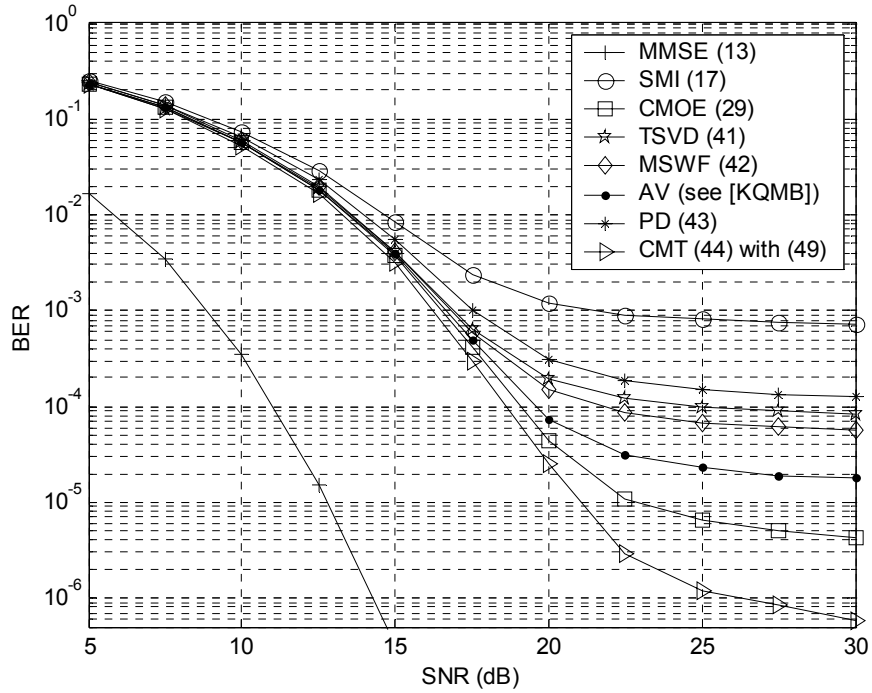


Fig. 18. BER of the regularized detectors (blind channel estimation, $K = 10$, $P = 372$).

Moreover, Fig. 18 compares the BER of the different regularized detectors. The optimum parameter of the CMOE, and the TSVD detectors is the same than in the first scenario, while the optimum parameter for the MSWF, the AV, and the PD detectors is $r = 3$, $r = 3$, and $r = 31$, respectively. At high SNR, the CMT with exponential profile (49) gives the best performance among all the estimated detectors. In particular, the full-rank regularized detectors (CMT and CMOE) present a lower BER with respect to the reduced-rank detectors, maybe because of the higher number of degrees of freedom offered by the MN -dimensional subspace. At low SNR, no significant BER differences are recorded.

3. NONLINEAR AMPLIFIER DISTORTIONS IN DS-CDMA SYSTEMS

A well-known feature of the DS-CDMA technique is its small sensitivity to nonlinear distortions with respect to multicarrier systems. Indeed, when phase-shift keying (PSK) modulations are used, the single-user DS-CDMA signal is characterized by an almost constant envelope, and therefore the transmitting high-power amplifier (HPA) can work efficiently, i.e., close to the saturation, without introducing significant distortions.

However, the constant envelope characteristic is missed when many independent DS-CDMA signals have to be transmitted, because the constructive and destructive superposition of these signals gives rise to an aggregate signal characterized by a high peak-to-average ratio (PAR). This effect is evident in the downlink scenario, where the base station has to serve all the active users of a specific cell. Indeed, in the downlink, due to the high variability of the input signal, the HPA may introduce significant nonlinear distortions, as it happens in multicarrier CDMA (MC-CDMA) systems [FaKa].

In the technical literature, few papers consider the presence of nonlinear distortions in DS-CDMA systems. The papers [LeMi] and [Lau] analyzed the PAR behavior and its reduction in downlink scenarios. In [CDT], a BER analysis of the matched filter (MF) receiver in AWGN channels is presented, considering BPSK and quaternary PSK (QPSK) modulations. In [GuMi], a mobile user is allowed to occupy multiple spreading codes, and the BER performance of the MF in AWGN is analyzed in the uplink. Also some methods to reduce the nonlinear distortions are examined.

Although the AWGN condition can be appropriate under some circumstances, e.g., in satellite channels with a strong line-of-sight (LOS) component, in many cases DS-CDMA systems have to face a frequency-selective fading channel due to the multipath delay spread.

This effect is especially emphasized in third generation cellular systems, which are characterized by a wide frequency band [PrOj]. Since frequency-selective channels destroy the user orthogonality, high performance improvements can be obtained making use of MUD techniques [Verd], because of their capability in reducing the MAI at the receiver side. However, the sensitivity of CDMA systems to nonlinear distortions is higher when the receiver employs MUD techniques rather than conventional matched filtering. Indeed, multiuser detectors tolerate a higher multiuser interference (i.e., more users) than the MF, leading to a HPA input signal with higher PAR. Therefore, if we want to exploit the high capacity of DS-CDMA systems by means of multiuser detectors, the performance degradation introduced by the nonlinear HPA should be carefully taken into account. Unfortunately, most of the research dealing with the performance analysis of multiuser detectors neglects the presence of nonlinear amplifiers, as testified by [PoVe][JuLa][MHM][ZvBr] and by the references in [Verd].

In this chapter, we evaluate the symbol-error rate (SER) performance of linear multiuser detectors in downlink channels, taking into account the presence of a nonlinear HPA at the transmitter. We underscore that our aim is to outline the performance degradation induced by the HPA when multiuser detectors designed for linear scenarios are employed. More sophisticated detectors specially designed for nonlinear environments [ReZh][MeGe] are not considered herein. Firstly, we present a statistical characterization of the nonlinear distortions. Successively, we extend to the linear decorrelating detector (LDD) and to the MMSE detector some of the results obtained in [CDT] for the MF in AWGN channels. Moreover, the degradation induced by the nonlinear amplifier is analyzed in fading channels. For flat Rayleigh fading channels, a closed-form SER expression for the LDD is derived. For frequency-selective fading channels, a semi-analytic SER expression is obtained. We also evaluate the total degradation (TD), which is a parameter that allows to optimize the mean output power for a given HPA and a target SER. Simulation results, which validate the analytical approach, are presented for the RAKE receiver, the LDD, and the MMSE detector.

3.1. SYSTEM MODEL WITH NONLINEAR AMPLIFIERS

We consider the downlink of a DS-CDMA system. Since the base station attends all the users that are active in a given cell, the signal to be transmitted is expressed by

$$x(t) = \sum_{k=1}^K x_k(t), \quad (50)$$

where $x_k(t)$ represents the signal component relative to the k th user, and K is the number of active users. Each signal $x_k(t)$ can be expressed by

$$x_k(t) = A_k \sum_{i=-\infty}^{+\infty} b_k[i] s_k(t - iT_s), \quad (51)$$

where T_s is the symbol interval, A_k , $s_k(t)$, and $b_k[i]$ are the amplitude, the spreading waveform, and the i th symbol, respectively, of the user k . The spreading waveform is expressed by $s_k(t) = \sum_{j=0}^{N-1} c_k[j] \psi(t - jT_c)$, where N is the processing gain, $T_c = T_s / N$ is the chip duration, $\psi(t)$ is the chip pulse shaping waveform with unit energy, and $c_k[j]$ is the j th value of the k th user spreading code, with $|c_k[j]| = 1/\sqrt{N}$. It is assumed that the data symbols $\{b_k[i]\}$ belong to a set of independent and equiprobable random variables, drawn from the QPSK set $\{\pm\sqrt{2}/2 \pm j\sqrt{-2}/2\}$.

If the transmitting HPA is supposed to be instantaneous, it can be modeled by its amplitude modulation to amplitude modulation (AM/AM) and amplitude modulation to phase modulation (AM/PM) distortion curves $G(\cdot)$ and $\Phi(\cdot)$, respectively [KGE], or equivalently by a complex nonlinear distorting function $F(\cdot) = G(\cdot)\exp[j\Phi(\cdot)]$. Hence, the signal $x(t)$ in (50) is transformed by the HPA into

$$w(t) = F(|x(t)|) e^{j\arg(x(t))}, \quad (52)$$

which represents the baseband-equivalent input-output relationship for the nonlinear amplifier. As motivated in the next section, the HPA output signal in (52) can be alternatively expressed as

$$w(t) = \alpha_0 x(t) + n_d(t), \quad (53)$$

where α_0 represents the average linear amplification gain, and $n_d(t)$ is the nonlinear distortion (NLD) noise.

We assume that the signal $w(t)$, which is transmitted by the base station, passes through a slowly varying multipath channel, characterized by an impulse response

$$g(\tau) = \sum_{q=1}^Q \beta_q e^{j\theta_q} \delta(\tau - \tau_q), \quad (54)$$

where Q is the number of paths of the channel, β_q , θ_q , and τ_q are the gain, the phase-shift, and the propagation delay, respectively, of the q th path, and $\delta(\cdot)$ is the Dirac delta function.

By exploiting (53), the signal $r(t)$ at the input of the receiver can be expressed by

$$r(t) = \int_{-\infty}^{+\infty} g(\tau)w(t-\tau)d\tau + n(t) = r_{\text{SOI}}(t) + r_{\text{NLD}}(t) + n(t), \quad (55)$$

where the function $r_{\text{SOI}}(t) = \sum_{q=1}^Q \beta_q |\alpha_0| e^{j\theta_q + j\arg(\alpha_0)} x(t - \tau_q)$ contains the signal of interest (SOI), $r_{\text{NLD}}(t) = \sum_{q=1}^Q \beta_q e^{j\theta_q} n_d(t - \tau_q)$ denotes the NLD noise, and $n(t)$ stands for the thermal noise.

At the receiver side, assuming perfect synchronization and channel state information, $r(t)$ is filtered by a chip-matched filter, and then sampled at the chip rate, thus obtaining

$$r_n[l] = \int_{-\infty}^{+\infty} r(t)\psi^*(t - lT - nT_c)dt = r_{\text{SOI},n}[l] + r_{\text{NLD},n}[l] + r_{\text{AWGN},n}[l], \quad (56)$$

where

$$r_{\text{SOI},n}[l] = \int_{-\infty}^{+\infty} r_{\text{SOI}}(t)\psi^*(t - lT - nT_c)dt, \quad (57)$$

$$r_{\text{NLD},n}[l] = \int_{-\infty}^{+\infty} r_{\text{NLD}}(t)\psi^*(t - lT - nT_c)dt, \quad (58)$$

$$r_{\text{AWGN},n}[l] = \int_{-\infty}^{+\infty} n(t)\psi^*(t - lT - nT_c)dt. \quad (59)$$

The received chip $r_n[l]$, expressed by (56), is characterized by three additive parts: $r_{\text{SOI},n}[l]$ is the useful component related to $x(t)$, $r_{\text{NLD},n}[l]$ is the in-band NLD noise introduced by the quantity $n_d(t)$, and $r_{\text{AWGN},n}[l]$ is the in-band thermal noise, with power expressed by

$$\sigma_{\text{AWGN}}^2 = E\{|r_{\text{AWGN},n}[l]|^2\}.$$

Assuming that the maximum delay spread of the channel is smaller than the symbol interval, the channel spreads the information related to a particular symbol over two symbol intervals, and consequently a receiver window of $2N$ consecutive chips contains all the energy related to the symbol of interest. Hence, we consider a receiving window of two symbol intervals. However, the extension to longer windows is straightforward.

The discrete-time equivalent impulse response of the channel is expressed by

$$g[l] = \left[\int_{-\infty}^{+\infty} g(\tau) R_{\psi\psi}(t-\tau) d\tau \right]_{t=lT_c}, \quad (60)$$

where $R_{\psi\psi}(\tau)$ is the autocorrelation function of the pulse waveform $\psi(t)$. Defining the channel order as $L = \lceil \max\{\tau_Q\}/T_c \rceil$, it holds true that $g[l] = 0$ when $l > L$ and when $l < 0$.

Moreover, we define the column vectors expressed by $\mathbf{c}_k = [c_k[0] \cdots c_k[N-1]]^T$, $\mathbf{b}[l] = [b_1[l] \cdots b_K[l]]^T$, $\mathbf{r}[l] = [r_0[l] \cdots r_{N-1}[l]]^T$, $\mathbf{r}_{\text{AWGN}}[l] = [r_{\text{AWGN},0}[l] \cdots r_{\text{AWGN},N-1}[l]]^T$, $\mathbf{r}_{\text{NLD}}[l] = [r_{\text{NLD},0}[l] \cdots r_{\text{NLD},N-1}[l]]^T$, $\mathbf{r}[l] = [\mathbf{r}[l]^T \mathbf{r}[l+1]^T]^T$, $\mathbf{r}_{\text{NLD}}[l] = [\mathbf{r}_{\text{NLD}}[l]^T \mathbf{r}_{\text{NLD}}[l+1]^T]^T$, $\mathbf{r}_{\text{AWGN}}[l] = [\mathbf{r}_{\text{AWGN}}[l]^T \mathbf{r}_{\text{AWGN}}[l+1]^T]^T$, and $\mathbf{b}[l] = [\mathbf{b}[l-1]^T \mathbf{b}[l]^T \mathbf{b}[l+1]^T]^T$, and the matrices $\mathbf{C} = [\mathbf{c}_1 \cdots \mathbf{c}_K]$, $\tilde{\mathbf{C}} = [\mathbf{C}]_{N-L+1:N,:}$, $\mathbf{A} = \text{diag}(A_1, \dots, A_K)$, $\underline{\mathbf{A}} = \mathbf{I}_3 \otimes \mathbf{A}$,

$$\underline{\mathbf{G}} = \begin{bmatrix} g[L] & \cdots & g[0] & 0 & \cdots & 0 \\ 0 & \ddots & \ddots & \ddots & \ddots & \vdots \\ \vdots & \ddots & \ddots & \ddots & \ddots & 0 \\ 0 & \cdots & 0 & g[L] & \cdots & g[0] \end{bmatrix}_{2N \times 2N+L}, \quad (61)$$

and

$$\underline{\mathbf{C}} = \begin{bmatrix} \tilde{\mathbf{C}} & \mathbf{0}_{L \times K} & \mathbf{0}_{L \times K} \\ \mathbf{0}_{N \times K} & \mathbf{C} & \mathbf{0}_{N \times K} \\ \mathbf{0}_{N \times K} & \mathbf{0}_{N \times K} & \mathbf{C} \end{bmatrix}_{2N+L \times 3K}, \quad (62)$$

thus obtaining the received vector $\underline{\mathbf{r}}[l]$, which is expressed by

$$\underline{\mathbf{r}}[l] = |\alpha_0| e^{j\arg(\alpha_0)} \underline{\mathbf{G}} \underline{\mathbf{C}} \underline{\mathbf{A}} \mathbf{b}[l] + \mathbf{r}_{\text{NLD}}[l] + \mathbf{r}_{\text{AWGN}}[l]. \quad (63)$$

For any linear detector, the decision variable is obtained by a linear combination of the

elements of the received vector $\mathbf{r}[l]$ in (63). Focusing on the user k , and assuming QPSK modulation, the estimate $\hat{b}_k[l]$ of the transmitted symbol $b_k[l]$ is expressed by

$$\hat{b}_k[l] = 2^{-1/2} \text{csgn}(\mathbf{d}_k \mathbf{r}[l]), \quad (64)$$

where the $2N$ -row vector \mathbf{d}_k represents a linear receiver chosen according to the detection criterion, e.g., MF, zero-forcing (ZF), or MMSE. The extension of such a model to other constellations or longer delay spreads is straightforward.

3.2. CHARACTERIZATION OF THE NONLINEAR DISTORTIONS

The signal $x(t)$, as summarized by (50), is the sum of those signals belonging to the K active users. If all the amplitudes A_k are nearly equal with one another, and K is sufficiently high (e.g., $K > 20$), then $x(t)$ can be approximated by a Gaussian random process [CDT] because of the central limit theorem (CLT) [Papo]. The Gaussian distribution of $x(t)$ holds true even if the number K of active users is high enough to group the users in subgroups, with each subgroup satisfying the above hypotheses. In practice, since K is always upper bounded, $x(t)$ is not always truly Gaussian and the following approximation has to be checked. However, the hypothesis of a DS-CDMA system with many active users seems to be realistic when multiuser detectors at the receiver side counteract the introduced MAI. Moreover, for multicode transmissions, it is possible to interpret K as the number of physical channels belonging to \tilde{K} users, with $\tilde{K} < K$.

The signal $x(t)$ in (50) is a zero-mean random process, because the signals $\{x_k(t)\}_{k=1}^K$ are uncorrelated and zero-mean random processes as well. By the previous considerations, the HPA input $x(t)$ can be modeled as a zero-mean Gaussian random process, and consequently, using the complex extension of the Busgang theorem [Papo][CDT][DTV], the HPA output is characterized by two mutually uncorrelated components $\alpha(t)x(t)$ and $n_d(t)$, as expressed by

$$w(t) = \alpha(t)x(t) + n_d(t), \quad (65)$$

$$E\{x^*(t)n_d(t+\tau)\} = 0, \quad \forall t, \forall \tau. \quad (66)$$

The linear gain $\alpha(t)$, for Gaussian inputs $x(t)$, is expressed by

$$\alpha(t) = \frac{E\{w(t)x^*(t+\tau)\}}{E\{x(t)x^*(t+\tau)\}} = \frac{E\{w(t)x^*(t)\}}{E\{|x(t)|^2\}}, \quad (67)$$

and it depends only on $E\{|x(t)|^2\}$ and on the amplifier nonlinearity $F(\cdot)$ [Rowe]. As an example, for the ideally predistorted amplifier (IPA) with stationary Gaussian inputs, the linear gain $\alpha(t)$ is expressed by [BaCa]

$$\alpha(t) = 1 - e^{-\text{IBO}} + \sqrt{\pi \text{IBO}} Q(\sqrt{2 \text{IBO}}), \quad (68)$$

where the input back-off (IBO), defined as

$$\text{IBO} = \frac{P_{\text{SAT},x}}{E\{|x(t)|^2\}}, \quad (69)$$

is the ratio between the saturating power $P_{\text{SAT},x}$ and the average power $E\{|x(t)|^2\}$ of the HPA input. Equivalently, the linear gain can be expressed as a function of the output back-off (OBO), which is the ratio between the saturating power $P_{\text{SAT},w}$ and the average power $E\{|w(t)|^2\}$ of the HPA output, as expressed by

$$\text{OBO} = \frac{P_{\text{SAT},w}}{E\{|w(t)|^2\}}, \quad (70)$$

by exploiting the relation between IBO and OBO. For the IPA, such a relation is [BaCa]

$$\text{OBO} = \frac{\text{IBO}}{1 - e^{-\text{IBO}}}. \quad (71)$$

If the HPA input $x(t)$ is stationary, then the linear gain is time-invariant, i.e., $\alpha(t) = \alpha_0$, because both the numerator and the denominator in (67) are independent of the time index t . In such a situation, the relation between the autocorrelation $R_{ww}(\tau)$ of the HPA output signal $w(t)$ and the autocorrelation $R_{xx}(\tau)$ of the HPA input signal $x(t)$ is expressed by

[DaRo]

$$R_{ww}(\tau) = \sum_{i=0}^{+\infty} \gamma_i R_{xx}(\tau)^{2i+1}, \quad (72)$$

where the coefficients γ_i , which depend on the nonlinear function $F(\cdot)$ and on the input power $E\{|x(t)|^2\}$, or equivalently on the IBO or the OBO, can be calculated by numerical integration or by means of closed form expressions [DaRo][BaCa]. Using (53) and exploiting (66), it is easy to split the output autocorrelation $R_{ww}(\tau)$ in (72) as the sum of the useful part $|\alpha_0|^2 R_{xx}(\tau)$ and of the nonlinear noise part $R_{n_d n_d}(\tau)$, as expressed by

$$R_{ww}(\tau) = |\alpha_0|^2 R_{xx}(\tau) + R_{n_d n_d}(\tau), \quad (73)$$

where

$$R_{n_d n_d}(\tau) = \sum_{i=1}^{+\infty} \gamma_i R_{xx}(\tau)^{2i+1}. \quad (74)$$

However, in the downlink of a DS-CDMA system, the signal $x(t)$ is not stationary. In our scenario, $x(t)$ is cyclostationary with a period equal to the duration T_s of the short spreading codes. By defining the time varying crosscorrelation function [Papo] of two random processes $u(t)$ and $v(t)$ as $R_{uv}(t, t+\tau) = E\{u^*(t)v(t+\tau)\}$, a relation similar to (73) can be derived from (65) and (66), which is

$$R_{ww}(t, t+\tau) = \alpha^*(t)\alpha(t+\tau)R_{xx}(t, t+\tau) + R_{n_d n_d}(t, t+\tau). \quad (75)$$

It should be observed that, if $E\{|x(t)|^2\}$ is almost constant with time, the linear gain $\alpha(t)$ in (67) is characterized by a small time variability, which yields $\alpha(t) \approx \alpha(t+\tau) \approx \alpha_0$. This property is realistic in many circumstances, e.g., when the pulse shaping waveform is rectangular, or when it is a raised cosine function with a small roll-off factor [CDT]. Assuming that such kind of pulse shaper is used, the time dependence of the linear gain $\alpha(t)$ can be neglected, thereby motivating the use of α_0 in (53).

It is noteworthy that the cyclostationarity of the input $x(t)$ holds true in the strict sense, since $x(t)$ is regarded as Gaussian. The output $w(t)$ is also cyclostationary (in the strict

sense) with the same period T_s , because the amplifier is modeled as memoryless. By defining the time-averaged crosscorrelation function [Proa] of two cyclostationary processes $u(t)$ and $v(t)$ as $\bar{R}_{uv}(\tau) = \frac{1}{T_s} \int_0^{T_s} R_{uv}(t, t+\tau) dt$, the hypothesis of the slow time variability of $\alpha(t) \approx \alpha_0$ allows us to express (75) as

$$\bar{R}_{ww}(\tau) = |\alpha_0|^2 \bar{R}_{xx}(\tau) + \bar{R}_{n_d n_d}(\tau). \quad (76)$$

Equivalently, (76) can be interpreted as the output autocorrelation function of the stationary random process $\tilde{w}(t) = w(t + \Theta)$, where the random variable Θ is uniformly distributed between 0 and T_s . As a consequence, $\bar{R}_{ww}(\tau)$ can be expressed as a power series expansion of $\bar{R}_{xx}(\tau)$ as in (72), with the same coefficients γ_i . Analogously, $\bar{R}_{n_d n_d}(\tau)$ in (76) can be evaluated by replacing in (74) the quantity $R_{xx}(\tau)$ with $\bar{R}_{xx}(\tau)$, thus obtaining

$$\bar{R}_{n_d n_d}(\tau) = \sum_{i=1}^{+\infty} \gamma_i \bar{R}_{xx}(\tau)^{2i+1}. \quad (77)$$

The knowledge of the quantities $|\alpha_0|^2$ and $\bar{R}_{n_d n_d}(\tau)$, which summarize the linear gain and the NLD noise, respectively, allows a complete characterization of both the effects produced by the nonlinear amplification.

3.3. PERFORMANCE OF LINEAR MULTIUSER DETECTORS

3.3.1. SER Performance in AWGN Channels

In AWGN channels, since $L = 0$, the channel matrix $\underline{\mathbf{G}}$ in (61) becomes $\underline{\mathbf{G}} = g_0 \mathbf{I}_{2N}$, where $g_0 = g[0]$, and hence a receiving window of one symbol interval (i.e., of N samples) is wide enough to recover the symbol of interest. In this situation, (63) simply reduces to

$$\mathbf{r}[l] = \mathbf{r}_{\text{SOI}}[l] + \mathbf{r}_{\text{NLD}}[l] + \mathbf{r}_{\text{AWGN}}[l], \quad (78)$$

where $\mathbf{r}_{\text{SOI}}[l] = |\alpha_0 g_0| e^{j\varphi_0} \mathbf{C} \mathbf{A} \mathbf{b}[l]$, and $\varphi_0 = \arg(\alpha_0 g_0)$ is the phase-shift due to both the channel and the HPA. Therefore the receiver of the k th user can be expressed by an N -row

vector

$$\mathbf{d}_k = e^{-j\varphi_0} [\mathbf{D}]_{k,:}, \quad (79)$$

where \mathbf{D} is the $K \times N$ matrix that contains the detectors of all the users. For the MF receiver, the detector acts like a simple despreading device. Therefore \mathbf{D} becomes

$$\mathbf{D}_{\text{MF}} = \mathbf{C}^H, \quad (80)$$

and the SER performance can be obtained in closed form by modeling the MAI and the NLD noise as Gaussian random variables. These approximations are reasonably justified by the high number K of active users and by the high processing gain $N \geq K$ [CDT], as detailed in the following for the NLD noise. In fact, the NLD noise at the decision variable is obtained as the linear combination of the N elements of $\mathbf{r}_{\text{NLD}}[l]$, by the N elements of \mathbf{d}_k . Therefore, if N is high enough, the NLD noise can be approximated as a zero-mean Gaussian variable because of the CLT. The accuracy of this approximation depends on the processing gain N , and on the used spreading code matrix \mathbf{C} that affects the values of the weighting vector \mathbf{d}_k . Indeed, if few elements of \mathbf{d}_k have amplitudes higher than the others, only these dominant elements will contribute to the NLD noise at the decision variable, and hence the Gaussian approximation will tend to fail. On the contrary, if many elements of \mathbf{d}_k have a high modulus, the corresponding elements of $\mathbf{r}_{\text{NLD}}[l]$ are weighted with coefficients having almost-equal values, and consequently the approximation will be very good.

Moreover, also the HPA working point has a significant impact on the Gaussian assumption of the NLD noise. Indeed, when the IBO is very high, most of the elements of $\mathbf{r}_{\text{NLD}}[l]$ are close to zero, at least for class A amplifiers. Consequently, for high values of the IBO, the NLD noise at the decision variable is practically obtained by the linear combination of few significant elements, thus violating the CLT hypothesis.

As a consequence of the Gaussian approximations, the SER $P_{\text{AWGN},k}$ of the user k can be expressed by

$$P_{\text{AWGN},k} = 2Q \left(\sqrt{\frac{\sigma_{\text{SOI},k}^2}{\sigma_{\text{MAI},k}^2 + \sigma_{\text{NLD},k}^2 + \sigma_{\text{AWGN},k}^2}} \right) - Q^2 \left(\sqrt{\frac{\sigma_{\text{SOI},k}^2}{\sigma_{\text{MAI},k}^2 + \sigma_{\text{NLD},k}^2 + \sigma_{\text{AWGN},k}^2}} \right), \quad (81)$$

where

$$\sigma_{\text{SOI},k}^2 = |\alpha_0 g_0|^2 A_k^2, \quad (82)$$

$$\sigma_{\text{MAI},k}^2 = |\alpha_0 g_0|^2 \sum_{\substack{j=1 \\ j \neq k}}^K |[\mathbf{P}]_{k,j}|^2 A_j^2, \quad (83)$$

$$\sigma_{\text{AWGN},k}^2 = \sigma_{\text{AWGN}}^2, \quad (84)$$

and $\mathbf{P} = \mathbf{C}^H \mathbf{C}$ is the matrix that contains the crosscorrelation coefficients of the spreading codes. In [CDT], the theoretical evaluation of the NLD noise power $\sigma_{\text{NLD},k}^2$ has been carried out supposing a rectangular chip waveform $\psi(t)$, leading to

$$\sigma_{\text{NLD},k}^2 = |g_0|^2 \bar{R}_{\text{ww}}(0) - |\alpha_0 g_0|^2 \bar{R}_{\text{xx}}(0). \quad (85)$$

Anyway, this assumption is not always realistic in bandlimited channels. By assuming a more realistic bandlimited chip waveform $\psi(t)$, the NLD noise power can be evaluated as

$$\sigma_{\text{NLD},k}^2 = |g_0|^2 [\mathbf{C}^H \mathbf{\Psi} \mathbf{C}]_{k,k}, \quad (86)$$

where the $N \times N$ matrix $\mathbf{\Psi}$ is expressed by $[\mathbf{\Psi}]_{m,n} = [\bar{R}_{n_d n_d}(\tau) * R_{\psi\psi}(\tau)]_{\tau=(n-m)T_c}$, with $\bar{R}_{n_d n_d}(\tau)$ computed using (77).

Assuming that the code matrix \mathbf{C} is full rank, by using the LDD (also known as ZF detector), expressed by

$$\mathbf{D}_{\text{LDD}} = \mathbf{C}^\dagger, \quad (87)$$

the MAI is completely eliminated [Verd]. The SER can be expressed as in (81), with

$$\sigma_{\text{SOI},k}^2 = |\alpha_0 g_0|^2 A_k^2, \quad (88)$$

$$\sigma_{\text{MAI},k}^2 = 0, \quad (89)$$

$$\sigma_{\text{NLD},k}^2 = |g_0|^2 [\mathbf{C}^\dagger \boldsymbol{\Psi} \mathbf{C}^{\dagger H}]_{k,k}, \quad (90)$$

$$\sigma_{\text{AWGN},k}^2 = \varepsilon_k \sigma_{\text{AWGN}}^2, \quad (91)$$

where the quantity $\varepsilon_k = [\mathbf{P}^{-1}]_{k,k} \geq 1$ is the thermal noise amplification factor due to the decorrelating operation. Also in this case the NLD noise at the decision variable can be considered Gaussian because of the high processing gain N .

Moreover, if the spreading sequences are characterized by good autocorrelation properties, as it is usual in DS-CDMA systems, the elements $\{[\boldsymbol{\Psi}]_{m,n}\}$ with $m \neq n$ are very small with respect to the elements on the main diagonal $\{[\boldsymbol{\Psi}]_{m,m}\}$. Therefore, since the matrix $\boldsymbol{\Psi}$ is nearly diagonal, it can be well approximated by $\sigma_{\text{NLD}}^2 \mathbf{I}_N$, where

$$\sigma_{\text{NLD}}^2 = [\boldsymbol{\Psi}]_{m,m} = [\bar{R}_{n_d n_d}(\tau) * \bar{R}_{\psi\psi}(\tau)]_{\tau=0} \quad (92)$$

is the NLD noise at the detector input. In this case, the NLD noise power on the decision variable reduces to

$$\sigma_{\text{NLD},k}^2 = \varepsilon_k \sigma_{\text{NLD}}^2. \quad (93)$$

A scaled version of the MMSE receiver can be expressed by

$$\mathbf{D}_{\text{MMSE}} = \mathbf{M}, \quad (94)$$

where [Kay]

$$\mathbf{M} = (\mathbf{I}_K + |\alpha_0 g_0|^2 \mathbf{A} \mathbf{C}^H \mathbf{W}^{-1} \mathbf{C} \mathbf{A})^{-1} \mathbf{A} \mathbf{C}^H \mathbf{W}^{-1} \quad (95)$$

$$= \mathbf{A} \mathbf{C}^H (|\alpha_0 g_0|^2 \mathbf{C} \mathbf{A}^2 \mathbf{C}^H + \mathbf{W})^{-1} \quad (96)$$

and $\mathbf{W} = |g_0|^2 \boldsymbol{\Psi} + \sigma_{\text{AWGN}}^2 \mathbf{I}_N$ is the covariance matrix of the total colored noise term $\mathbf{r}_{\text{NLD}}[l] + \mathbf{r}_{\text{AWGN}}[l]$. As far as the SER of the MMSE detector is concerned, we propose to model the NLD noise as Gaussian. Moreover, as shown in [PoVe], even the residual MAI at the MMSE output is well approximated by a Gaussian random variable. Therefore, the SER can be expressed by (81) as well, where

$$\sigma_{\text{SOL},k}^2 = |\alpha_0 g_0|^2 A_k^2 |[\mathbf{M} \mathbf{C}]_{k,k}|^2, \quad (97)$$

$$\sigma_{\text{MAI},k}^2 = |\alpha_0 g_0|^2 \sum_{\substack{j=1 \\ j \neq k}}^K |[\mathbf{MC}]_{k,j}|^2 A_j^2, \quad (98)$$

$$\sigma_{\text{NLD},k}^2 = |g_0|^2 [\mathbf{M}\Psi\mathbf{M}^H]_{k,k}, \quad (99)$$

$$\sigma_{\text{AWGN},k}^2 = [\mathbf{M}\mathbf{M}^H]_{k,k} \sigma_{\text{AWGN}}^2. \quad (100)$$

Also in this case, for spreading codes with good correlation properties, (99) can be well approximated by

$$\sigma_{\text{NLD},k}^2 = [\mathbf{M}\mathbf{M}^H]_{k,k} \sigma_{\text{NLD}}^2. \quad (101)$$

3.3.2. SER Performance in Flat-Fading Channels

In this section, we assume that the channel has a single resolvable path, characterized by a Rayleigh statistic. Consequently, we assume that the FIR channel (60) degenerates to a single-path channel, with $L=0$ and $g[0]=g_0$, and that the absolute value of g_0 is characterized by a Rayleigh probability density function (PDF) with $E\{|g_0|^2\}=1$, as expressed by

$$p(|g_0|) = 2|g_0|e^{-|g_0|^2}. \quad (102)$$

Since $\sigma_{\text{SOI},k}^2$, $\sigma_{\text{MAI},k}^2$, and $\sigma_{\text{NLD},k}^2$ depends on $|g_0|$, the SER can be obtained by averaging (81) over the PDF of the channel gain $|g_0|$. This operation can be done in different ways. The easiest way consists in generating many realizations of the channel gain $|g_0|$, in calculating $\sigma_{\text{SOI},k}^2$, $\sigma_{\text{MAI},k}^2$, $\sigma_{\text{NLD},k}^2$, and $\sigma_{\text{AWGN},k}^2$ for each realization of $|g_0|$, and in averaging Equation (81) semi-analytically. However, in many cases, such a semi-analytical procedure can be avoided, and the average of (81) over the statistic of $|g_0|$ can be done in closed form. As an example, we consider the LDD performance. In this case, by taking into account (88)-(91) and (93), the signal-to-interference plus noise (SINR) at the decision variable can be expressed by

$$\text{SINR} = \frac{\sigma_{\text{SOI},k}^2}{\sigma_{\text{MAI},k}^2 + \sigma_{\text{NLD},k}^2 + \sigma_{\text{AWGN},k}^2} = \frac{|g_0|^2 |\alpha_0|^2 A_k^2}{|g_0|^2 \varepsilon_k \sigma_{\text{NLD}}^2 + \varepsilon_k \sigma_{\text{AWGN}}^2}. \quad (103)$$

The SER is then obtained by neglecting the term that depends on the square of the Q-function as

$$P_{\text{FLAT},k} \approx \int_0^{+\infty} 4 |g_0| e^{-|g_0|^2} Q \left(\sqrt{\frac{|g_0|^2 \mu_k^2}{|g_0|^2 \nu^2 + 1}} \right) d |g_0|, \quad (104)$$

where

$$\mu_k^2 = \frac{|\alpha_0|^2 A_k^2}{\varepsilon_k \sigma_{\text{AWGN}}^2}, \quad (105)$$

$$\nu^2 = \frac{\sigma_{\text{NLD}}^2}{\sigma_{\text{AWGN}}^2}. \quad (106)$$

The analytical computation of the integral in (104) has been derived in Appendix B. The final result, which is not included in [SiAl], can be expressed as a series of generalized hypergeometric functions ${}_2F_0(\cdot, \cdot; \cdot; \cdot)$ [GrRy][AbSt], as expressed by

$$P_{\text{FLAT},k} \approx 1 - \frac{\sqrt{2}}{2} \mu_k e^{-\frac{\mu_k^2}{2\nu^2}} \sum_{m=0}^{+\infty} \frac{1}{m!} \left(\frac{\mu_k^2}{2\nu^2} \right)^m {}_2F_0 \left(m + \frac{3}{2}, \frac{1}{2}; \cdot; -\nu^2 \right). \quad (107)$$

It can be observed that the series expansion in (107) can be conveniently truncated without affecting its accuracy. Such a truncation criterion, which can be found in Appendix C, allows to obtain the range $[m_{\min}, m_{\max}]$ of the terms to be considered in the summation of (107).

It is important to underline that a similar computation can be performed for the RAKE receiver, as long as the MAI term can be associated with the NLD noise term. However, in this case, also the parameter in (106) depends on the user index k .

On the contrary, the result (107) is not valid for the MMSE receiver, because the matrix \mathbf{M} in (95) depends on $|g_0|$, and therefore $\sigma_{\text{SOI},k}^2$, $\sigma_{\text{MAI},k}^2$, and $\sigma_{\text{NLD},k}^2$, are not proportional to $|g_0|^2$. As a consequence, the error probability cannot be expressed as in (104). However,

the computation can be applied to a modified version of the MMSE receiver, in order to obtain an upper bound on the SER performance of the MMSE receiver. Such a detector, which can be called approximated MMSE (AMMSE) receiver, is obtained by replacing in (95) the instantaneous fading gain $|g_0|^2$ with its mean value $E\{|g_0|^2\}=1$, thereby obtaining

$$\tilde{\mathbf{M}} = (\mathbf{I}_K + |\alpha_0|^2 \mathbf{A}\mathbf{C}^H \mathbf{W}^{-1} \mathbf{C}\mathbf{A})^{-1} \mathbf{A}\mathbf{C}^H \mathbf{W}^{-1}. \quad (108)$$

3.3.3. SER Performance in Frequency-Selective Fading Channels

For frequency-selective channels, the detector $\underline{\mathbf{d}}_k$, expressed by

$$\underline{\mathbf{d}}_k = e^{-j\arg(\alpha_0)} [\underline{\mathbf{D}}]_{K+k,:}, \quad (109)$$

has to consider not only the MAI but it has also to combine the resolvable paths. The received vector expression in (63) suggests to treat the multipath situation, summarized by $\underline{\mathbf{G}}$, like the AWGN scenario in (78), with a modified code matrix expressed by

$$\underline{\mathbf{H}} = \underline{\mathbf{G}}\underline{\mathbf{C}}. \quad (110)$$

As a consequence, as in (80), (87), and (94), for frequency-selective channels we can define the RAKE receiver, the LDD and the MMSE detector, respectively, as

$$\underline{\mathbf{D}}_{\text{RAKE}} = \underline{\mathbf{H}}^H, \quad (111)$$

$$\underline{\mathbf{D}}_{\text{LDD}} = \underline{\mathbf{H}}^\dagger, \quad (112)$$

$$\underline{\mathbf{D}}_{\text{MMSE}} = \underline{\mathbf{M}}, \quad (113)$$

where

$$\underline{\mathbf{M}} = (\mathbf{I}_{3K} + |\alpha_0|^2 \underline{\mathbf{A}}\underline{\mathbf{H}}^H \underline{\mathbf{W}}^{-1} \underline{\mathbf{H}}\underline{\mathbf{A}})^{-1} \underline{\mathbf{A}}\underline{\mathbf{H}}^H \underline{\mathbf{W}}^{-1} \quad (114)$$

$$= \underline{\mathbf{A}}\underline{\mathbf{H}}^H (|\alpha_0|^2 \underline{\mathbf{H}}\underline{\mathbf{A}}^2 \underline{\mathbf{H}}^H + \underline{\mathbf{W}})^{-1} \quad (115)$$

and $\underline{\mathbf{W}} = \underline{\mathbf{G}}\underline{\mathbf{\Psi}}\underline{\mathbf{G}}^H + \sigma_{\text{AWGN}}^2 \mathbf{I}_{2N}$, with $\underline{\mathbf{\Psi}}$ equivalent to the square matrix $\mathbf{\Psi}$, but with higher

dimension $2N + L$.

By applying the detector $\underline{\mathbf{D}}$ to the received signal $\underline{\mathbf{r}}[l]$ in (63), we obtain

$$\underline{\mathbf{y}}[l] = e^{-j\arg(\alpha_0)} \underline{\mathbf{D}} \underline{\mathbf{r}}[l] = \underline{\mathbf{s}}_k[l] + \underline{\mathbf{m}}_k[l] + \underline{\mathbf{n}}[l] + \underline{\mathbf{a}}[l] \quad (116)$$

where

$$\underline{\mathbf{s}}_k[l] = |\alpha_0| \underline{\mathbf{D}} \underline{\mathbf{H}}_{\text{SOI},k} \underline{\mathbf{A}} \underline{\mathbf{b}}[l] \quad (117)$$

contains the useful signal of the user k ,

$$\underline{\mathbf{m}}_k[l] = |\alpha_0| \underline{\mathbf{D}} \underline{\mathbf{H}}_{\text{MAI},k} \underline{\mathbf{A}} \underline{\mathbf{b}}[l] \quad (118)$$

represents the ISI-plus-MAI term,

$$\underline{\mathbf{n}}[l] = e^{-j\arg(\alpha_0)} \underline{\mathbf{D}} \underline{\mathbf{r}}_{\text{NLD}}[l] \quad (119)$$

stands for the NLD noise, and

$$\underline{\mathbf{a}}[l] = e^{-j\arg(\alpha_0)} \underline{\mathbf{D}} \underline{\mathbf{r}}_{\text{AWGN}}[l] \quad (120)$$

is due to the thermal AWGN. The matrices $\underline{\mathbf{H}}_{\text{SOI},k} = [\mathbf{0}_{2N \times K+k-1} \quad [\underline{\mathbf{H}}]_{:,K+k} \quad \mathbf{0}_{2N \times 2K-k}]$ and $\underline{\mathbf{H}}_{\text{MAI},k} = [[\underline{\mathbf{H}}]_{:,1:K+k-1} \quad \mathbf{0}_{2N \times 1} \quad [\underline{\mathbf{H}}]_{:,K+k+1:3K}]$ in (117) and (118) are obtained by partitioning the channel-code matrix $\underline{\mathbf{H}}$ in (110) as $\underline{\mathbf{H}} = \underline{\mathbf{H}}_{\text{SOI},k} + \underline{\mathbf{H}}_{\text{MAI},k}$.

As in the AWGN scenario, we suppose that both the MAI and the NLD noise can be approximated as Gaussian. As we will verify in the simulation section, these approximations work reasonably well in AWGN channels. Therefore a similar behavior is expected in multipath channels, because the received signal can be thought as the superposition of many replicas of AWGN-like contributions, and the sum of Gaussian random variables is still Gaussian. By (109), the decision variable $\underline{\mathbf{d}}_k \underline{\mathbf{r}}[l]$ in (64) is equal to the $(K+k)$ th element of the vector $\underline{\mathbf{y}}[l]$ in (116). Therefore, in order to evaluate the conditional SER given the channel realization $g(\tau)$, we need to calculate the power of the $(K+k)$ th element of the vectors in the right hand side of (116).

As far as the thermal noise is concerned, the elements of the vector $\underline{\mathbf{a}}[l]$ are jointly complex Gaussian random variables, because obtained as linear combination $\underline{\mathbf{D}}$ of the jointly

complex Gaussian random variables contained in $\underline{\mathbf{r}}_{\text{AWGN}}[l]$. The covariance matrix $\underline{\Phi}_{\text{AWGN}} = E\{\underline{\mathbf{a}}[l]\underline{\mathbf{a}}[l]^H\}$ is expressed by $\underline{\Phi}_{\text{AWGN}} = \sigma_{\text{AWGN}}^2 \underline{\mathbf{D}}\underline{\mathbf{D}}^H$, and hence the $(K+k)$ th element of the thermal noise vector $\underline{\mathbf{a}}[l]$ in (120) has power $\sigma_{\Delta,k}^2$ expressed by

$$\sigma_{\Delta,k}^2 = [\underline{\mathbf{D}}\underline{\mathbf{D}}^H]_{K+k,K+k} \sigma_{\text{AWGN}}^2. \quad (121)$$

For the NLD noise, we observe that the element $[\underline{\mathbf{n}}[l]]_{K+k}$ of the vector $\underline{\mathbf{n}}[l]$ is the sum of the $2N$ elements of $\underline{\mathbf{r}}_{\text{NLD}}[l]$, weighted by the $2N$ elements of $[\underline{\mathbf{D}}]_{K+k,:}$, and consequently, if the processing gain N is high enough, the NLD noise $[\underline{\mathbf{n}}[l]]_{K+k}$ can be well approximated as a Gaussian random variable. The accuracy of this approximation depends not only on the processing gain N , but also on the channel realization, which affects the values of the weighting vector $[\underline{\mathbf{D}}]_{K+k,:}$ by means of $\underline{\mathbf{H}}$. Indeed, for some channel realizations, few elements of $[\underline{\mathbf{D}}]_{K+k,:}$ are characterized by higher amplitudes with respect to the others, and consequently the CLT and the Gaussian approximation will tend to fail. On the contrary, for other channel realizations, many elements of $[\underline{\mathbf{D}}]_{K+k,:}$ have significant amplitude, and hence the approximation accuracy is very good, because many elements of the vector $\underline{\mathbf{n}}[l]$ are weighted with coefficients having almost-equal values. Moreover, in multipath scenarios, the IBO plays the same role than in AWGN channels.

As a consequence of the Gaussian approximation, the covariance matrix $\underline{\Phi}_{\text{NLD}}$ of the vector $\underline{\mathbf{n}}[l]$, expressed by $\underline{\Phi}_{\text{NLD}} = \underline{\mathbf{D}}\underline{\mathbf{G}}\underline{\Psi}\underline{\mathbf{G}}^H\underline{\mathbf{D}}^H$, completely characterizes the statistical properties of the NLD noise, and the power $\sigma_{\text{N},k}^2$ of the $(K+k)$ th element of the $\underline{\mathbf{n}}[l]$ in (116) is expressed by

$$\sigma_{\text{N},k}^2 = [\underline{\mathbf{D}}\underline{\mathbf{G}}\underline{\Psi}\underline{\mathbf{G}}^H\underline{\mathbf{D}}^H]_{K+k,K+k}. \quad (122)$$

As far as the ISI-plus-MAI term $\underline{\mathbf{m}}_k[l]$ in (116) is concerned, the good accuracy of the Gaussian approximation has been already tested in [JuLa] for the RAKE and MMSE receivers in linear scenarios. Since the covariance matrix $\underline{\Phi}_{\text{MAI}}$ of the column vector $\underline{\mathbf{m}}_k[l]$ is expressed by $\underline{\Phi}_{\text{MAI}} = |\alpha_0|^2 \underline{\mathbf{D}}\underline{\mathbf{H}}_{\text{MAI},k}\underline{\mathbf{A}}^2\underline{\mathbf{H}}_{\text{MAI},k}^H\underline{\mathbf{D}}^H$, the $(K+k)$ th element of the vector $\underline{\mathbf{m}}_k[l]$ in (116) is characterized by a power $\sigma_{\text{M},k}^2$ expressed by

$$\sigma_{\underline{\mathbf{M}},k}^2 = |\alpha_0|^2 [\underline{\mathbf{D}}\underline{\mathbf{H}}_{\underline{\mathbf{MAI}},k}\underline{\mathbf{A}}^2\underline{\mathbf{H}}_{\underline{\mathbf{MAI}},k}^H\underline{\mathbf{D}}^H]_{K+k,K+k}. \quad (123)$$

Finally, analogously to the MAI case, the power of the $(K+k)$ th element of the signal vector $\underline{\mathbf{s}}_k[l]$ in (116) can be obtained as

$$\sigma_{\underline{\mathbf{S}},k}^2 = |\alpha_0|^2 [\underline{\mathbf{D}}\underline{\mathbf{H}}_{\underline{\mathbf{SOI}},k}\underline{\mathbf{A}}^2\underline{\mathbf{H}}_{\underline{\mathbf{SOI}},k}^H\underline{\mathbf{D}}^H]_{K+k,K+k}. \quad (124)$$

Given the channel realization $g(\tau)$, the conditional symbol-error probability $P_k(g)$ is equal to

$$P_k(g) = 2Q\left(\sqrt{\frac{\sigma_{\underline{\mathbf{S}},k}^2}{\sigma_{\underline{\mathbf{M}},k}^2 + \sigma_{\underline{\mathbf{N}},k}^2 + \sigma_{\underline{\mathbf{A}},k}^2}}\right) - Q^2\left(\sqrt{\frac{\sigma_{\underline{\mathbf{S}},k}^2}{\sigma_{\underline{\mathbf{M}},k}^2 + \sigma_{\underline{\mathbf{N}},k}^2 + \sigma_{\underline{\mathbf{A}},k}^2}}\right), \quad (125)$$

where the quantities $\sigma_{\underline{\mathbf{S}},k}^2$, $\sigma_{\underline{\mathbf{M}},k}^2$, $\sigma_{\underline{\mathbf{N}},k}^2$ and $\sigma_{\underline{\mathbf{A}},k}^2$ are defined in (121)-(124). Like for the flat-fading case, the average SER can be obtained by averaging (125) over the joint PDF $p(\beta_1, \dots, \beta_Q, \theta_1, \dots, \theta_Q, \tau_1, \dots, \tau_Q)$ of the channel parameters $\beta_1, \dots, \beta_Q, \theta_1, \dots, \theta_Q, \tau_1, \dots, \tau_Q$ contained in $g(\tau)$, as expressed by

$$P_{\text{SEL},k} = \int P_k(g) p(\beta_1, \dots, \beta_Q, \theta_1, \dots, \theta_Q, \tau_1, \dots, \tau_Q) d\beta_1 \cdots d\beta_Q d\theta_1 \cdots d\theta_Q d\tau_1 \cdots d\tau_Q. \quad (126)$$

The solution of the multivariate integral (126) seems to be quite prohibitive, even for simple statistical channel characterizations (e.g., Rayleigh fading channels). Consequently, $P_{\text{SEL},k}$ can be estimated using a semi-analytical approach by

$$\hat{P}_{\text{SEL},k} = \frac{1}{N_{ch}} \sum_{i=1}^{N_{ch}} P_k(g^{(i)}(\tau)), \quad (127)$$

where the N_{ch} channel realizations $\{g^{(i)}(\tau)\}$ are generated according to the joint PDF $p(\beta_1, \dots, \beta_Q, \theta_1, \dots, \theta_Q, \tau_1, \dots, \tau_Q)$, and $P_k(g^{(i)}(\tau))$ is calculated as in (125).

It should be noted that our approach used to estimate (126) is quite similar to the one of [JuLa] for linear scenarios, and it is valid for frequency-selective channels with any statistical characterization. The main difference with [JuLa] is that, since we assume the spreading codes as fixed, the average over the spreading codes is not necessary.

3.3.4. Total Degradation

The TD to obtain a target SER, can be defined as [KGE][CDT]

$$[\text{TD}]_{\text{dB}} = [\Delta\text{SNR}]_{\text{dB}} + [\text{OBO}]_{\text{dB}}, \quad (128)$$

where

$$[\Delta\text{SNR}]_{\text{dB}} = [\text{SNR}_{\text{APP}}]_{\text{dB}} - [\text{SNR}_{\text{EFF}}]_{\text{dB}}, \quad (129)$$

$$\text{SNR}_{\text{APP}} = \frac{\sigma_{\text{SOI}}^2 + \sigma_{\text{NLD}}^2}{\sigma_{\text{AWGN}}^2}, \quad (130)$$

is the apparent SNR measured at the detector input, and

$$\text{SNR}_{\text{EFF}} = \frac{\sigma_{\text{SOI}}^2}{\sigma_{\text{NLD}}^2 + \sigma_{\text{AWGN}}^2} \quad (131)$$

is the effective SNR at the detector input, which coincides with the apparent SNR in the linear scenario, where $\alpha_0 = 1$ and $\sigma_{\text{NLD}}^2 = 0$. Consequently, in (128), ΔSNR represents the power penalty with respect to the linear scenario, whereas the OBO represents the power penalty with respect to the maximum output power of the HPA.

For a selected target SER, it is obviously desirable to have both low ΔSNR (i.e., low transmitted power) and low OBO (i.e., high HPA efficiency). These two requirements are clearly in competition with one another. Indeed, if the OBO is decreased, the HPA introduces a higher distortion and consequently the required ΔSNR , for the target SER, must be greater. As a consequence, the minimization of the TD, which balances both the requirements, is a fair criterion for the selection of the optimum OBO value, provided that other effects, e.g., the adjacent channel interference (ACI), can be neglected or eliminated by linear filtering. The ACI generated by the spectral regrowth at the HPA output can be estimated by Fourier transform of (76).

It can be pointed out that, in AWGN and in flat Rayleigh fading, the TD can be evaluated analytically. Indeed, for each OBO value, the SER formulas in Section 3.3.1 and Section 3.3.2 can be used to find the ΔSNR required at the detector input.

3.4. VALIDATION BY SIMULATION RESULTS

In this section, we present some simulation results in order to check the approximations introduced in the theoretical analysis. The scenario with a base station that transmits data to K users is considered. Unless otherwise stated, it is assumed that $K = 40$ users are active, and that the amplitudes $\{A_k\}$ are equal for all the K users. Real-valued Gold sequences [DiJa] of length $N = 63$ have been chosen for the short spreading codes $\{c_k[j]\}$. For the chip pulse shaping waveform $\psi(t)$, a square-root raised cosine with roll-off factor equal to $\rho = 0.22$ has been chosen. An oversampling factor equal to 10, with respect to the chip rate $1/T_c$, has been used, leading to a simulation sampling frequency approximately 8 times higher than the Nyquist rate. The (apparent) SNR is defined at the input of the detector as

$$\text{SNR} = \frac{E\{|r_n[l] - r_{\text{AWGN},n}[l]|^2\}}{E\{|r_{\text{AWGN},n}[l]|^2\}}. \quad (132)$$

The nonlinearities considered for the HPA model are the soft-limiter [KGE], which is the envelope input-output characteristic of an IPA, with AM/AM and AM/PM curves expressed by

$$G(|x|) = \begin{cases} |x| & , \quad |x| \leq A_{\text{SAT}} \\ A_{\text{SAT}} & , \quad |x| > A_{\text{SAT}} \end{cases} \quad \Phi(|x|) = 0, \quad (133)$$

where A_{SAT} is the maximum amplitude of the amplifier, and the Saleh HPA model [Sale], with AM/AM and AM/PM expressed by

$$G(|x|) = \frac{2|x|}{1+|x|^2} \quad \Phi(|x|) = \frac{\pi}{3} \frac{|x|^2}{1+|x|^2}. \quad (134)$$

We want to underline that, although only these two models are considered in this thesis, the theoretical analysis is valid for any solid state power amplifier (SSPA) or traveling-wave tube amplifier (TWTA) that can be modeled as memoryless by means of its AM/AM and AM/PM curves.

Fig. 19 illustrates the normalized power spectral density (PSD) of the HPA output signal,

versus the normalized frequency, when the Saleh model (134) is used. It is evident the very small mismatch between the PSD predicted by the theoretical approach, obtained by fast Fourier transform (FFT) of (76), and the estimated PSD, obtained by FFT of the estimated autocorrelation function of the HPA output signal.

Fig. 20 shows the SER of the LDD as a function of the SNR in AWGN channels, when an IPA is used. It is noteworthy the good agreement between the theoretical curves and the simulated points for all the OBO values. On the contrary, when the Saleh HPA model replaces the IPA (Fig. 21), there is a good agreement at high back-off (OBO \approx 4 dB), while at low OBO values (OBO = 1.72 dB) the simulated performance does not perfectly match with the theoretical one. Indeed, since the PDF of the NLD noise is not exactly Gaussian, the simulated SER slightly diverges from the theoretical one only when the NLD noise is dominant with respect to the AWGN, i.e., when the SNR is high and at the same time the OBO is not too high. However, the good agreement between simulated and theoretical performance at low SNR for any OBO values proves that the signal loss induced by the HPA is correctly modeled by the coefficient $|\alpha_0|$. Moreover, for very low OBO values, (i.e., OBO \approx 1 dB), the Gaussian approximation is accurate, despite of the increased NLD noise. Fig. 22 shows the SER performance of the MMSE receiver in AWGN channels when the soft-limiter model (133) is used for the HPA. Similar considerations holds true.

It is also of interest to check the differences between analytical and simulated performance when the operating conditions are not exactly the ones assumed in the theoretical model. Specifically, we checked the model accuracy in three different conditions:

- The powers $\{A_k^2\}$ of the users' signals are not exactly equal;
- The number K of active users is not high enough to assume a Gaussian PDF for the HPA input;
- The processing gain N is not high enough to assume a Gaussian PDF for the NLD noise at the output of the detector.

Particularly, we focused on the two extreme scenarios with high and very low OBO values. To begin with the first case, we consider the situation with AWGN and IPA, even though

analogous considerations hold true for other channels or amplifiers. In the first scenario, we assume that the power of the $K = 40$ users' signals varies in a linear manner, in such a way that the last user has double power with respect to the first user, which is the user of interest. In this case, the simulated performance exactly matches the analytical model when the OBO is high or very low, as shown in Fig. 23. In the second scenario, we assume that 20 out of 40 users, including the one of interest, have double power with respect to the others. In this case, at low OBO values, Fig. 24 presents a little mismatch in the saturating point of the SER curve, as in Fig. 21.

Moreover, Fig. 25 shows that the analysis is still accurate when the number of active (equal power) users is reduced to $K = 20$. However, when the base station attends a smaller number of users, e.g., $K = 10$ users, the HPA input is no more Gaussian. Therefore, when $\text{SER} < 10^{-4}$, the analytical results are pessimistic if compared with the simulated ones, as shown in Fig. 26. In Fig. 27, we assume that $N = 31$ and that $K = 20$ users are active. The simulation results exhibit good agreement with the analytical model also in such a scenario.

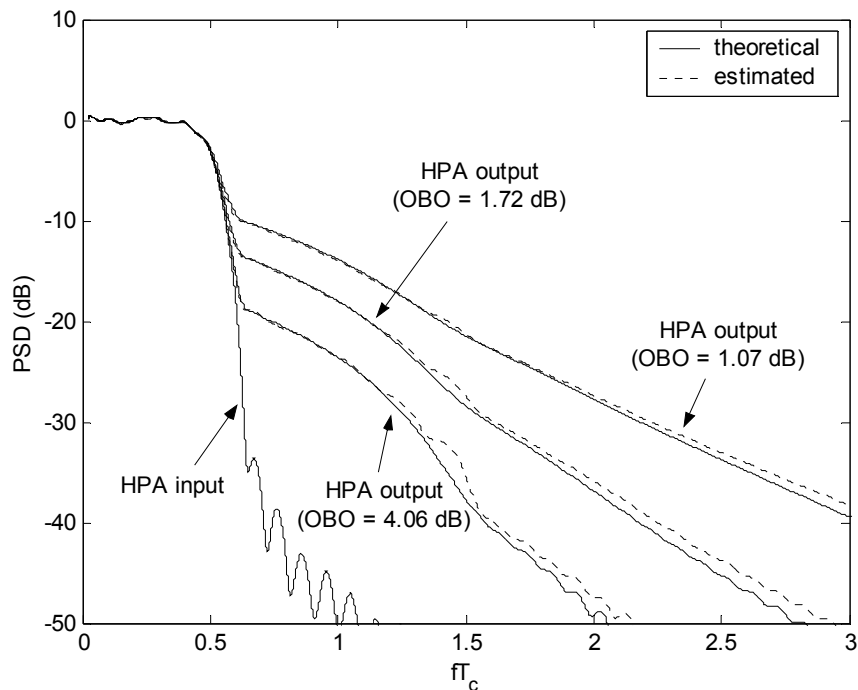


Fig. 19. PSD of the signal at the HPA output (Saleh model, $K = 40$, $N = 63$).

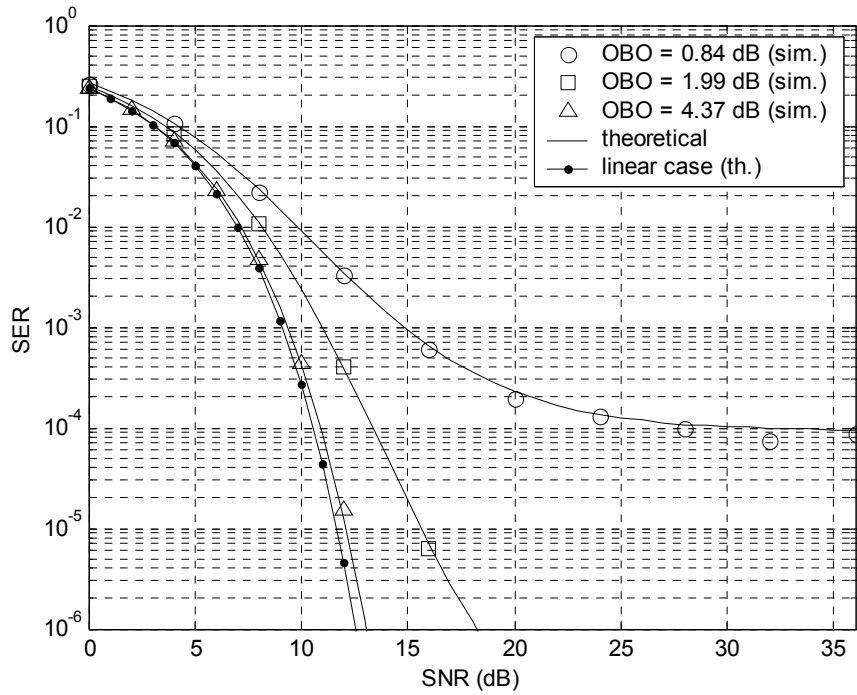


Fig. 20. SER of the LDD in AWGN channels (IPA model, $K = 40$, $N = 63$).

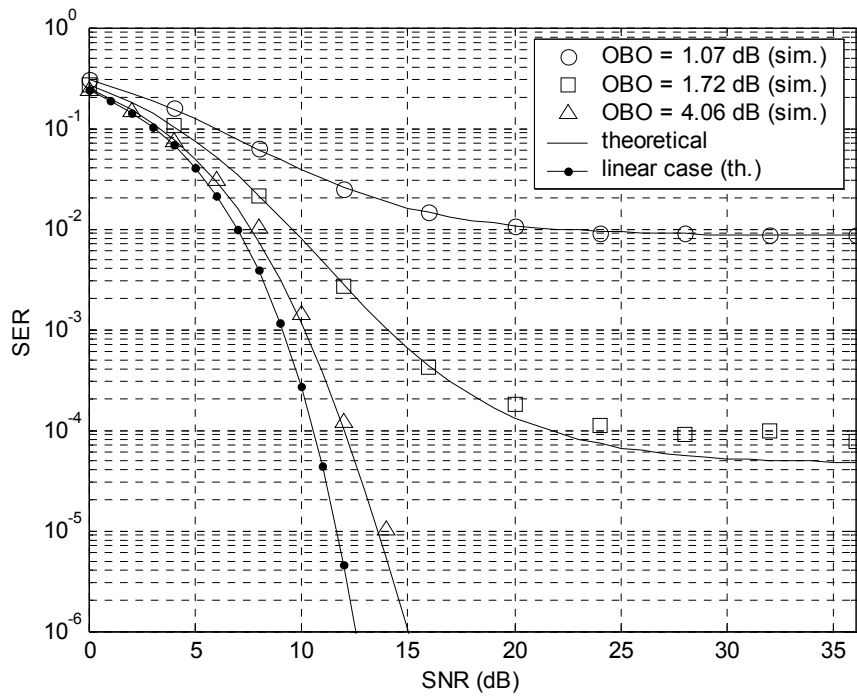


Fig. 21. SER of the LDD in AWGN channels (Saleh model, $K = 40$, $N = 63$).

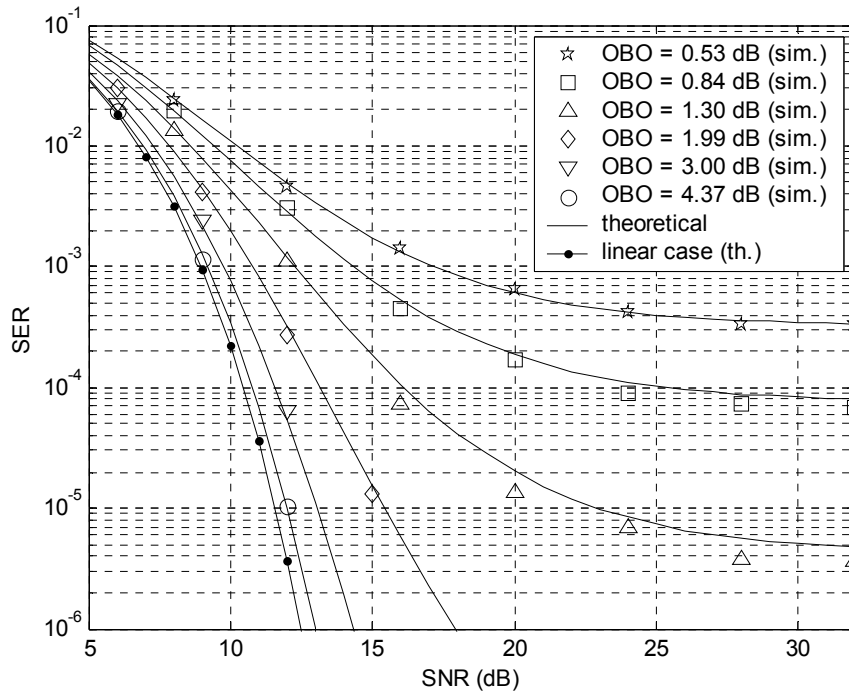


Fig. 22. SER of the MMSE in AWGN channels (IPA model, $K = 40$, $N = 63$).

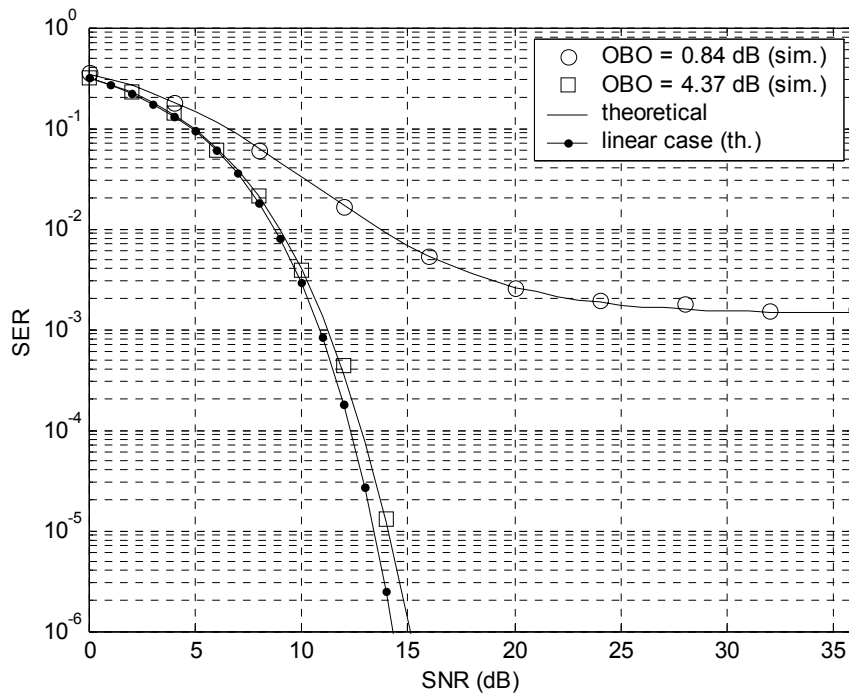


Fig. 23. SER of the LDD in AWGN (Signals with unequal powers, first scenario).

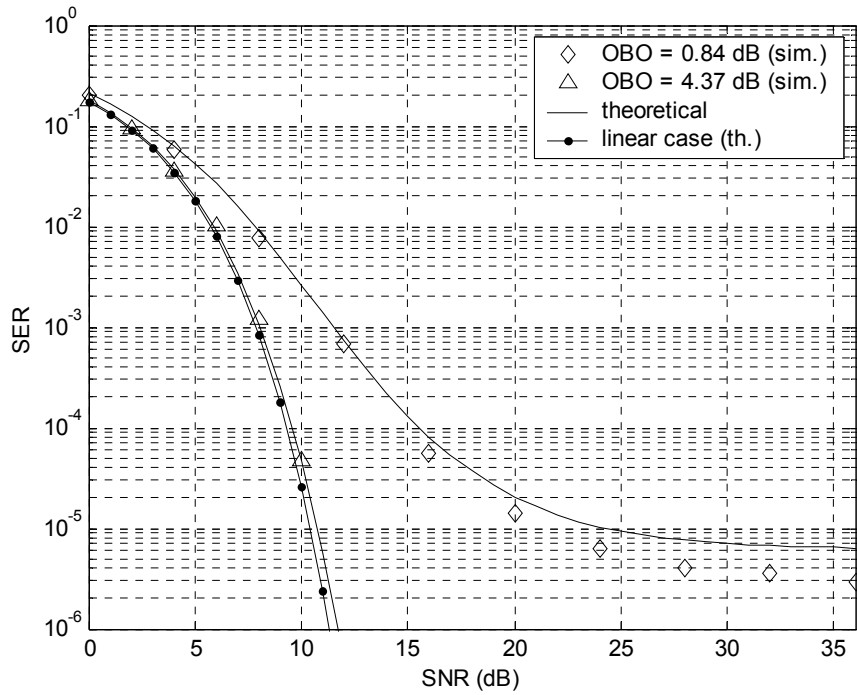


Fig. 24. SER of the LDD in AWGN (Signals with unequal powers, second scenario).

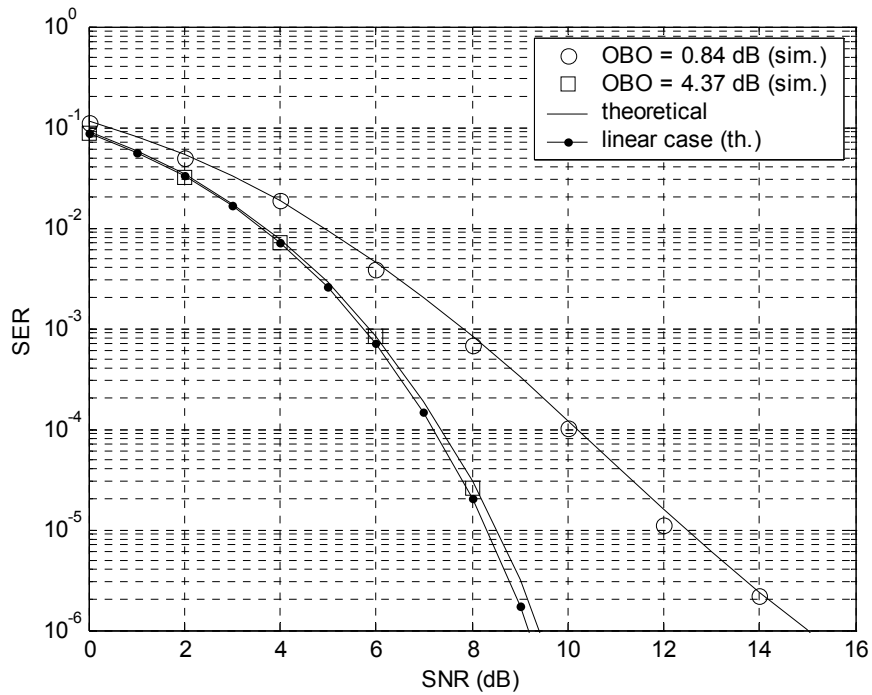


Fig. 25. SER of the LDD in AWGN channels (IPA model, $K = 20$, $N = 63$).

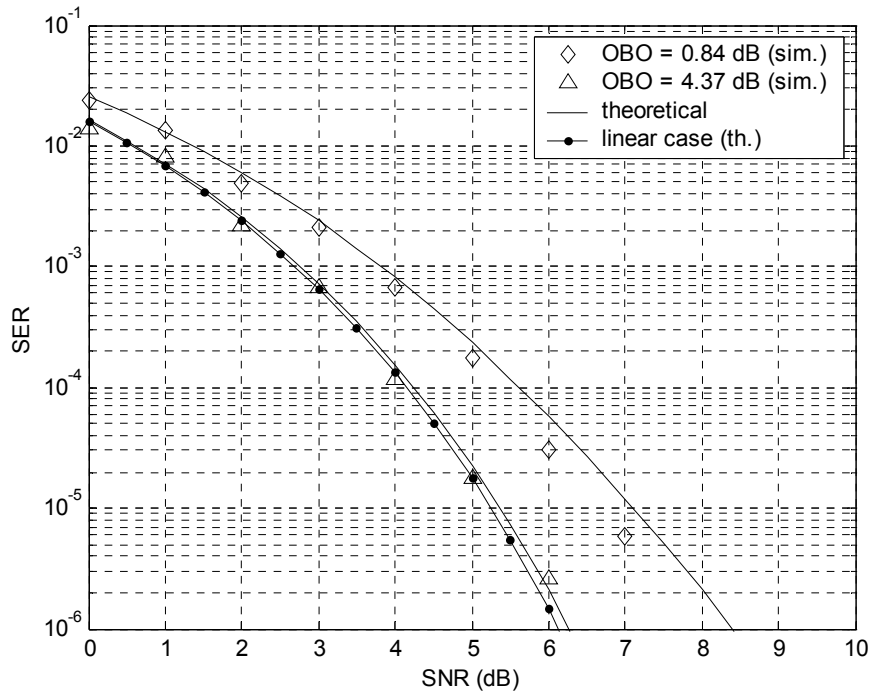


Fig. 26. SER of the LDD in AWGN channels (IPA model, $K = 10$, $N = 63$).

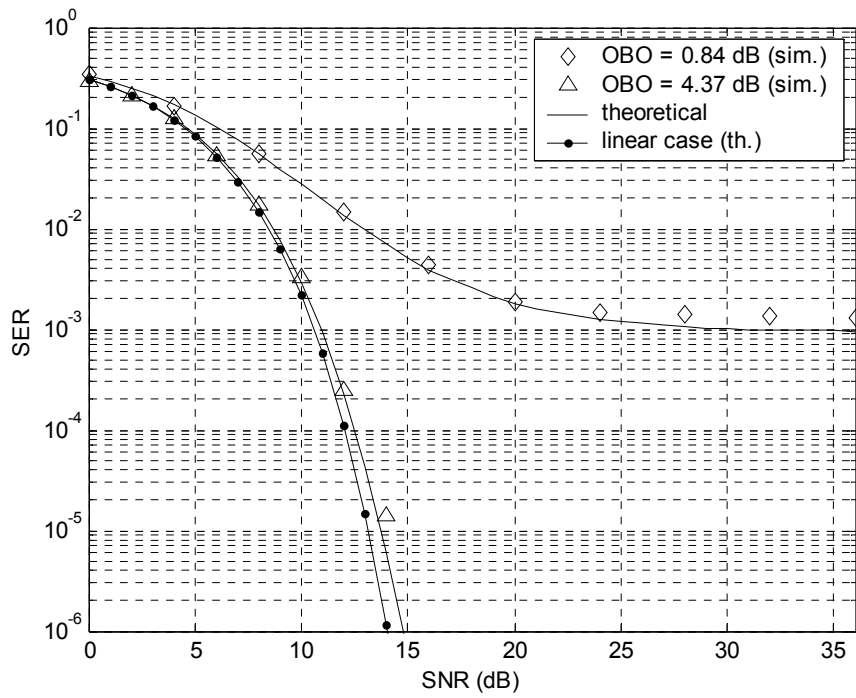


Fig. 27. SER of the LDD in AWGN channels (IPA model, $K = 20$, $N = 31$).

Fig. 28 and Fig. 29 exhibit the SER performance of the LDD in flat-fading channels, assuming the IPA and the Saleh model, respectively. We can observe that, as in AWGN channels, there exists some mismatch only at high SNR, when the OBO assumes low-to-medium values.

Fig. 30 shows the TD of the LDD for an uncoded $\text{SER} = 10^{-3}$. The TD is obtained using the approximated analytical model, since little mismatch with the simulations is introduced at this target SER. For the IPA (Saleh) model, the optimum OBO is approximately equal to 2.5 dB (3 dB) in AWGN channels, while it is approximately 1.3 dB (2 dB) in flat Rayleigh fading environments. It should be also observed that for any OBO value the TD is smaller in flat-fading scenarios rather than in AWGN channels. This can be intuitively explained by the following consideration. In flat-fading channels, the NLD noise is affected by the fading gain, and therefore its power is small (high) when the useful signal power also is small (high). Since most of the errors caused by the NLD noise are committed when the useful signal power is small, the NLD noise is partially masked by the thermal noise, whose power is independent of the fading gain.

Fig. 31, Fig. 32, and Fig. 33 show the SER performance of the three linear receivers (RAKE, LDD, and MMSE) in frequency-selective channels for different OBO values. The soft-limiter model (133) has been chosen for the HPA. The amplitudes $\{\beta_q \exp(j\theta_q)\}$ of the $Q=15$ channel paths are modeled as independent zero-mean complex Gaussian random variables with variance $E\{|\beta_q|^2\} = 1/Q$, while the path delays $\{\tau_q\}$ are fixed quantities, multiple of the chip duration T_c . The theoretical SER has been evaluated by averaging (125) over $N_{ch} = 400$ independent channel realizations. As expected, the MMSE receiver, which takes into account the presence of the NLD noise, outperforms the other two detectors.

Fig. 34 and Fig. 35 illustrate the SER performance of the MMSE detector for different OBO values, using the frequency-selective channel model described above, and the HPA models (133) and (134), respectively. As in AWGN channels, for practical uncoded SERs, there is a good agreement between analytical model and simulation results, especially if the OBO is very low or quite high. Moreover, a little mismatch exists when the OBO is roughly 2 dB.

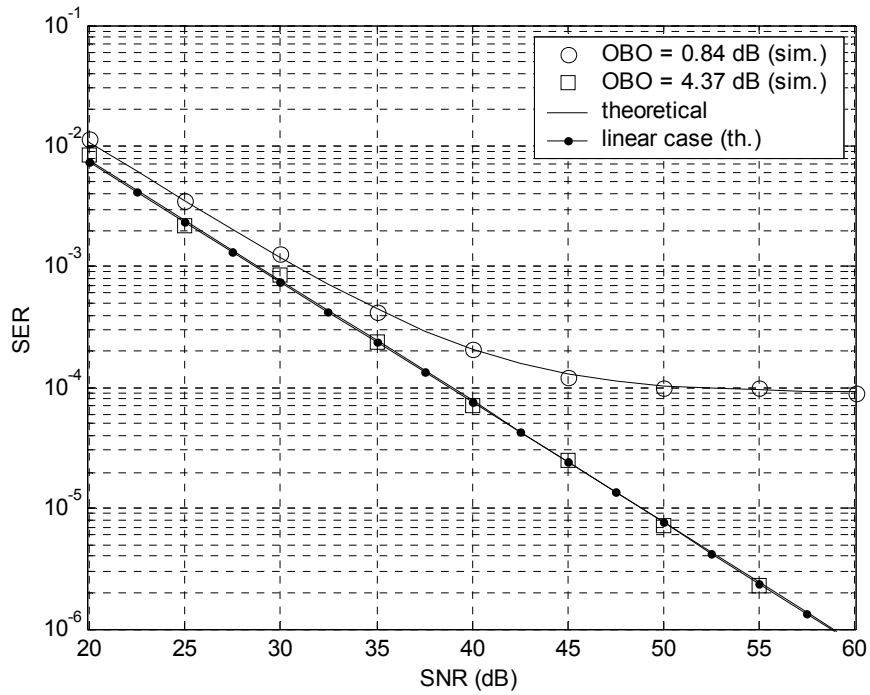


Fig. 28. SER of the LDD in flat-fading channels (IPA model, $K = 40$, $N = 63$).

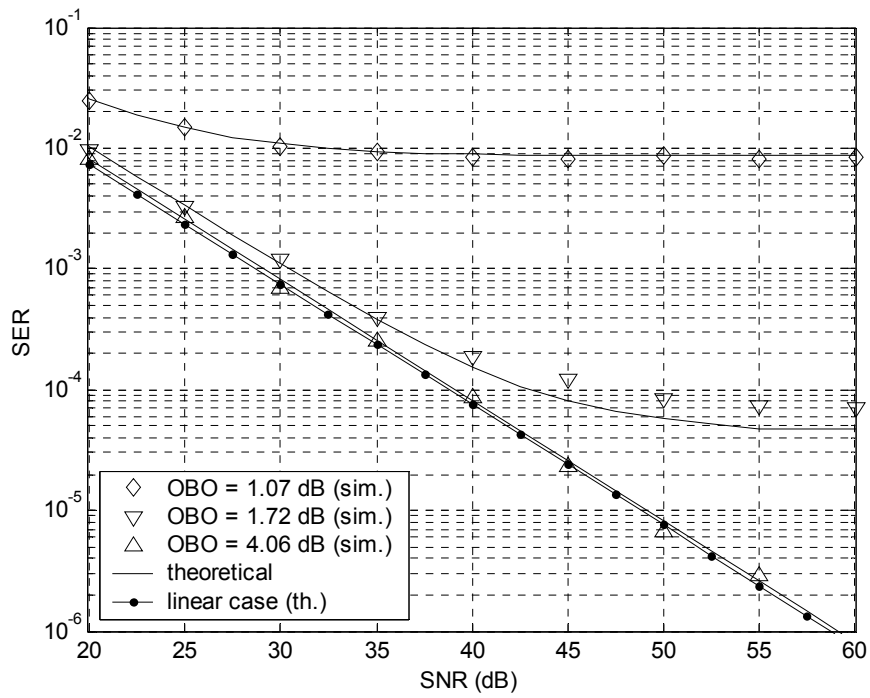


Fig. 29. SER of the LDD in flat-fading channels (Saleh model, $K = 40$, $N = 63$).

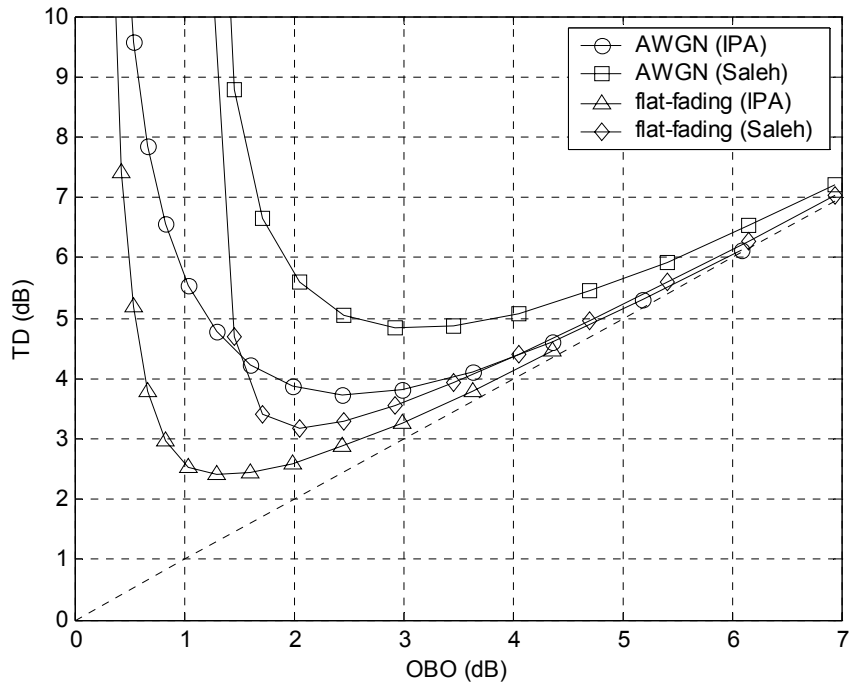


Fig. 30. TD of the LDD at $SER = 10^{-3}$ ($K = 40$, $N = 63$).

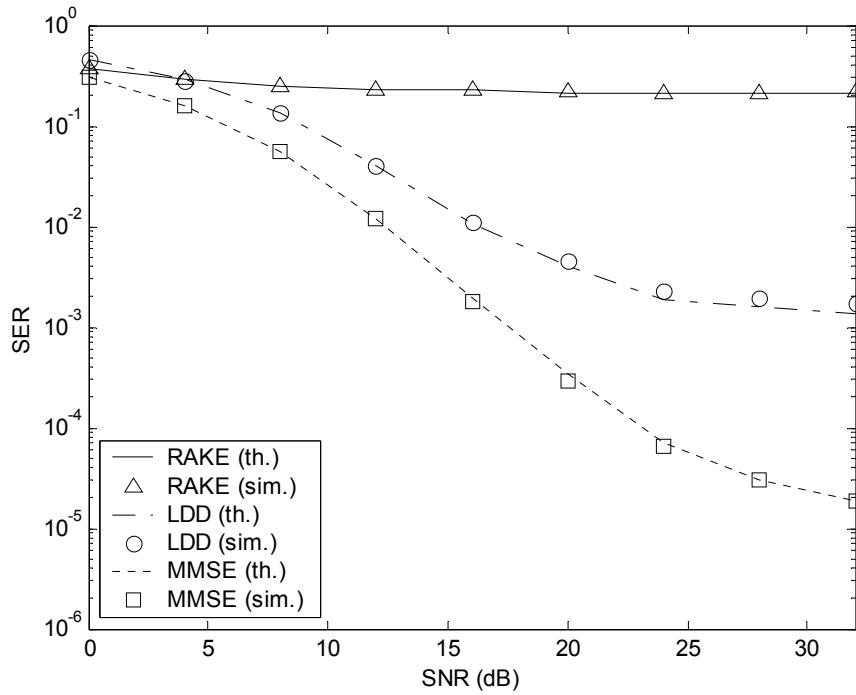


Fig. 31. SER in frequency-selective channels (IPA, OBO = 1.30 dB, $K = 40$, $N = 63$).

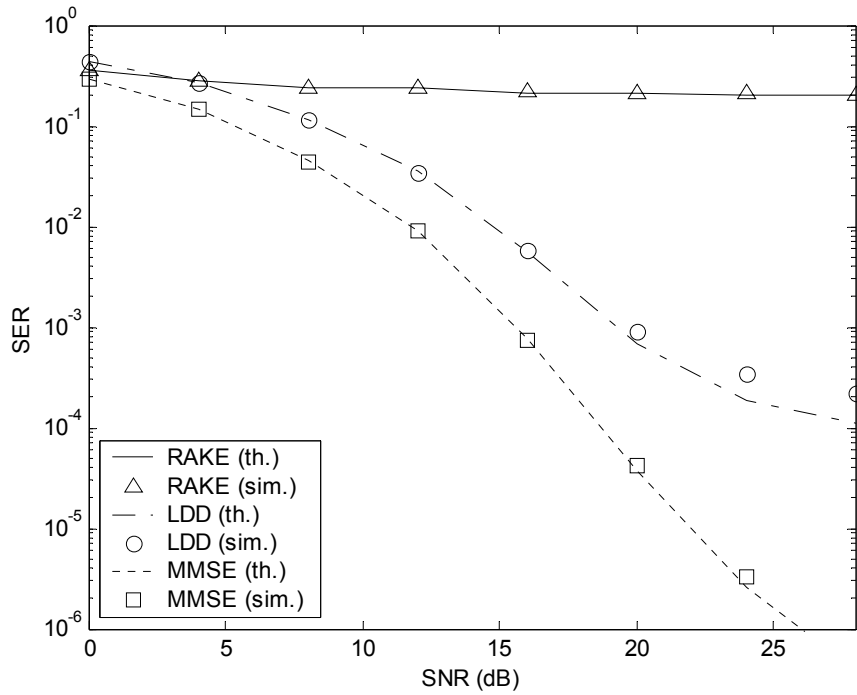


Fig. 32. SER in frequency-selective channels (IPA, OBO = 1.99 dB, $K = 40$, $N = 63$).

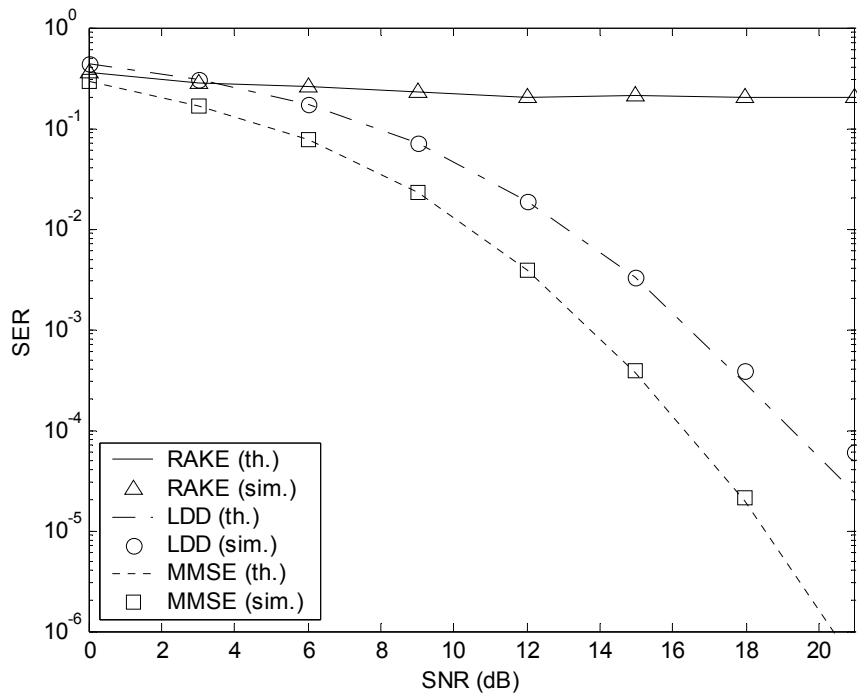


Fig. 33. SER in frequency-selective channels (IPA, OBO = 3.00 dB, $K = 40$, $N = 63$).

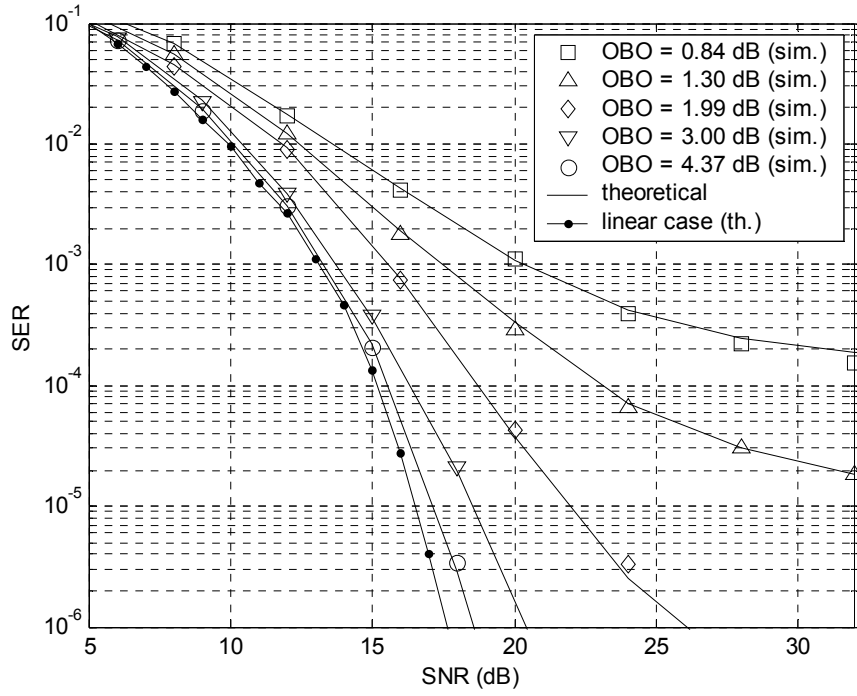


Fig. 34. SER of the MMSE in frequency-selective channels (IPA model, $K = 40$, $N = 63$).

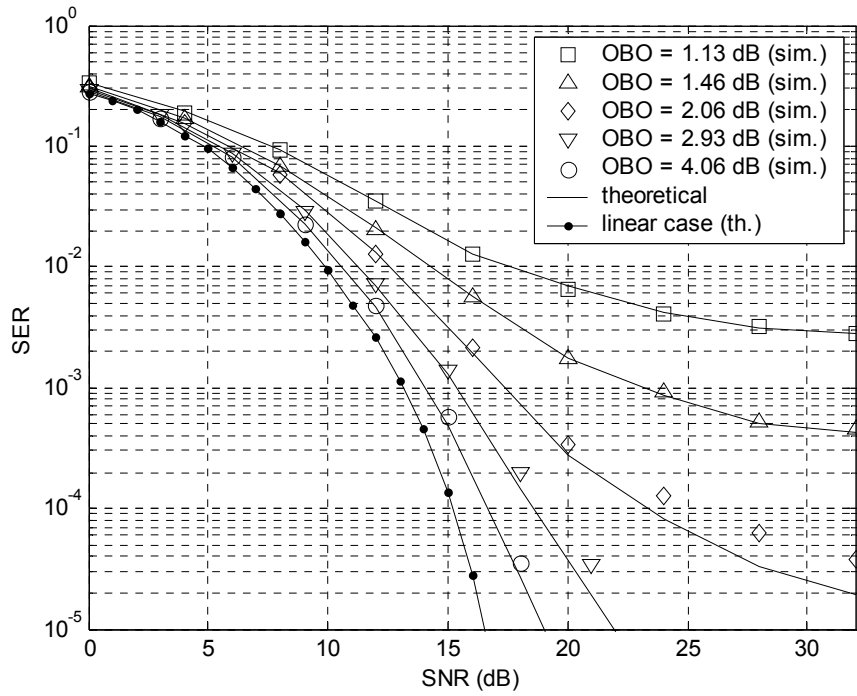


Fig. 35. SER of the MMSE in frequency-selective channels (Saleh model, $K = 40$, $N = 63$).

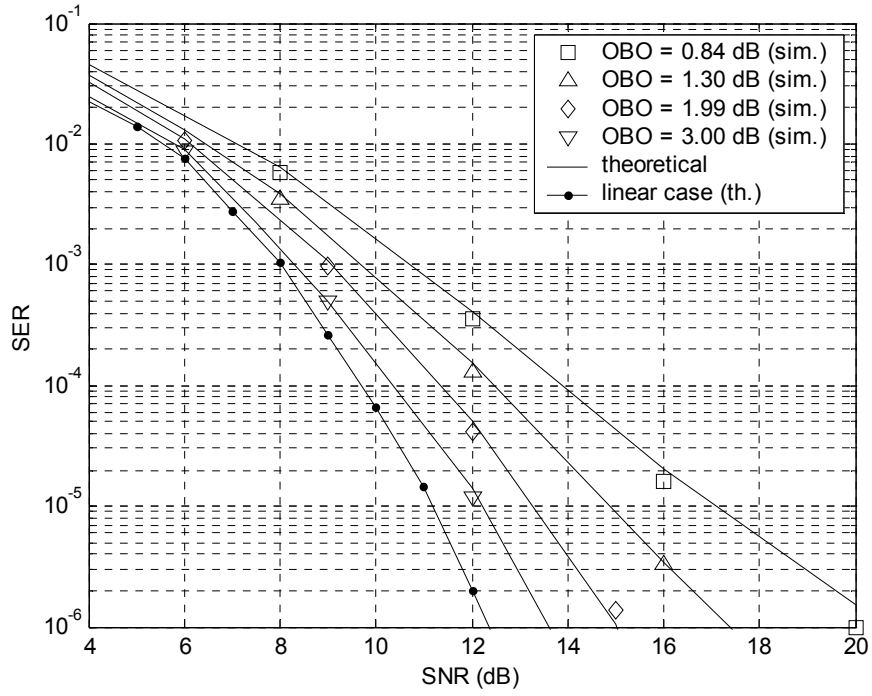


Fig. 36. SER of the MMSE in frequency-selective channels (IPA model, $K = 20$, $N = 63$).

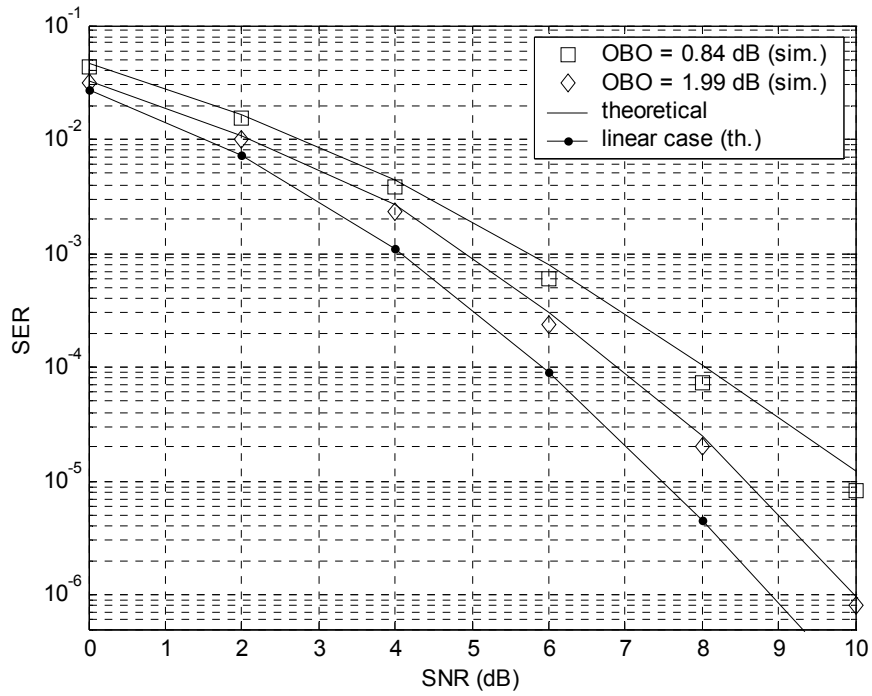


Fig. 37. SER of the MMSE in frequency-selective channels (IPA model, $K = 10$, $N = 63$).

Finally, Fig. 36 and Fig. 37 show the SER performance when the number of active users is reduced to $K = 20$ and to $K = 10$, respectively. We consider the MMSE detector in frequency-selective channels, assuming the soft-limiter model (133) as HPA. In both the figures, it is evident that the SER analysis is less accurate with respect to the case with $K = 40$ active users. However, the SER mismatch is quite small, and therefore the SER analysis could be useful also in these cases.

4. FREQUENCY SYNCHRONIZATION ERRORS AND NONLINEAR AMPLIFIER DISTORTIONS IN MULTICARRIER DS-CDMA SYSTEMS

In the last years, several multicarrier multiple-access schemes [HaPr] have been proposed by combining orthogonal frequency-division multiplexing (OFDM) and DS-CDMA, with the goal of incorporating the advantages of both techniques. Specifically, the low complexity equalization of cyclic prefixed OFDM systems, and the MAI mitigation capabilities offered by DS-CDMA systems, make MC-CDMA techniques attractive for future mobile broadband communications [FaFe].

Differently from single-carrier systems, one of the main problems of multicarrier schemes is the high sensitivity to frequency synchronization errors [PBM]. Indeed, the carrier frequency offset (CFO), which models the frequency mismatch between the transmitter and receiver oscillators, gives rise to intercarrier interference (ICI), thereby destroying the frequency-domain orthogonality of the transmitted data. The presence of a nonlinear amplifier (NLA) at the transmitter, which introduces both intermodulation distortion (IMD) and out-of-band interference, is another relevant source of impairment in multicarrier systems. Indeed, multicarrier signals are characterized by a high peak-to-average power ratio (PAPR) [OcIm], and hence they are significantly distorted when the NLA working point is chosen close to the saturation point.

Obviously, the typical impairments of multicarrier systems add to the sources of degradation that are generally present also in other multiple-access schemes, such as the MAI associated with multiple users in non-orthogonal systems [Verd], and the ISI introduced by the signal propagation over multipath channels. As a consequence, the degradation introduced by CFO and NLA, as well as MAI and multipath, should be taken into account when evaluating the

performance of multicarrier systems.

Specifically, this chapter deals with the effects of the mentioned impairments on the BER performance. The particular multicarrier scheme herein considered is commonly identified as multicarrier DS-CDMA (MC-DS-CDMA) [HaPr], where multiple users are discriminated by spreading the data in the time domain [DaSo]. Moreover, we focus on the performance at the mobile end (i.e., downlink), assuming that the receiver is equipped with a low-complexity MF detector. More complex RAKE receivers that exploit the frequency diversity of distant subcarriers [SoNa][KoMi] are not considered herein.

Previous works about MC-DS-CDMA performance considered the presence of either frequency synchronization errors or nonlinear distortions. For instance, the paper [StMo], evaluates the SNR degradation produced by the CFO in AWGN, without considering the NLA at the transmitter. On the other hand, the paper [JoSt] analyzes the effects of multipath and nonlinearities on the BER performance of a multicarrier spread-spectrum system, which basically is an MC-DS-CDMA scheme with one active user, assuming perfect frequency synchronization at the receiver side. The purpose of our work is to extend the results of [StMo] and [JoSt] in order to jointly take into account CFO, nonlinear distortions, and MAI, in multipath fading channels.

Besides, the results obtained in MC-DS-CDMA scenarios are also useful to characterize the BER performance degradation in OFDM scenarios. Indeed, OFDM systems can be thought as particular single-user MC-DS-CDMA systems, where no time-domain spreading is performed. Although wireless OFDM systems are generally considered single-user systems, more than one user can be supported by multiplexing the users' signals at the medium access control (MAC) level [DABN]. Furthermore, the results obtained for OFDM systems are equivalent to those in orthogonal frequency-division multiple-access (OFDMA) systems, where different subcarriers are employed to convey the data of different users.

In linearly modulated OFDM systems, the performance degradation caused by the CFO is often evaluated in terms of SNR loss [PBM][Moos][StFe]. Moreover, in [KeHa], the Gaussian approximation of the ICI is exploited to obtain an analytical BER expression in

AWGN channels. However, such an approximation is highly pessimistic when the BER is small. A more accurate BER expression that exploits the moments of the ICI distribution has been proposed by [ZhHä]. In addition, using the characteristic function of the ICI, the exact SER in AWGN channels can be derived [SaTe].

The main weakness of [KeHa], [ZhHä], and [SaTe] is that they consider the CFO effects only in AWGN channels, whereas OFDM systems are usually designed to cope with frequency-selective fading [NePr]. On this subject, by using the Gaussian approximation of the ICI, a BER analysis in Rayleigh fading channels is proposed in [ChHo]. By comparing theoretical and simulation results, we show that our solution is more accurate than the one in [ChHo].

In the following, we firstly consider MC-DS-CDMA systems in Rayleigh fading channels. Successively, we deal with OFDM systems, focusing the attention on frequency-selective fading channels. We point out that, for OFDM scenarios, the analysis takes also into account the Rician fading case.

4.1. MULTICARRIER DS-CDMA SYSTEM MODEL

In this chapter, we use a notation that is slightly different from the rest of the thesis. The reason is that we want to maintain the notation compatible with other works in the multicarrier area. We consider the downlink of an MC-DS-CDMA system with N subcarriers, spaced by $\Delta_f = 1/T$, and with K active users. Hence, assuming rectangular pulse-shaping, the chip duration is equal to T . The base station transmits N symbols of each user in parallel, one for each subcarrier, by spreading each symbol in the time domain employing a user-dependent spreading code. The spreading code of the k th user, which is the same for all the subcarriers, is denoted with $\mathbf{c}_k = [c_{k,0} \cdots c_{k,G-1}]^T$, where G is the processing gain. Assuming $|c_{k,g}| = 1/\sqrt{G}$, the vector \mathbf{c}_k has unit norm. As in conventional OFDM systems, the time-domain samples are obtained by N -dimensional inverse FFT

(IFFT) of the data on the N subcarriers, and a cyclic prefix of duration $\tau_{\text{CP}} = LT/N$ is attached to the IFFT output block in order to avoid channel-induced interblock interference (IBI). Consequently, the symbol rate of each user is equal to $N(1+L/N)^{-1}G^{-1}T^{-1}$.

By defining the $N \times N$ unitary FFT matrix \mathbf{F} as

$$[\mathbf{F}]_{m,n} = \frac{1}{\sqrt{N}} e^{-j \frac{2\pi(m-1)(n-1)}{N}}, \quad (135)$$

and the $(N+L) \times N$ cyclic prefix insertion matrix as $\mathbf{T}_{\text{CP}} = [\mathbf{I}_{\text{CP}}^T \ \mathbf{I}_N^T]^T$, where \mathbf{I}_{CP} contains the last L rows of the identity matrix \mathbf{I}_N , the transmitted block, at the input of the NLA, can be expressed by

$$\mathbf{u}_{\text{IN}}[lG+g] = \mathbf{T}_{\text{CP}} \mathbf{F}^H \mathbf{S}[l] \mathbf{c}[g], \quad (136)$$

where $\mathbf{u}_{\text{IN}}[lG+g]$ is a vector of dimension $P = N+L$, $\mathbf{S}[l]$ is the $N \times K$ matrix containing the data symbols, with $s_{n,k}[l] = [\mathbf{S}[l]]_{n,k}$ the l th symbol of the k th user on the n th subcarrier, and $\mathbf{c}[g] = [c_{1,g} \ \dots \ c_{K,g}]^T$ is the vector that contains the g th chip of the spreading codes of all the K users. The data symbols $\{s_{n,k}[l]\}$, drawn from an M -ary square quadrature amplitude modulation (QAM) constellation, are assumed to be independent and identically distributed with power σ_s^2 . Although in many cases we are dealing with continuous-time signals (i.e., at the NLA input and output, at the receiver input, and so on), we consider the equivalent discrete-time signals, to simplify the notation.

As in Chapter 2, we model the NLA as a memoryless device characterized by its AM/AM and AM/PM curves. After incorporating both the chip index g and the symbol index l into a single index $i = lG+g$, by the Busgang theorem [Papo], the transmitted block, at the output of the NLA, can be expressed as [BaCa][DTV]

$$\mathbf{u}_{\text{OUT}}[i] = \alpha \mathbf{u}_{\text{IN}}[i] + \bar{\mathbf{v}}_{\text{IMD}}[i], \quad (137)$$

where α represents the average linear amplification gain, and $\bar{\mathbf{v}}_{\text{IMD}}[i]$ is the IMD, uncorrelated with the linear part $\alpha \mathbf{u}_{\text{IN}}[i]$. The validity of (137), based on a Gaussian distribution of $\mathbf{u}_{\text{IN}}[i]$ in (136), is justified by the high number of subcarriers usually

employed in multicarrier systems (e.g., $N > 32$) [DVT]. In this case, as in single-carrier DS-CDMA systems, the average linear amplification gain can be evaluated as $\alpha = R_{u_{\text{OUT}} u_{\text{IN}}}(0) / R_{u_{\text{IN}} u_{\text{IN}}}(0)$, where $R_{u_{\text{OUT}} u_{\text{IN}}}(\tau)$ is the continuous-time crosscorrelation between the NLA output and input, and $R_{u_{\text{IN}} u_{\text{IN}}}(\tau)$ is the continuous-time autocorrelation function of the NLA input. Moreover, the elements of the matrix

$$\mathbf{R}_{\bar{\mathbf{v}}}(g, g') = E\{\bar{\mathbf{v}}_{\text{IMD}}[lG + g]\bar{\mathbf{v}}_{\text{IMD}}[lG + g']^H\} \quad (138)$$

can be predicted in advance by exploiting the knowledge of the continuous-time autocorrelation function $R_{u_{\text{OUT}} u_{\text{OUT}}}(\tau)$ of the NLA output.

After the parallel-to-serial conversion, the signal stream $u_{\text{OUT}}[iP + p] = [\mathbf{u}_{\text{OUT}}[i]]_{p+1}$, $p = 0, \dots, P-1$, is transmitted through a multipath channel, whose discrete-time equivalent impulse response is

$$h[b] = \sum_{q=1}^Q \beta_q R(bT_s - \tau_q), \quad (139)$$

where Q is the number of paths, β_q and τ_q are the complex amplitude and the propagation delay, respectively, of the q th path, $R(\tau)$ is the triangular autocorrelation function of the rectangular pulse shaping waveform, and $T_s = T/N$ is the sampling period. We assume that the channel amplitudes $\{\beta_q\}$ are zero-mean complex Gaussian random variables, giving rise to Rayleigh fading, and that the maximum delay spread $\tau_{\text{max}} = \max\{\tau_q\}$ is smaller than the cyclic prefix duration $\tau_{\text{CP}} = LT_s$, i.e., $h[b]$ may have non-zero entries only for $0 \leq b \leq L$.

At the receiver side, the samples obtained after matched filtering can be expressed as [MTGB]

$$x[a] = e^{j2\pi f_0 a T_s} \sum_{b=0}^L h[b] u_{\text{OUT}}[a-b] + x_{\text{AWGN}}[a], \quad (140)$$

where f_0 is the CFO caused by the frequency synchronization error at the receiver side, $x_{\text{AWGN}}[a]$ represents the AWGN, with $a = iP + p$. Throughout the paper, we assume that the timing information is available at the receiver. In multicarrier systems, such information could be acquired by exploiting timing synchronization algorithms designed to work in the

presence of an unknown CFO [ScCo][MZB][LWBÖ]. In any case, when timing errors are significant, the BER expressions we will derive can be considered as lower bounds.

The P received samples relative to the g th chip (of the l th symbol) are grouped in the vector $\mathbf{x}[i] = \mathbf{x}[lG + g]$, thus obtaining [MTGB]

$$\mathbf{x}[i] = e^{j2\pi\varepsilon i P/N} \tilde{\mathbf{D}}(\mathbf{H}_0 \mathbf{u}_{\text{OUT}}[i] + \mathbf{H}_1 \mathbf{u}_{\text{OUT}}[i-1]) + \mathbf{x}_{\text{AWGN}}[i], \quad (141)$$

where $[\mathbf{x}[i]]_{p+1} = x[iP + p]$, $\varepsilon = f_0 T$ is the normalized CFO, $\tilde{\mathbf{D}}$ is a $P \times P$ diagonal matrix, defined by $[\tilde{\mathbf{D}}]_{p,p} = e^{j\frac{2\pi\varepsilon(p-1)}{N}}$, that models the block-independent phase-shift introduced by the CFO, and \mathbf{H}_0 and \mathbf{H}_1 are $P \times P$ Toeplitz matrices defined by [WaGi]

$$\mathbf{H}_0 = \begin{bmatrix} h[0] & 0 & \cdots & \cdots & 0 \\ \vdots & \ddots & \ddots & & \vdots \\ h[L] & & \ddots & \ddots & \vdots \\ \vdots & \ddots & & \ddots & 0 \\ 0 & \cdots & h[L] & \cdots & h[0] \end{bmatrix}, \quad \mathbf{H}_1 = \begin{bmatrix} 0 & \cdots & h[L] & \cdots & h[1] \\ \vdots & \ddots & & \ddots & \vdots \\ 0 & & \ddots & & h[L] \\ \vdots & \ddots & & \ddots & \vdots \\ 0 & \cdots & 0 & \cdots & 0 \end{bmatrix}. \quad (142)$$

The cyclic prefix elimination, which is employed by many multicarrier-based systems to eliminate the IBI, can be represented by the left multiplication of the matrix $\mathbf{R}_{\text{CP}} = [\mathbf{0}_{N \times L} \ \mathbf{I}_N]$ with the received vector in (141), which leads to the $N \times 1$ vector [MTGB]

$$\mathbf{y}[i] = \mathbf{R}_{\text{CP}} \mathbf{x}[i] = e^{j2\pi\varepsilon(iP+L)/N} \mathbf{D} \mathbf{R}_{\text{CP}} \mathbf{H}_0 \mathbf{u}_{\text{OUT}}[i] + \mathbf{y}_{\text{AWGN}}[i], \quad (143)$$

where \mathbf{D} is an $N \times N$ diagonal matrix defined by $[\mathbf{D}]_{n,n} = e^{j\frac{2\pi\varepsilon(n-1)}{N}}$, and $\mathbf{y}_{\text{AWGN}}[i] = \mathbf{R}_{\text{CP}} \mathbf{x}_{\text{AWGN}}[i]$ stands for the AWGN term. By using (136) and (137), the vector $\mathbf{y}[i] = \mathbf{y}[lG + g]$ in (143) can also be expressed as

$$\mathbf{y}[lG + g] = e^{j2\pi\varepsilon((lG+g)P+L)/N} \mathbf{D} \mathbf{H} (\alpha \mathbf{F}^H \mathbf{S}[l] \mathbf{c}[g] + \tilde{\mathbf{v}}_{\text{IMD}}[lG + g]) + \mathbf{y}_{\text{AWGN}}[lG + g], \quad (144)$$

where $\mathbf{H} = \mathbf{R}_{\text{CP}} \mathbf{H}_0 \mathbf{T}_{\text{CP}}$ is the equivalent channel matrix expressed by $[\mathbf{H}]_{m,n} = h[(m-n)_{\text{mod} N}]$, and $\tilde{\mathbf{v}}_{\text{IMD}}[lG + g] = \mathbf{R}_{\text{CP}} \bar{\mathbf{v}}_{\text{IMD}}[lG + g]$. Since \mathbf{H} is circulant [WaGi], it can be expressed as $\mathbf{H} = \mathbf{F}^H \mathbf{\Lambda} \mathbf{F}$ [HoJo1], where $\mathbf{\Lambda} = \text{diag}(\boldsymbol{\lambda})$ is the $N \times N$ diagonal matrix with elements expressed by

$$\boldsymbol{\lambda} = \sqrt{N} \mathbf{F} \mathbf{h}, \quad (145)$$

where $\mathbf{h} = [h[0] \cdots h[N-1]]^T$ and $\boldsymbol{\lambda} = [\lambda_1 \cdots \lambda_n]^T$ are the channel vectors in the time and frequency domain, respectively. Consequently, the recovery of the transmitted data is accomplished by applying the FFT at the receiver, thus obtaining $\mathbf{z}[lG+g] = \mathbf{F}\mathbf{y}[lG+g]$, which, by (144), can be rearranged as

$$\mathbf{z}[lG+g] = e^{j2\pi\epsilon((lG+g)P+L)/N} \boldsymbol{\Phi} \boldsymbol{\Lambda} (\alpha \mathbf{S}[l] \mathbf{c}[g] + \mathbf{v}_{\text{IMD}}[lG+g]) + \mathbf{z}_{\text{AWGN}}[lG+g], \quad (146)$$

where $\boldsymbol{\Phi} = \mathbf{F} \mathbf{D} \mathbf{F}^H$ is the $N \times N$ circulant matrix that models the ICI due to the CFO, $\mathbf{v}_{\text{IMD}}[lG+g] = \mathbf{F} \tilde{\mathbf{v}}_{\text{IMD}}[lG+g]$ is the IMD after the FFT operation, and the vector $\mathbf{z}_{\text{AWGN}}[lG+g] = \mathbf{F} \mathbf{y}_{\text{AWGN}}[lG+g]$ represents the AWGN after the FFT operation.

Due to the spreading in the time domain, in order to decode the N data symbols $\mathbf{s}_k[l] = [s_{1,k}[l] \cdots s_{N,k}[l]]^T$ relative to the l th interval, the receiver of the k th user has to collect G consecutive chip vectors $\{\mathbf{z}[lG+g]\}_{g=0, \dots, G-1}$ in (146). By defining the $N \times G$ matrices $\mathbf{Z}[l] = [\mathbf{z}[lG] \cdots \mathbf{z}[lG+G-1]]$, $\mathbf{V}_{\text{IMD}}[l] = [\mathbf{v}_{\text{IMD}}[lG] \cdots \mathbf{v}_{\text{IMD}}[lG+G-1]]$, and $\mathbf{Z}_{\text{AWGN}}[l] = [\mathbf{z}_{\text{AWGN}}[lG] \cdots \mathbf{z}_{\text{AWGN}}[lG+G-1]]$, from (146) we obtain

$$\mathbf{Z}[l] = e^{j2\pi\epsilon l/N} \boldsymbol{\Phi} \boldsymbol{\Lambda} (\alpha \mathbf{S}[l] \mathbf{C} + \mathbf{V}_{\text{IMD}}[l]) \mathbf{E}[l] + \mathbf{Z}_{\text{AWGN}}[l], \quad (147)$$

where $\mathbf{C} = [\mathbf{c}[0] \cdots \mathbf{c}[G-1]] = [\mathbf{c}_1 \mathbf{c}_2 \cdots \mathbf{c}_K]^T$ is the $K \times G$ matrix whose rows contain the spreading codes of the K users, and $\mathbf{E}[l]$ is a $G \times G$ diagonal matrix defined as $[\mathbf{E}[l]]_{g+1, g+1} = e^{j2\pi\epsilon(lG+g)P/N}$, $g = 0, \dots, G-1$.

The matrix model expressed by (147) allows a nice representation of the MC-DS-CDMA received signal. Indeed, the number of rows of $\mathbf{Z}[l]$ in (147) is equal to the number of subcarriers, while the number of columns of $\mathbf{Z}[l]$ is equal to the processing gain. Consequently, we are able to represent linear frequency-domain operations (such as the equalization) by matrix multiplications on the left side of $\mathbf{Z}[l]$, and linear time-domain operations (such as the despreading) by matrix multiplications on the right side of $\mathbf{Z}[l]$.

Expression (147) shows the effects of both nonlinear distortions and frequency synchronization errors on the coded-data matrix $\mathbf{S}[l] \mathbf{C}$. Specifically, the NLA introduces the constant complex gain α and the additive term $\mathbf{V}_{\text{IMD}}[l]$, which represents the IMD. Moreover, the NLA-distorted signal, after passing through the multipath channel

summarized by the diagonal matrix Λ , is affected by the CFO-induced ICI, because the matrix Φ is not diagonal. In addition, the CFO produces two phase-shift effects. The first one is a time-invariant phase-shift $\varphi = e^{j2\pi\epsilon L/N} e^{j\pi\epsilon(N-1)/N}$ (the factor $e^{j\pi\epsilon(N-1)/N}$ is contained in the main diagonal of Φ), which adds to the phase-shift caused by the NLA. The second effect is a time varying phase-shift, which is represented by the diagonal matrix $\mathbf{E}[l]$. In this thesis, we assume that the receiver is able to perfectly compensate for the time-invariant phase-shift term φ , which could also be seen as part of the channel-induced distortion. As far as the compensation for the time-variant phase-shift is concerned, we consider two different hypotheses:

- Hypothesis H1: The receiver obtains an accurate phase-shift estimate in each chip interval, as assumed in [StMo]. As a consequence, by the knowledge of $\mathbf{E}[l]$ at the receiver side, the estimated phase-shift matrix can be expressed by

$$\hat{\mathbf{E}}[l] = \hat{\mathbf{E}}[l]_{\text{H1}} = \mathbf{E}[l]. \quad (148)$$

- Hypothesis H2: The receiver does not track the time-variant phase-shift at the chip level, estimating only the average phase-shift within a symbol interval. Hence, by the knowledge of the mean of the elements in $\mathbf{E}[l]$, the estimated phase-shift matrix $\hat{\mathbf{E}}[l] = \hat{\mathbf{E}}[l]_{\text{H2}}$ is diagonal, with elements

$$[\hat{\mathbf{E}}[l]_{\text{H2}}]_{g+1, g+1} = \exp\left(j \frac{1}{G} \sum_{g=0}^{G-1} \frac{2\pi\epsilon(lG + g)P}{N}\right) = \exp\left(j \frac{2\pi\epsilon P}{N} \left(lG + \frac{G-1}{2}\right)\right). \quad (149)$$

In this chapter, we assume that the receiver performs MF detection. The motivation of considering such a detector is twofold. Firstly, in the absence of NLA- and CFO-induced impairments, the MF is the optimum detector when orthogonal spreading codes are employed. In other words, in MC-DS-CDMA downlink systems subject to slow time varying fading channels, the MF with frequency-domain equalization is able to eliminate the all the MAI. Moreover, from the computational complexity point of view, MF receivers are less demanding than multiuser detectors, thereby reducing the power consumption of the mobile terminals.

The MF receiver can perform the despreading operation after the phase-shift compensation and the channel equalization. Thus, by assuming perfect channel state information (CSI) at the receiver side, the equalized data matrix can be constructed as

$$\mathbf{Z}_{\text{EQ}}[l] = \varphi^* \alpha^{-1} \Lambda^{-1} \mathbf{Z}[l] \hat{\mathbf{E}}[l]^{-1}. \quad (150)$$

From (147), $\mathbf{Z}_{\text{EQ}}[l]$ becomes equal to

$$\mathbf{Z}_{\text{EQ}}[l] = \Lambda^{-1} \mathbf{M} \Lambda \mathbf{S}[l] \mathbf{C} \Theta + \mathbf{Z}_{\text{EQ,IMD}}[l] + \mathbf{Z}_{\text{EQ,AWGN}}[l], \quad (151)$$

where $\mathbf{M} = e^{-j\pi\epsilon(N-1)/N} \Phi$ represents the phase-compensated ICI matrix,

$$\mathbf{Z}_{\text{EQ,IMD}}[l] = \alpha^{-1} \Lambda^{-1} \mathbf{M} \Lambda \mathbf{V}_{\text{IMD}}[l] \Theta \quad (152)$$

represents the IMD after the channel equalization,

$$\mathbf{Z}_{\text{EQ,AWGN}}[l] = \varphi^* \alpha^{-1} \Lambda^{-1} \mathbf{Z}_{\text{AWGN}}[l] \hat{\mathbf{E}}[l]^{-1} \quad (153)$$

represents the effect of the AWGN on the equalized data, and $\Theta = \mathbf{E}[l] \hat{\mathbf{E}}[l]^{-1}$ is a diagonal matrix equal to $\Theta_{\text{H1}} = \mathbf{I}_G$ under the Hypothesis H1, and defined as

$$[\Theta_{\text{H2}}]_{g+1,g+1} = \exp\left(j \frac{2\pi\epsilon P}{N} \left(g - \frac{G-1}{2}\right)\right) \quad (154)$$

under the Hypothesis H2. The despreading operation leads to an N -dimensional vector that contains the N decision variables of the k th user, as expressed by

$$\mathbf{z}_{\text{DESPR},k}[l] = \mathbf{Z}_{\text{EQ}}[l] \mathbf{c}_k^* = \Lambda^{-1} \mathbf{M} \Lambda \mathbf{S}[l] \mathbf{C} \Theta \mathbf{c}_k^* + \mathbf{z}_{\text{DESPR,IMD},k}[l] + \mathbf{z}_{\text{DESPR,AWGN},k}[l], \quad (155)$$

where $\mathbf{z}_{\text{DESPR,IMD},k}[l] = \mathbf{Z}_{\text{EQ,IMD}}[l] \mathbf{c}_k^*$, and $\mathbf{z}_{\text{DESPR,AWGN},k}[l] = \mathbf{Z}_{\text{EQ,AWGN}}[l] \mathbf{c}_k^*$. The decision over $\mathbf{z}_{\text{DESPR},k}[l]$ is successively done according to the proper constellation size M .

It should be pointed out that the K -dimensional vector $\mathbf{C} \Theta \mathbf{c}_k^*$ represents the effect of the CFO-induced time varying phase-shift on the spreading-despreading operation. If the time varying phase-shift can be perfectly compensated for, i.e., under the Hypothesis H1, this vector becomes equal to $\mathbf{C} \mathbf{c}_k^*$. Therefore, if the users employ orthogonal spreading codes, the multiuser interference is perfectly eliminated, because the product $\mathbf{S}[l] \mathbf{C} \Theta_{\text{H1}} \mathbf{c}_k^*$ in

(155) is equal to $\mathbf{s}_k[l] = [\mathbf{S}[l]]_{:,k}$. On the contrary, under the Hypothesis H2, the multiuser interference cannot be completely eliminated. Indeed, when $k' \neq k$, we have

$$\rho_{k,k'}^{(H2)} = [\mathbf{C}\mathbf{\Theta}_{H2}\mathbf{c}_k^*]_{k'} = \mathbf{c}_{k'}^T \mathbf{\Theta}_{H2} \mathbf{c}_k^* = \sum_{g=0}^{G-1} e^{j\frac{2\pi\epsilon P}{N}\left(g-\frac{G-1}{2}\right)} c_{k',g} c_{k,g}^*, \quad (156)$$

which is, in general, different from zero even for orthogonal sequences (characterized by $\mathbf{c}_{k'}^T \mathbf{c}_k^* = \sum_{g=0}^{G-1} c_{k',g} c_{k,g}^* = 0$). An interesting matter could be the search for spreading sequences that minimize (156), following the lines suggested by [YiNg]. However, this topic is beyond the scope of this thesis.

Furthermore, since $\rho_{k,k}^{(H2)} = \mathbf{c}_k^T \mathbf{\Theta}_{H2} \mathbf{c}_k^* < 1$, the time-variant phase-shift also introduces an attenuation factor of the useful signal, given by

$$\rho_{k,k}^{(H2)} = \frac{1}{G} \sum_{g=0}^{G-1} e^{j\frac{2\pi\epsilon P}{N}\left(g-\frac{G-1}{2}\right)} = \frac{\sin(\pi\epsilon P G / N)}{G \sin(\pi\epsilon P / N)}. \quad (157)$$

For a given maximum tolerable frequency offset ϵ , the attenuation factor in (157) limits the maximum value G of the processing gain. Indeed, $\rho_{k,k}^{(H2)}$ is close to 1 only if $\epsilon \ll N(N+L)^{-1} G^{-1} \approx G^{-1}$. On the contrary, under the Hypothesis H1, $\rho_{k,k}^{(H1)} = \mathbf{c}_k^T \mathbf{\Theta}_{H1} \mathbf{c}_k^* = 1$, and hence no attenuation is introduced by the spreading-despreading operation. It should be observed that $\rho_{k,k}$ is independent of the user index k in both hypotheses, and hence, in the following, it will be denoted with ρ .

4.2. PERFORMANCE ANALYSIS IN MULTICARRIER DS-CDMA SYSTEMS

In this section, we evaluate the effect of the previously described impairments when the channel exhibits a fading behavior. We start with channels characterized by frequency-flat fading. The results obtained in this preliminary case will be useful for the performance evaluation in frequency-selective fading channels, developed in Section 4.2.2.

4.2.1. BER Performance in Flat-Fading Channels

In the flat-fading case, all the subcarriers experience the same channel gain. Consequently, since $\mathbf{\Lambda} = \lambda \mathbf{I}_N$, (155) can be simplified to

$$\mathbf{z}_{\text{DESPR},k}[l] = \mathbf{MS}[l]\mathbf{C}\mathbf{\Theta}\mathbf{c}_k^* + \alpha^{-1}\mathbf{M}\mathbf{V}_{\text{IMD}}[l]\mathbf{\Theta}\mathbf{c}_k^* + \varphi^* \alpha^{-1} \lambda^{-1} \mathbf{Z}_{\text{AWGN}}[l]\hat{\mathbf{E}}[l]\mathbf{c}_k^*. \quad (158)$$

For convenience, we consider the scaled version of (158) obtained by multiplying $\mathbf{z}_{\text{DESPR},k}[l]$ with $\lambda|\alpha|$. Therefore, we obtain $\mathbf{z}_{\text{SC},k}[l] = \lambda|\alpha|\mathbf{z}_{\text{DESPR},k}[l]$, and, by focusing on the n th subcarrier, it yields

$$z_{\text{SC},n,k}[l] = [\mathbf{z}_{\text{SC},k}[l]]_n = \lambda|\alpha| \mathbf{m}_n^T \mathbf{S}[l] \mathbf{C} \mathbf{\Theta} \mathbf{c}_k^* + z_{\text{SC,IMD},n,k}[l] + z_{\text{SC,AWGN},n,k}[l], \quad (159)$$

where

$$z_{\text{SC,IMD},n,k}[l] = \lambda e^{-j\arg(\alpha)} \mathbf{m}_n^T \mathbf{V}_{\text{IMD}}[l] \mathbf{\Theta} \mathbf{c}_k^*, \quad (160)$$

$$z_{\text{SC,AWGN},n,k}[l] = \varphi^* e^{-j\arg(\alpha)} \mathbf{z}_{\text{AWGN},n}[l]^T \hat{\mathbf{E}}[l] \mathbf{c}_k^*, \quad (161)$$

where $\mathbf{z}_{\text{AWGN},n}[l]^T$ is the n th row of $\mathbf{Z}_{\text{AWGN}}[l]$, and $\mathbf{m}_n = [m_{n,1} \cdots m_{n,N}]^T$ collects the elements on the n th row of \mathbf{M} . It can be verified that

$$m_{n,n'} = [\mathbf{M}]_{n,n'} = \frac{\sin(\pi((n'-n)_{\text{mod } N} + \mathcal{E}))}{N \sin\left(\frac{\pi}{N}((n'-n)_{\text{mod } N} + \mathcal{E})\right)} e^{j\pi \frac{N-1}{N}(n'-n)_{\text{mod } N}}, \quad (162)$$

where $m_{n,n'}$ represents the ICI coefficient relative to the n' th subcarrier when $n' \neq n$, and an additional attenuation factor, denoted with $m = m_{n,n}$, when $n' = n$. Since

$$\mathbf{S}[l] \mathbf{C} \mathbf{\Theta} \mathbf{c}_k^* = \rho \mathbf{s}_k[l] + \sum_{\substack{k'=1 \\ k' \neq k}}^K \rho_{k,k'} \mathbf{s}_{k'}[l], \quad (163)$$

by dropping the symbol index l for the sake of simplicity, (159) can be rewritten as

$$z_{\text{SC},n,k} = \lambda(|\alpha| \rho m s_{n,k} + z_{\text{ICI},n,k} + z_{\text{MAI},n,k} + z_{\text{MAICI},n,k} + z_{\text{IMD},n,k}) + z_{\text{AWGN},n,k}, \quad (164)$$

where the quantity

$$z_{\text{ICI},n,k} = |\alpha| \rho \sum_{\substack{n'=1 \\ n' \neq n}}^N m_{n,n'} s_{n',k} \quad (165)$$

represents the ICI coming from the symbols of the k th user,

$$z_{\text{MAI},n,k} = |\alpha| m \sum_{\substack{k'=1 \\ k' \neq k}}^K \rho_{k,k'} s_{n,k'} \quad (166)$$

corresponds to the MAI coming from the symbols of the other users on the n th subcarrier,

$$z_{\text{MAICI},n,k} = |\alpha| \sum_{\substack{k'=1 \\ k' \neq k}}^K \rho_{k,k'} \sum_{\substack{n'=1 \\ n' \neq n}}^N m_{n,n'} s_{n',k'} \quad (167)$$

represents the multiple-access ICI (MAICI) coming from the symbols of the other users on the other subcarriers,

$$z_{\text{IMD},n,k} = e^{-j \arg(\alpha)} \mathbf{m}_n^T \mathbf{V}_{\text{IMD}} \mathbf{\Theta} \mathbf{c}_k^* \quad (168)$$

represents the IMD, and

$$z_{\text{AWGN},n,k} = \varphi^* e^{-j \arg(\alpha)} \mathbf{z}_{\text{AWGN},n}^T \hat{\mathbf{E}} \mathbf{c}_k^* \quad (169)$$

stands for the AWGN.

In order to find the BER of the k th user on the n th subcarrier, we will firstly evaluate the conditional bit-error probability $P_{\text{BE},n,k}(\lambda)$ for a given channel gain λ , and we will successively average the obtained $P_{\text{BE},n,k}(\lambda)$ over the PDF $f_\lambda(\lambda)$ of the channel gain. Therefore, we will determine the BER by making use of the expressions

$$(\text{BER})_{n,k} = \int_{\lambda} P_{\text{BE},n,k}(\lambda) f_\lambda(\lambda) d\lambda, \quad (170)$$

$$P_{\text{BE},n,k}(\lambda) = \int_{\mathbf{S}} P_{\text{BE},n,k}(\mathbf{S}, \lambda) f_{\mathbf{S}}(\mathbf{S}) d\mathbf{S}, \quad (171)$$

where $P_{\text{BE},n,k}(\mathbf{S}, \lambda)$ is the bit-error probability conditioned on both the channel gain λ and the data symbols in the matrix $\mathbf{S}[l]$, and $f_{\mathbf{S}}(\mathbf{S})$ is the multidimensional PDF of the data symbols in $\mathbf{S}[l]$.

From (164), we observe that we have five noise terms, each one with different statistical characterization. Hence, the computation of the conditional probability $P_{\text{BE},n,k}(\lambda)$ seems to be quite complicated. As a consequence, a reasonable way to proceed relies on finding simple (yet accurate) approximations that allow a mathematical treatment. Along this way, we observe that the ICI term $z_{\text{ICI},n,k}$ in (165) is obtained by the linear combination of $N-1$ symbols, each one weighted by a different coefficient $m_{n,n'}$. If the frequency offset ε is not too high (e.g., $\varepsilon < 0.1$), the coefficients $\{m_{n,n'}\}_{n \neq n'}$ have comparable amplitudes [KeHa]. Therefore, under the hypothesis of high number N of subcarriers, the ICI term in (165) can be well approximated by a zero-mean Gaussian random variable with power

$$\sigma_{\text{ICI},n,k}^2 = |\alpha\rho|^2 \sum_{\substack{n'=1 \\ n' \neq n}}^N |m_{n,n'}|^2 \sigma_s^2 = |\alpha\rho|^2 \left(1 - \frac{\sin^2(\pi\varepsilon)}{N^2 \sin^2(\pi\varepsilon/N)} \right) \sigma_s^2. \quad (172)$$

We want also to underline that the hypotheses of high N and low CFO seem to be realistic. Indeed, multicarrier systems usually employ many active subcarriers, from $N=52$ in wireless local area network (WLAN) environments to $N \approx 6000$ in broadcasting applications [NePr]. Moreover, in the presence of high CFO, the BER will be very high (e.g., $\text{BER} > 0.1$), and therefore in this case the BER analysis seems to be of limited practical interest.

It should be pointed out that the ICI power in (172) does not depend on the user index k as long as σ_s^2 remains the same for all the users. However, the result could be extended to take into account different user powers. Moreover, our BER analysis can be easily extended in order to take into account the presence of N_{VS} switched-off subcarriers that are used as guard frequency bands, because a switched-off subcarrier does not contribute to the ICI and to the MAICI. As an example, assume that the switched-off subcarriers are the ones with $n \in \{N - N_{\text{VS}} + 1, N - N_{\text{VS}} + 2, \dots, N\}$. The only modification to our analysis is that $s_{n,k} = 0$ for these subcarriers. Therefore, the BER analysis remains still valid, provided that the summations over the subcarrier index n are truncated up to $n = N - N_{\text{VS}}$.

As far as the MAI term is concerned, we similarly observe that $z_{\text{MAI},n,k}$ in (166) is obtained

as the sum of the $K-1$ elements $\{s_{n,k'}\}$, weighted by almost-equal elements $\{\rho_{k,k'}\}$. Therefore, when the number K of users is sufficiently high, we can exploit the Gaussian approximation as we did for the ICI term. The MAI power can be expressed as

$$\sigma_{\text{MAI},n,k}^2 = |\alpha m|^2 \sum_{\substack{k'=1 \\ k' \neq k}}^K |\rho_{k,k'}|^2 \sigma_S^2. \quad (173)$$

Since high bit rates are expected in the downlink of fourth generation systems, also the hypothesis of high K seems to be realistic, because many spreading codes can be assigned to the same user in order to provide higher bit rates. Therefore, K can be interpreted as the number of spreading codes assigned to \tilde{K} active users, with $\tilde{K} < K$. Moreover we remark that, under the Hypothesis H1, the MAI term can be set to zero by employing orthogonal codes, and hence no accurate MAI characterization is necessary in this case.

Because of the previous assumptions about the number K of equivalent users and the number N of subcarriers, the MAICI term can be approximated by a zero-mean Gaussian variable as well, with power equal to

$$\sigma_{\text{MAICI},n,k}^2 = |\alpha|^2 \sum_{\substack{k'=1 \\ k' \neq k}}^K |\rho_{k,k'}|^2 \sum_{\substack{n'=1 \\ n' \neq n}}^N |m_{n,n'}|^2 \sigma_S^2 \quad (174)$$

$$= |\alpha|^2 \sum_{\substack{k'=1 \\ k' \neq k}}^K |\rho_{k,k'}|^2 \left(1 - \frac{\sin^2(\pi\epsilon)}{N^2 \sin^2(\pi\epsilon/N)} \right) \sigma_S^2. \quad (175)$$

We still remark that, under the Hypothesis H1, also the MAICI term vanishes when the codes are orthogonal.

We also observe that the IMD term $z_{\text{IMD},n,k}$ in (168) can equivalently be expressed as

$$z_{\text{IMD},n,k} = \sum_{g=0}^{G-1} e^{-j \arg(\alpha)} \theta_{g+1} c_{k,g}^* \mathbf{m}_n^T \mathbf{v}_{\text{IMD},g}, \quad (176)$$

where $\theta_{g+1} = [\Theta]_{g+1,g+1}$, and $\mathbf{v}_{\text{IMD},g}$ is the g th column of \mathbf{V}_{IMD} . Since \mathbf{V}_{IMD} is evaluated at the output of the receiver FFT, the assumption of high N allows to approximate the PDF of $\mathbf{v}_{\text{IMD},g}$ as a multidimensional Gaussian PDF. Moreover, \mathbf{V}_{IMD} is transformed in $z_{\text{IMD},n,k}$ by

linear operations, and hence $z_{\text{IMD},n,k}$ also can be modeled as a zero-mean Gaussian random variable, with power expressed by

$$\sigma_{\text{IMD},n,k}^2 = \sum_{g=0}^{G-1} \sum_{g'=0}^{G-1} \theta_{g+1} \theta_{g'+1}^* c_{k,g}^* c_{k,g'} \mathbf{m}_n^T \mathbf{R}_v(g, g') \mathbf{m}_n^*, \quad (177)$$

where

$$\mathbf{R}_v(g, g') = E\{\mathbf{v}_{\text{IMD},g} \mathbf{v}_{\text{IMD},g'}^H\} = \mathbf{F} \mathbf{R}_{\text{CP}} \mathbf{R}_v(g, g') \mathbf{R}_{\text{CP}}^T \mathbf{F}^H, \quad (178)$$

which depends on the indexes g and g' , can be calculated by exploiting the knowledge of the IMD autocorrelation function, summarized by $\mathbf{R}_v(g, g')$ in (138).

Since the interference terms in (164) are modeled as zero-mean Gaussian random variables, also the aggregate noise can be considered as Gaussian. Indeed, the data of different users or different subcarriers are uncorrelated with one another, as well as the ICI, the MAI, and the MAICI terms are uncorrelated with one another and with the useful signal. Moreover, thanks to the Bussgang theorem [Papo], the IMD term also is uncorrelated with the other terms. Consequently, the power of the aggregate noise is equal to the sum of the powers of the individual noise terms. Hence, the conditional bit-error probability $P_{\text{BE},n,k}(\lambda)$, for square M -QAM with Gray coding, can be expressed by [ChYo]

$$P_{\text{BE},n,k}(\lambda) = \frac{1}{\log_2 \sqrt{M}} \sum_{q=1}^{\log_2 \sqrt{M}} P_{n,k}(q, \lambda), \quad (179)$$

$$P_{n,k}(q, \lambda) = \frac{1}{\sqrt{M}} \sum_{i=0}^{(1-2^{-q})\sqrt{M}-1} \left\{ (-1)^{\lfloor \frac{2^{q-1}i}{\sqrt{M}} \rfloor} \left(2^q - 2 \left\lfloor \frac{2^{q-1}i}{\sqrt{M}} - \frac{1}{2} \right\rfloor \right) Q \left((2i+1) \sqrt{\frac{3}{M-1}} \gamma_{n,k}(\lambda) \right) \right\}, \quad (180)$$

with the SINR $\gamma_{n,k}(\lambda)$ expressed by

$$\gamma_{n,k}(\lambda) = \frac{|\lambda|^2 |\alpha \rho m|^2 \sigma_s^2}{|\lambda|^2 (\sigma_{\text{ICI},n,k}^2 + \sigma_{\text{MAI},n,k}^2 + \sigma_{\text{MAICI},n,k}^2 + \sigma_{\text{IMD},n,k}^2) + \sigma_{\text{AWGN}}^2}. \quad (181)$$

In order to perform the average over the channel statistics, for convenience, we rewrite (179)-(180) as

$$P_{\text{BE},n,k}(\lambda) = \sum_{i=0}^{\sqrt{M}-2} a_i Q\left(\sqrt{b_i \gamma_{n,k}(\lambda)}\right), \quad (182)$$

where the coefficients $\{a_i\}$ and $\{b_i\}$, calculated from (179)-(180), depend on the modulation size M . Therefore the resultant BER, which is obtained by inserting in (170) the expressions (181), (182), and the specific PDF $f_\lambda(\lambda)$ of the channel, can be expressed as the sum of $\sqrt{M}-1$ integrals. Each integral can then be evaluated by numerical techniques.

We want to highlight that such an approach can be used regardless of the statistical characterization of the channel. However, when the channel is characterized by Rayleigh fading, we can circumvent the numerical integration by evaluating a suitable series expansion. As an example, for 4-QAM or QPSK, (182) becomes $P_{\text{BE},n,k}(\lambda) = Q\left(\sqrt{\gamma_{n,k}(\lambda)}\right)$, and, by exploiting the results in Appendix B, (170) becomes

$$(\text{BER})_{n,k} = \int_0^{+\infty} Q\left(\sqrt{\gamma(\lambda)}\right) \frac{2|\lambda|}{\sigma_\lambda^2} e^{-\frac{|\lambda|^2}{\sigma_\lambda^2}} d|\lambda| \quad (183)$$

$$= \frac{1}{2} - \frac{\sqrt{2\mu_{n,k}^2}}{4} e^{-\frac{\mu_{n,k}^2}{2\nu_{n,k}^2}} \sum_{i=0}^{+\infty} \frac{1}{i!} \left(\frac{\mu_{n,k}^2}{2\nu_{n,k}^2}\right)^i {}_2F_0\left(i + \frac{3}{2}, \frac{1}{2}; ; -\nu_{n,k}^2\right), \quad (184)$$

where ${}_pF_q$ denotes the generalized hypergeometric function [GrRy][AbSt], $\sigma_\lambda^2 = E\{|\lambda|^2\}$, and $\mu_{n,k}^2$ and $\nu_{n,k}^2$ are expressed by

$$\mu_{n,k}^2 = \mu^2 = \frac{|\alpha \rho m|^2 \sigma_s^2 \sigma_\lambda^2}{\sigma_{\text{AWGN}}^2}, \quad (185)$$

$$\nu_{n,k}^2 = \frac{(\sigma_{\text{ICI},n,k}^2 + \sigma_{\text{MAI},n,k}^2 + \sigma_{\text{MAICI},n,k}^2 + \sigma_{\text{IMD},n,k}^2) \sigma_\lambda^2}{\sigma_{\text{AWGN}}^2}. \quad (186)$$

As a consequence of (182) and (183), the general M -QAM case leads to a resultant BER that is expressed as the sum of $\sqrt{M}-1$ series expansions. Note that each series expansion in the form of (184) can be conveniently truncated without affecting significantly the BER value (see Appendix C for a simple and accurate truncation criterion).

4.2.2. BER Performance in Frequency-Selective Fading Channels

For frequency-selective fading channels, we follow a two-step approach similar to the one adopted for frequency-flat channels. By denoting with $\lambda_n = [\mathbf{\Lambda}]_{n,n}$ the channel gain of the n th subcarrier, the frequency-selective counterparts of (170) and (171) can be expressed by

$$(\text{BER})_{n,k} = \int_{\lambda_n} P_{\text{BE},n,k}(\lambda_n) f_{\lambda_n}(\lambda_n) d\lambda_n, \quad (187)$$

$$P_{\text{BE},n,k}(\lambda_n) = \int_{\mathbf{s}, \bar{\lambda}_n} P_{\text{BE},n,k}(\mathbf{S}, \boldsymbol{\lambda}) f_{\bar{\lambda}_n | \lambda_n}(\bar{\lambda}_n | \lambda_n) f_{\mathbf{S}}(\mathbf{S}) d\mathbf{S} d\bar{\lambda}_n, \quad (188)$$

where $f_{\lambda_n}(\lambda_n)$ is the PDF of λ_n , $f_{\bar{\lambda}_n | \lambda_n}(\bar{\lambda}_n | \lambda_n)$ is the conditional PDF of the channel vector $\bar{\lambda}_n = [\lambda_1 \cdots \lambda_{n-1} \lambda_{n+1} \cdots \lambda_N]^T$ of the other subcarriers given the subcarrier of interest λ_n , and $P_{\text{BE},n,k}(\mathbf{S}, \boldsymbol{\lambda})$ is the bit-error probability conditioned on both the channel gains in $\boldsymbol{\lambda}$ and the data symbols in $\mathbf{S}[l]$. By multiplying (155) with $\lambda_n |\alpha|$, the scaled decision variable $z_{\text{SC},n,k}[l]$ can be expressed by

$$z_{\text{SC},n,k}[l] = |\alpha| \mathbf{m}_n^T \mathbf{\Lambda} \mathbf{S}[l] \mathbf{C} \boldsymbol{\Theta} \mathbf{c}_k^* + e^{-j \arg(\alpha)} \mathbf{m}_n^T \mathbf{\Lambda} \mathbf{V}_{\text{IMD}}[l] \boldsymbol{\Theta} \mathbf{c}_k^* + \varphi^* e^{-j \arg(\alpha)} \mathbf{z}_{\text{AWGN},n}[l]^T \hat{\mathbf{E}}[l] \mathbf{c}_k^*. \quad (189)$$

By exploiting

$$\mathbf{S}[l] \mathbf{C} \boldsymbol{\Theta} \mathbf{c}_k^* = \rho \mathbf{s}_k[l] + \sum_{\substack{k'=1 \\ k' \neq k}}^K \rho_{k,k'} \mathbf{s}_{k'}[l], \quad (190)$$

and dropping the index l , (189) becomes

$$z_{\text{SC},n,k} = |\alpha| \rho m \lambda_n s_{n,k} + z_{\text{SC,ICI},n,k} + z_{\text{SC,MAI},n,k} + z_{\text{SC,MAICI},n,k} + z_{\text{SC,IMD},n,k} + z_{\text{AWGN},n,k}, \quad (191)$$

where

$$z_{\text{SC,ICI},n,k} = |\alpha| \rho \sum_{\substack{n'=1 \\ n' \neq n}}^N m_{n,n'} \lambda_{n'} s_{n',k}, \quad (192)$$

$$z_{\text{SC,MAI},n,k} = |\alpha| m \lambda_n \sum_{\substack{k'=1 \\ k' \neq k}}^K \rho_{k,k'} s_{n,k'}, \quad (193)$$

$$z_{\text{SC,MAICI},n,k} = |\alpha| \sum_{\substack{n'=1 \\ n' \neq n}}^N m_{n,n'} \lambda_{n'} \sum_{\substack{k'=1 \\ k' \neq k}}^K \rho_{k,k'} s_{n',k'}, \quad (194)$$

$$z_{\text{SC,IMD},n,k} = \sum_{g=0}^{G-1} e^{-j \arg(\alpha)} \theta_{g+1} c_{k,g}^* \sum_{n'=1}^N m_{n,n'} \lambda_{n'} v_{\text{IMD},n',g}, \quad (195)$$

$$z_{\text{AWGN},n,k} = \varphi^* e^{-j \arg(\alpha)} \mathbf{z}_{\text{AWGN},n}^T \hat{\mathbf{E}} \mathbf{c}_k^*, \quad (196)$$

and $v_{\text{IMD},n,g}$ in (195) is the (n,g) th element of \mathbf{V}_{IMD} . Equation (191) clearly illustrates the presence of four interference terms (ICI, MAI, MAICI, and IMD). By constructing the conditional random variable $t_{\text{SC},n,k} = z_{\text{SC},n,k} | \lambda_n$, from (191) we obtain

$$\begin{aligned} t_{\text{SC},n,k} &= \lambda_n |\alpha| \rho m s_{n,k} + |\alpha| \rho \sum_{\substack{n'=1 \\ n' \neq n}}^N m_{n,n'} \hat{\lambda}_{n',n} s_{n',k} + \lambda_n |\alpha| m \sum_{\substack{k'=1 \\ k' \neq k}}^K \rho_{k,k'} s_{n,k'} \\ &+ |\alpha| \sum_{\substack{n'=1 \\ n' \neq n}}^N m_{n,n'} \hat{\lambda}_{n',n} \sum_{\substack{k'=1 \\ k' \neq k}}^K \rho_{k,k'} s_{n',k'} + \lambda_n e^{-j \arg(\alpha)} m \sum_{g=0}^{G-1} \theta_{g+1} c_{k,g}^* v_{\text{IMD},n,g} \\ &+ e^{-j \arg(\alpha)} \sum_{g=0}^{G-1} \theta_{g+1} c_{k,g}^* \sum_{\substack{n'=1 \\ n' \neq n}}^N m_{n,n'} \hat{\lambda}_{n',n} v_{\text{IMD},n',g} + z_{\text{AWGN},n,k}, \end{aligned} \quad (197)$$

where $\hat{\lambda}_{n',n} = \lambda_{n'} | \lambda_n$ is the random variable that indicates the channel gain value on the n' th subcarrier conditioned to the channel gain on the n th subcarrier. Note that in (197) the IMD relative to the subcarrier of interest and the IMD coming from the other subcarriers are considered separately. As shown in [Kay], the $(N-1) \times 1$ vector

$$\hat{\boldsymbol{\lambda}}_n = [\hat{\lambda}_{1,n} \ \dots \ \hat{\lambda}_{n-1,n} \ \hat{\lambda}_{n+1,n} \ \dots \ \hat{\lambda}_{N,n}]^T \quad (198)$$

is still a Gaussian random vector, with mean value $\boldsymbol{\eta}_{\hat{\boldsymbol{\lambda}}_n} = E\{\hat{\boldsymbol{\lambda}}_n\}$ and covariance $\mathbf{R}_{\hat{\boldsymbol{\lambda}}_n} = E\{\hat{\boldsymbol{\lambda}}_n \hat{\boldsymbol{\lambda}}_n^H\}$ expressed by [Kay]

$$\boldsymbol{\eta}_{\hat{\boldsymbol{\lambda}}_n} = \lambda_n r_{\lambda_n}^{-1} \mathbf{r}_{\bar{\boldsymbol{\lambda}}_n \lambda_n}, \quad (199)$$

$$\mathbf{R}_{\hat{\boldsymbol{\lambda}}_n} = \mathbf{R}_{\bar{\boldsymbol{\lambda}}_n} - r_{\lambda_n}^{-1} \mathbf{r}_{\bar{\boldsymbol{\lambda}}_n \lambda_n} \mathbf{r}_{\bar{\boldsymbol{\lambda}}_n \lambda_n}^H, \quad (200)$$

where $r_{\lambda_n, \lambda_n} = E\{\lambda_n \lambda_n^*\}$ is the statistical correlation between the channels on the n 'th and the n th subcarrier, $\mathbf{r}_{\bar{\lambda}_n, \lambda_n} = E\{\bar{\lambda}_n \lambda_n^*\}$ is the crosscorrelation vector between the channel of interest and the other channels, and $\mathbf{R}_{\bar{\lambda}_n} = E\{\bar{\lambda}_n \bar{\lambda}_n^H\}$ is the covariance matrix of the other channels. Consequently, by defining the $(N-1) \times 1$ zero-mean Gaussian random vector

$$\boldsymbol{\pi}_n = \hat{\boldsymbol{\lambda}}_n - \boldsymbol{\eta}_{\hat{\lambda}_n} = [\pi_{1,n} \ \cdots \ \pi_{n-1,n} \ \pi_{n+1,n} \ \cdots \ \pi_{N,n}]^T, \quad (201)$$

(197) becomes

$$\begin{aligned} t_{\text{SC},n,k} &= \lambda_n (|\alpha| \rho m s_{n,k} + z_{\text{ICI},n,k} + z_{\text{MAI},n,k} + z_{\text{MAICI},n,k} + z_{\text{IMD},n,k}) \\ &+ \tilde{z}_{\text{ICI},n,k} + \tilde{z}_{\text{MAICI},n,k} + \tilde{z}_{\text{IMD},n,k} + z_{\text{AWGN},n,k}, \end{aligned} \quad (202)$$

where

$$z_{\text{ICI},n,k} = |\alpha| \rho r_{\lambda_n, \lambda_n}^{-1} \sum_{\substack{n'=1 \\ n' \neq n}}^N m_{n,n'} r_{\lambda_n, \lambda_n} s_{n',k}, \quad (203)$$

$$z_{\text{MAI},n,k} = |\alpha| m \sum_{\substack{k'=1 \\ k' \neq k}}^K \rho_{k,k'} s_{n,k'}, \quad (204)$$

$$z_{\text{MAICI},n,k} = |\alpha| r_{\lambda_n, \lambda_n}^{-1} \sum_{\substack{n'=1 \\ n' \neq n}}^N m_{n,n'} r_{\lambda_n, \lambda_n} \sum_{\substack{k'=1 \\ k' \neq k}}^K \rho_{k,k'} s_{n',k'}, \quad (205)$$

$$z_{\text{IMD},n,k} = e^{-j \arg(\alpha)} r_{\lambda_n, \lambda_n}^{-1} \sum_{g=0}^{G-1} \theta_{g+1} c_{k,g}^* \sum_{n'=1}^N m_{n,n'} r_{\lambda_n, \lambda_n} v_{\text{IMD},n',g}, \quad (206)$$

$$\tilde{z}_{\text{ICI},n,k} = |\alpha| \rho \sum_{\substack{n'=1 \\ n' \neq n}}^N m_{n,n'} \pi_{n',n} s_{n',k}, \quad (207)$$

$$\tilde{z}_{\text{MAICI},n,k} = |\alpha| \sum_{\substack{n'=1 \\ n' \neq n}}^N m_{n,n'} \pi_{n',n} \sum_{\substack{k'=1 \\ k' \neq k}}^K \rho_{k,k'} s_{n',k'}, \quad (208)$$

and

$$\tilde{z}_{\text{IMD},n,k} = e^{-j\arg(\alpha)} \sum_{g=0}^{G-1} \theta_{g+1} c_{k,g}^* \sum_{\substack{n'=1 \\ n' \neq n}}^N m_{n,n'} \pi_{n',n} \mathcal{V}_{\text{IMD},n',g}. \quad (209)$$

By means of (202), we want to highlight that in the frequency-selective case the ICI consists of two different components. The first one, $\lambda_n z_{\text{ICI},n,k}$, is proportional to the channel amplitude λ_n of the useful signal, and therefore it represents the ICI that fades coherently with the useful signal. On the other hand, the second part $\tilde{z}_{\text{ICI},n,k}$ represents the ICI that fades independently of λ_n . Indeed, since $\tilde{z}_{\text{ICI},n,k}$ in (207) is a linear combination of the Gaussian coefficients $\{\pi_{n',n}\}$, $\tilde{z}_{\text{ICI},n,k}$ is Gaussian with mean equal to zero and power expressed by

$$\tilde{\sigma}_{\text{ICI},n,k}^2 = |\alpha \rho|^2 \sum_{\substack{n'=1 \\ n' \neq n}}^N |m_{n,n'}|^2 (r_{\lambda_n, \lambda_n} - r_{\lambda_n, \lambda_n}^{-1} |r_{\lambda_n, \lambda_n}|^2) \sigma_S^2, \quad (210)$$

which does not depend on the actual channel gain λ_n . Also the MAICI and the IMD, similarly to the ICI, consist of two parts. In both cases, the first part is proportional to λ_n , while the second one is Gaussian with power independent of λ_n . The powers of the Gaussian components are expressed respectively by

$$\tilde{\sigma}_{\text{MAICI},n,k}^2 = |\alpha|^2 \sum_{\substack{n'=1 \\ n' \neq n}}^N |m_{n,n'}|^2 (r_{\lambda_n, \lambda_n} - r_{\lambda_n, \lambda_n}^{-1} |r_{\lambda_n, \lambda_n}|^2) \sum_{\substack{k'=1 \\ k' \neq k}}^K |\rho_{k,k'}|^2 \sigma_S^2, \quad (211)$$

$$\tilde{\sigma}_{\text{IMD},n,k}^2 = \sum_{g=0}^{G-1} \sum_{g'=0}^{G-1} \theta_{g+1} \theta_{g'+1}^* c_{k,g}^* c_{k,g'} \sum_{\substack{n'=1 \\ n' \neq n}}^N \sum_{\substack{n''=1 \\ n'' \neq n}}^N m_{n,n'} m_{n,n''}^* [\mathbf{J}_n^T \mathbf{R}_{\lambda_n} \mathbf{J}_n]_{n',n''} [\mathbf{R}_v(g, g')]_{n',n''}, \quad (212)$$

where $\mathbf{R}_v(g, g')$ is the same as in (178), and the $(N-1) \times N$ matrix \mathbf{J}_n is obtained from the identity matrix \mathbf{I}_N by removing the n th row. The conditional SINR can be expressed as

$$\gamma_{n,k}(\lambda_n) = \frac{|\lambda_n|^2 |\alpha \rho m|^2 \sigma_S^2}{|\lambda_n|^2 \sigma_{n,k}^2 + \tilde{\sigma}_{n,k}^2}, \quad (213)$$

where

$$\sigma_{n,k}^2 = \sigma_{\text{ICI},n,k}^2 + \sigma_{\text{MAI},n,k}^2 + \sigma_{\text{MAICI},n,k}^2 + \sigma_{\text{IMD},n,k}^2, \quad (214)$$

$$\tilde{\sigma}_{n,k}^2 = \tilde{\sigma}_{\text{ICL},n,k}^2 + \tilde{\sigma}_{\text{MAICL},n,k}^2 + \tilde{\sigma}_{\text{IMD},n,k}^2 + \sigma_{\text{AWGN}}^2, \quad (215)$$

$$\sigma_{\text{ICL},n,k}^2 = |\alpha \rho r_{\lambda_n, \lambda_n}^{-1}|^2 \sum_{\substack{n'=1 \\ n' \neq n}}^N |m_{n,n'} r_{\lambda_n, \lambda_n}|^2 \sigma_S^2, \quad (216)$$

$$\sigma_{\text{MAICL},n,k}^2 = |\alpha r_{\lambda_n, \lambda_n}^{-1}|^2 \sum_{\substack{n'=1 \\ n' \neq n}}^N |m_{n,n'} r_{\lambda_n, \lambda_n}|^2 \sum_{\substack{k'=1 \\ k' \neq k}}^K |\rho_{k,k'}|^2 \sigma_S^2, \quad (217)$$

$$\sigma_{\text{IMD},n,k}^2 = r_{\lambda_n, \lambda_n}^{-2} \sum_{g=0}^{G-1} \sum_{g'=0}^{G-1} \theta_{g+1} \theta_{g'+1}^* c_{k,g}^* c_{k,g'} \bar{\mathbf{m}}_n^T \mathbf{R}_v(\mathbf{g}, \mathbf{g}') \bar{\mathbf{m}}_n^*, \quad (218)$$

$$[\bar{\mathbf{m}}_n]_{n'} = m_{n,n'} r_{\lambda_n, \lambda_n}, \quad (219)$$

and $\sigma_{\text{MAI},n,k}^2$, $\tilde{\sigma}_{\text{ICL},n,k}^2$, $\tilde{\sigma}_{\text{MAICL},n,k}^2$, and $\tilde{\sigma}_{\text{IMD},n,k}^2$ are expressed by (173), (210), (211), and (212), respectively. Moreover, as in the previous section, we exploit the hypotheses of a high number of subcarriers and a high number of users in order to approximate as Gaussian the four interference terms in (202) that are proportional to λ_n . The resultant BER can therefore be obtained by inserting (213), (182) and the Rayleigh PDF of $|\lambda_n|$ in (187).

Also in this case the BER can be calculated by means of series expansions that involve generalized hypergeometric functions. For 4-QAM, the BER expression is the same as in (183), with

$$\mu_{n,k}^2 = \frac{|\alpha \rho m|^2 \sigma_S^2 \sigma_\lambda^2}{\tilde{\sigma}_{n,k}^2}, \quad \nu_{n,k}^2 = \frac{\sigma_{n,k}^2 \sigma_\lambda^2}{\tilde{\sigma}_{n,k}^2}. \quad (220)$$

4.3. PERFORMANCE ANALYSIS IN OFDM SYSTEMS

In this section, we consider a special case of MC-DS-CDMA system with only one active user ($K=1$). In this case, the processing gain can be selected equal to $G=1$, thereby reducing the MC-DS-CDMA system to an OFDM system. In this case, the signal at the

HPA input becomes

$$\mathbf{u}_{\text{IN}}[l] = \mathbf{T}_{\text{CP}} \mathbf{F}^H \mathbf{s}[l], \quad (221)$$

where $\mathbf{s}[l]$ is the N -dimensional vector that contains the OFDM data symbols. The transmitted block, at the output of the NLA, can be expressed as [BaCa][DTV]

$$\mathbf{u}_{\text{OUT}}[i] = \alpha \mathbf{u}_{\text{IN}}[i] + \bar{\mathbf{v}}_{\text{IMD}}[i], \quad (222)$$

where α and $\bar{\mathbf{v}}_{\text{IMD}}[i]$ represent the same quantities as in (137). After the parallel-to-serial conversion, the signal stream $u_{\text{OUT}}[iP + p] = [\mathbf{u}_{\text{OUT}}[i]]_{p+1}$, $p = 0, \dots, P-1$, is transmitted through the multipath FIR channel $h[b]$. We assume frequency-selective fading, with maximum delay spread smaller than the cyclic prefix duration. The channel amplitudes $\{\beta_q\}$ are assumed complex Gaussian random variables, giving rise to Rayleigh or Rician fading.

By employing the same assumptions made in the general MC-DS-CDMA case, the received signal, after the cyclic prefix discarding and the FFT operation, can be expressed as

$$\mathbf{z}[l] = e^{j2\pi\epsilon(IP+L)/N} \mathbf{\Phi} \mathbf{\Lambda} (\alpha \mathbf{s}[l] + \mathbf{v}_{\text{IMD}}[l]) + \mathbf{z}_{\text{AWGN}}[l], \quad (223)$$

where $\mathbf{\Phi}$ is the $N \times N$ circulant matrix that models the ICI due to the CFO, $\mathbf{v}_{\text{IMD}}[l]$ is the IMD noise, and $\mathbf{z}_{\text{AWGN}}[l]$ represents the AWGN. By incorporating the compensation for the time-invariant phase-shift $\varphi = e^{j2\pi\epsilon L/N} e^{j\pi\epsilon(N-1)/N}$ into the equalization step, the equalized vector can be expressed as

$$\mathbf{z}_{\text{EQ}}[l] = \varphi^* \alpha^{-1} \mathbf{\Lambda}^{-1} \mathbf{z}[l] \quad (224)$$

$$= \mathbf{\Lambda}^{-1} \mathbf{M} \mathbf{\Lambda} \mathbf{s}[l] + \alpha^{-1} \mathbf{\Lambda}^{-1} \mathbf{M} \mathbf{\Lambda} \mathbf{v}_{\text{IMD}}[l] + \varphi^* \alpha^{-1} \mathbf{\Lambda}^{-1} \mathbf{z}_{\text{AWGN}}[l]. \quad (225)$$

4.3.1. BER Performance in Rayleigh Channels

In order to obtain the BER performance, we follow the two-step approach previously introduced. By denoting with $\lambda_n = [\mathbf{\Lambda}]_{n,n}$ the channel gain of the n th subcarrier, the BER can be expressed by

$$(\text{BER})_n = \int_{\lambda_n} P_{\text{BE},n}(\lambda_n) f_{\lambda_n}(\lambda_n) d\lambda_n, \quad (226)$$

$$P_{\text{BE},n}(\lambda_n) = \int_{\mathbf{s}, \bar{\lambda}_n} P_{\text{BE},n}(\mathbf{s}, \boldsymbol{\lambda}) f_{\bar{\lambda}_n | \lambda_n}(\bar{\boldsymbol{\lambda}}_n | \lambda_n) f_{\mathbf{s}}(\mathbf{s}) d\mathbf{s} d\bar{\boldsymbol{\lambda}}_n, \quad (227)$$

where $P_{\text{BE},n}(\mathbf{s}, \boldsymbol{\lambda})$ is the bit-error probability on the n th subcarrier conditioned on both the channel gains in $\boldsymbol{\lambda}$ and the data symbols in $\mathbf{s}[l]$. By multiplying (225) with $\lambda_n |\alpha|$, the scaled decision variable $z_{\text{SC},n}[l] = \lambda_n |\alpha| [\mathbf{z}_{\text{EQ}}[l]]_n$ can be expressed by

$$z_{\text{SC},n}[l] = |\alpha| \mathbf{m}_n^T \boldsymbol{\Lambda} \mathbf{s}[l] + e^{-j \arg(\alpha)} \mathbf{m}_n^T \boldsymbol{\Lambda} \mathbf{v}_{\text{IMD}}[l] + \varphi^* e^{-j \arg(\alpha)} [\mathbf{z}_{\text{AWGN}}[l]]_n. \quad (228)$$

By dropping the index l , (228) becomes

$$z_{\text{SC},n} = |\alpha| m \lambda_n s_n + z_{\text{SC,ICI},n} + z_{\text{SC,IMD},n} + z_{\text{AWGN},n}, \quad (229)$$

where

$$z_{\text{SC,ICI},n} = |\alpha| \sum_{\substack{n'=1 \\ n' \neq n}}^N m_{n,n'} \lambda_{n'} s_{n'}, \quad (230)$$

$$z_{\text{SC,IMD},n} = e^{-j \arg(\alpha)} \sum_{n'=1}^N m_{n,n'} \lambda_{n'} v_{\text{IMD},n'}, \quad (231)$$

$$z_{\text{AWGN},n} = \varphi^* e^{-j \arg(\alpha)} [\mathbf{z}_{\text{AWGN}}[l]]_n, \quad (232)$$

with $v_{\text{IMD},n} = [\mathbf{v}_{\text{IMD}}[l]]_n$. By constructing the conditional random variable $t_{\text{SC},n} = z_{\text{SC},n} | \lambda_n$, we obtain

$$t_{\text{SC},n} = \lambda_n (|\alpha| m s_n + z_{\text{ICI},n} + z_{\text{IMD},n}) + \tilde{z}_{\text{ICI},n} + \tilde{z}_{\text{IMD},n} + z_{\text{AWGN},n}, \quad (233)$$

where

$$z_{\text{ICI},n} = |\alpha| r_{\lambda_n \lambda_n}^{-1} \sum_{\substack{n'=1 \\ n' \neq n}}^N m_{n,n'} r_{\lambda_n \lambda_n} s_{n'}, \quad (234)$$

$$z_{\text{IMD},n} = e^{-j \arg(\alpha)} r_{\lambda_n \lambda_n}^{-1} \sum_{n'=1}^N m_{n,n'} r_{\lambda_n \lambda_n} v_{\text{IMD},n'}, \quad (235)$$

$$\tilde{z}_{\text{ICI},n} = |\alpha| \sum_{\substack{n'=1 \\ n' \neq n}}^N m_{n,n'} \pi_{n',n} s_{n'}, \quad (236)$$

$$\tilde{z}_{\text{IMD},n} = e^{-j \arg(\alpha)} \sum_{\substack{n'=1 \\ n' \neq n}}^N m_{n,n'} \pi_{n',n} v_{\text{IMD},n'}. \quad (237)$$

As a consequence, the powers of the interference terms can be calculated as

$$\sigma_{\text{ICI},n}^2 = |\alpha r_{\lambda_n, \lambda_n}^{-1}|^2 \sum_{\substack{n'=1 \\ n' \neq n}}^N |m_{n,n'} r_{\lambda_n, \lambda_n}|^2 \sigma_S^2, \quad (238)$$

$$\sigma_{\text{IMD},n}^2 = r_{\lambda_n, \lambda_n}^{-2} \bar{\mathbf{m}}_n^T \mathbf{R}_v(0,0) \bar{\mathbf{m}}_n^*, \quad (239)$$

$$\tilde{\sigma}_{\text{ICI},n}^2 = |\alpha|^2 \sum_{\substack{n'=1 \\ n' \neq n}}^N |m_{n,n'}|^2 (r_{\lambda_n, \lambda_n} - r_{\lambda_n, \lambda_n}^{-1} |r_{\lambda_n, \lambda_n}|^2) \sigma_S^2, \quad (240)$$

$$\tilde{\sigma}_{\text{IMD},n}^2 = \sum_{\substack{n'=1 \\ n' \neq n}}^N \sum_{\substack{n''=1 \\ n'' \neq n}}^N m_{n,n'} m_{n,n''}^* [\mathbf{J}_n^T \mathbf{R}_{\hat{\lambda}_n} \mathbf{J}_n]_{n',n''} [\mathbf{R}_v(0,0)]_{n',n''}, \quad (241)$$

where the vector $\bar{\mathbf{m}}_n$ and the matrix $\mathbf{R}_v(0,0)$ are defined in (219) and (178), respectively, and \mathbf{J}_n is obtained from \mathbf{I}_N by expurgating the n th row. By exploiting the Gaussian approximation of $z_{\text{ICI},n}$ and $z_{\text{IMD},n}$, we are able to express the BER as a series of generalized hypergeometric functions, as in the general case. In particular, in the OFDM case the conditional SINR can be expressed by

$$\gamma_n(\lambda_n) = \frac{|\lambda_n|^2 |\alpha m|^2 \sigma_S^2}{|\lambda_n|^2 (\sigma_{\text{ICI},n}^2 + \sigma_{\text{IMD},n}^2) + \tilde{\sigma}_{\text{ICI},n}^2 + \tilde{\sigma}_{\text{IMD},n}^2 + \sigma_{\text{AWGN}}^2}. \quad (242)$$

It should be pointed out that the same analysis can be carried out in the downlink of OFDMA systems, where the base station uses different subcarriers to transmit the data of different users. Obviously, the BER result is the same than in single-user OFDM systems.

4.3.2. BER Performance in Rician Channels

In this section, we again assume a frequency-selective fading channel. However, differently from the previous section, we assume that both a LOS component and a non-line-of-sight (NLOS) Rayleigh component are present, leading to Rician fading. We denote by K_R the Rician factor, which is the power ratio between the LOS and the NLOS components. For the sake of simplicity, we only consider the effect of the ICI, and hence we assume that the nonlinear distortions are absent.

For Rician fading channels, we use the same approach adopted in the Rayleigh case. From [Kay], the conditional PDF of $\hat{\lambda}_n$ is an $(N-1)$ -dimensional Gaussian random vector, with mean value $\boldsymbol{\eta}_{\hat{\lambda}_n} = E\{\hat{\lambda}_n\}$ and covariance $\mathbf{R}_{\hat{\lambda}_n} = E\{\hat{\lambda}_n \hat{\lambda}_n^H\}$ expressed by

$$\boldsymbol{\eta}_{\hat{\lambda}_n} = \lambda_{\text{LOS}} \mathbf{1}_{N-1 \times 1} + \lambda_{\text{NLOS},n} r_{\lambda_n}^{-1} \mathbf{r}_{\bar{\lambda}_n, \lambda_n}, \quad (243)$$

$$\mathbf{R}_{\hat{\lambda}_n} = \mathbf{R}_{\bar{\lambda}_n} - r_{\lambda_n}^{-1} \mathbf{r}_{\lambda_n, \lambda_n} \mathbf{r}_{\bar{\lambda}_n, \lambda_n}^H, \quad (244)$$

where $\lambda_{\text{LOS}} = E\{\lambda_n\}$ is independent from the subcarrier index n , and $\lambda_{\text{NLOS},n} = \lambda_n - \lambda_{\text{LOS}}$ is the corresponding zero-mean complex Gaussian random variable, with

$$K_R = \frac{|\lambda_{\text{LOS}}|^2}{E\{|\lambda_{\text{NLOS},n}|^2\}}. \quad (245)$$

In this case, we obtain

$$z_{\text{SC},n} = m\lambda_{\text{LOS}}s_n + m\lambda_{\text{NLOS},n}s_n + \lambda_{\text{LOS}} \sum_{\substack{n'=1 \\ n' \neq n}}^N m_{n,n'}s_{n'} + \sum_{\substack{n'=1 \\ n' \neq n}}^N m_{n,n'}\lambda_{\text{NLOS},n'}s_{n'} + z_{\text{AWGN},n}, \quad (246)$$

and, by constructing the conditional random variable $t_{\text{SC},n} = z_{\text{SC},n} | \lambda_n$, it follows

$$t_{\text{SC},n} = m\lambda_{\text{LOS}}s_n + m\lambda_{\text{NLOS},n}s_n + z_{\text{ICI,LOS},n} + \lambda_{\text{NLOS},n}z_{\text{ICI},n} + \tilde{z}_{\text{ICI},n} + z_{\text{AWGN},n}, \quad (247)$$

where

$$z_{\text{ICI,LOS},n} = \lambda_{\text{LOS}} \sum_{\substack{n'=1 \\ n' \neq n}}^N m_{n,n'}s_{n'}, \quad (248)$$

$$z_{\text{ICI},n} = r_{\lambda_n, \lambda_n}^{-1} \sum_{\substack{n'=1 \\ n' \neq n}}^N m_{n,n'} r_{\lambda_n, \lambda_n} S_{n'} , \quad (249)$$

$$\tilde{z}_{\text{ICI},n} = \sum_{\substack{n'=1 \\ n' \neq n}}^N m_{n,n'} \pi_{n',n} S_{n'} . \quad (250)$$

By exploiting the Gaussian approximation of $z_{\text{ICI},\text{LOS},n}$ and $z_{\text{ICI},n}$, for Gray-mapped QAM, the conditional BER $P_{\text{BE},n}(\lambda_n)$ can be expressed as the sum of Q-type functions [ChYo], with conditional SINR given by

$$\gamma_n(\lambda_n) = \frac{|\lambda_n|^2 |m|^2 \sigma_S^2}{|\lambda_n - \lambda_{\text{LOS}}|^2 \sigma_{\text{ICI},n}^2 + 2\rho_{\text{ICI},n}(\lambda_n, \lambda_{\text{LOS}}) + \sigma_{\text{ICI},\text{LOS},n}^2(\lambda_{\text{LOS}}) + \tilde{\sigma}_{\text{ICI},n}^2 + \sigma_{\text{AWGN}}^2} , \quad (251)$$

where

$$\sigma_{\text{ICI},\text{LOS},n}^2(\lambda_{\text{LOS}}) = |\lambda_{\text{LOS}}|^2 \sum_{\substack{n'=1 \\ n' \neq n}}^N |m_{n,n'}|^2 \sigma_S^2 , \quad (252)$$

$$\sigma_{\text{ICI},n}^2 = |r_{\lambda_n, \lambda_n}^{-1}|^2 \sum_{\substack{n'=1 \\ n' \neq n}}^N |m_{n,n'} r_{\lambda_n, \lambda_n}|^2 \sigma_S^2 , \quad (253)$$

$$\tilde{\sigma}_{\text{ICI},n}^2 = \sum_{\substack{n'=1 \\ n' \neq n}}^N |m_{n,n'}|^2 (r_{\lambda_n, \lambda_n} - r_{\lambda_n, \lambda_n}^{-1} |r_{\lambda_n, \lambda_n}|^2) \sigma_S^2 , \quad (254)$$

$$\rho_{\text{ICI},n}(\lambda_n, \lambda_{\text{LOS}}) = r_{\lambda_n, \lambda_n}^{-1} \sum_{\substack{n'=1 \\ n' \neq n}}^N |m_{n,n'}|^2 \text{Re}(\lambda_{\text{LOS}}^* (\lambda_n - \lambda_{\text{LOS}}) r_{\lambda_n, \lambda_n}) \sigma_S^2 . \quad (255)$$

The BER is then obtained by Monte Carlo integration of (226), where $f_{\lambda_n}(\lambda_n)$ is the PDF of the Rician channel gain λ_n .

The performance analysis in the presence of nonlinear distortions can be obtained as follows. Firstly, from (229), we can evaluate the conditional random variable $t_{\text{SC},n} = z_{\text{SC},n} | \lambda_n$ by using the same approach employed for Rician channels in linear scenarios. Successively, as in Rayleigh channels, we can exploit the Gaussian

approximation of the NLD noise in order to get the conditional SINR. Finally, the BER is obtained by means of a semi-analytical approach that averages the Q-functions evaluated at the conditional SINR.

4.4. SIMULATION RESULTS

In this section, we validate the previous analysis by comparing the theoretical results with the simulated ones. In the first group of simulations, we consider an MC-DS-CDMA system with $N = 256$ subcarriers with a subcarrier separation of $\Delta_f = 1/T = 156.25$ kHz and a cyclic prefix of length $L = 64$. For brevity, we only consider data modulated by 4-QAM, which correspond to a gross bit rate of 4 Mb per second per user when the length of the spreading codes is equal to $G = 16$. We assume that each time-domain tap of the channel suffers independent Rayleigh fading, with an exponentially decaying power delay profile and a root mean square delay spread equal to 250 ns.

In the first scenario, we assume that the base station employs Walsh-Hadamard (WH) spreading codes [DiJa] of length $G = 16$. We also assume that the receiver is able to get an accurate estimate of the CFO-induced time varying phase-shift (Hypothesis H1). Fig. 38 and Fig. 39 show the BER performance versus the received E_b/N_0 when the number of active users is equal to $K = G = 16$. The received E_b/N_0 is defined before the despreading as the ratio between the noiseless signal power and the noise power, while the BER is obtained by averaging the BER over all the subcarriers and all the users. Fig. 38 shows the BER versus E_b/N_0 for different values of the normalized CFO ε , assuming linear amplification at the transmitter (i.e., without IMD). The good agreement between theoretical analysis and simulated BER for all practical values of ε is evident. This fact clearly testifies that, in frequency-selective fading scenarios, the Gaussian approximation of the ICI leads to accurate results.

Fig. 39 shows the impact of the NLA on the BER performance in the absence of CFO. We

assume the IPA model (133), i.e., that the amplifier behaves as a clipper of the NLA input envelope. From Fig. 39, we deduce that the Gaussian approximation of the IMD is slightly worse than the approximation of the ICI in Fig. 38, especially at the saturating BER. Indeed, for a clipping amplifier, the Gaussian approximation of the IMD is very accurate only when the SNR is not too high or the number of subcarriers is very high [NiJa]. However, in this case the BER mismatch seems to be quite small.

In Fig. 40 and 41, we still assume WH spreading codes of length $G = 16$, the Hypothesis H1 as true, and $\varepsilon = 0$, and we focus on the impact of the number K of active users on the BER performance. We also assume that each user employs a fixed spreading code, i.e., that the k th user employs the k th row of the $G \times G$ Hadamard matrix. Fig. 40 shows that at low SNR the BER increases with the number of active users, as expected. However, the BER floor at high SNR does not increase with the number of users. Such a behavior is due to the fact that the IMD powers in (212) and (218) depend on $\mathbf{R}_v(g, g')$, which is highly sensitive to the choice of the spreading codes among the ones provided by the Hadamard matrix. This fact is confirmed by the BER floors of Fig. 41, because $\mathbf{R}_v(g, g')$ is the same for $K = 4$, $K = 8$, and $K = 16$.

Fig. 42 shows the joint effect of CFO and NLA on the BER performance when $\varepsilon = 0.02$. The results show that, in the presence of a CFO, it is not convenient to increase the output NLA power back-off at the transmitter beyond a certain value (that obviously depends on ε), because the IMD reduction is masked by the presence of the ICI induced by the CFO.

In order to identify the optimum OBO value, we introduce the TD as in the previous chapter, as expressed by

$$[\text{TD}]_{\text{dB}} = [\Delta_{E_b/N_0}]_{\text{dB}} + [\text{OBO}]_{\text{dB}}, \quad (256)$$

where $[\Delta_{E_b/N_0}]_{\text{dB}} = [E_b/N_0(\text{OBO}, \varepsilon)]_{\text{dB}} - [E_b/N_0(+\infty, \varepsilon)]_{\text{dB}}$ is the SNR increase caused by the NLA to achieve a target BER for a fixed CFO ε . Fig. 43 shows the TD performance at $\text{BER} = 10^{-3}$ for different values of the CFO and number of users. It is evident that the optimum OBO mainly depends on the value of the CFO.

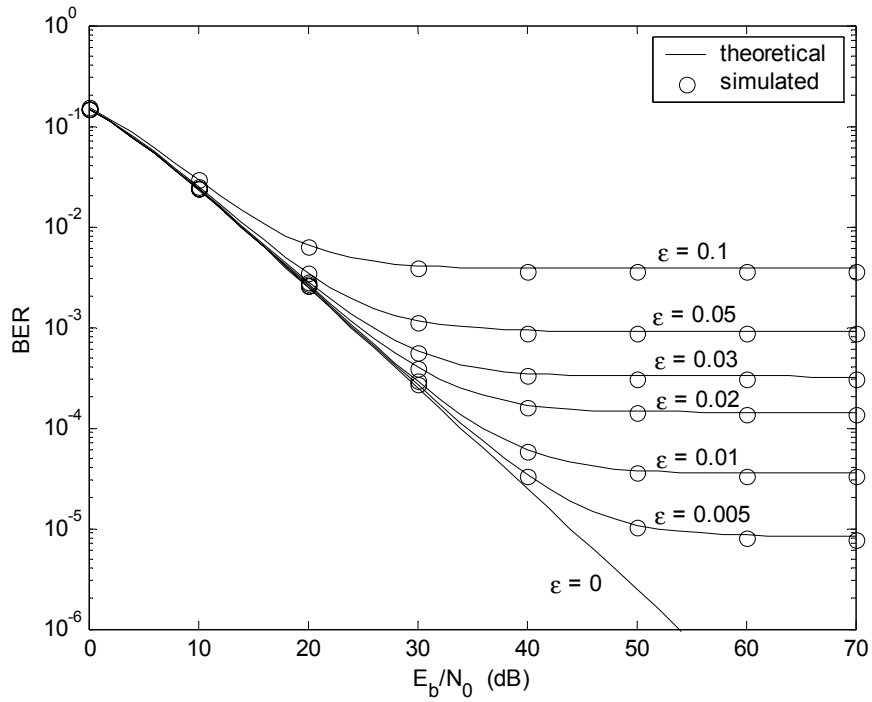


Fig. 38. Impact of the CFO ε on MC-DS-CDMA (WH codes, $K = G = 16$, no IMD).

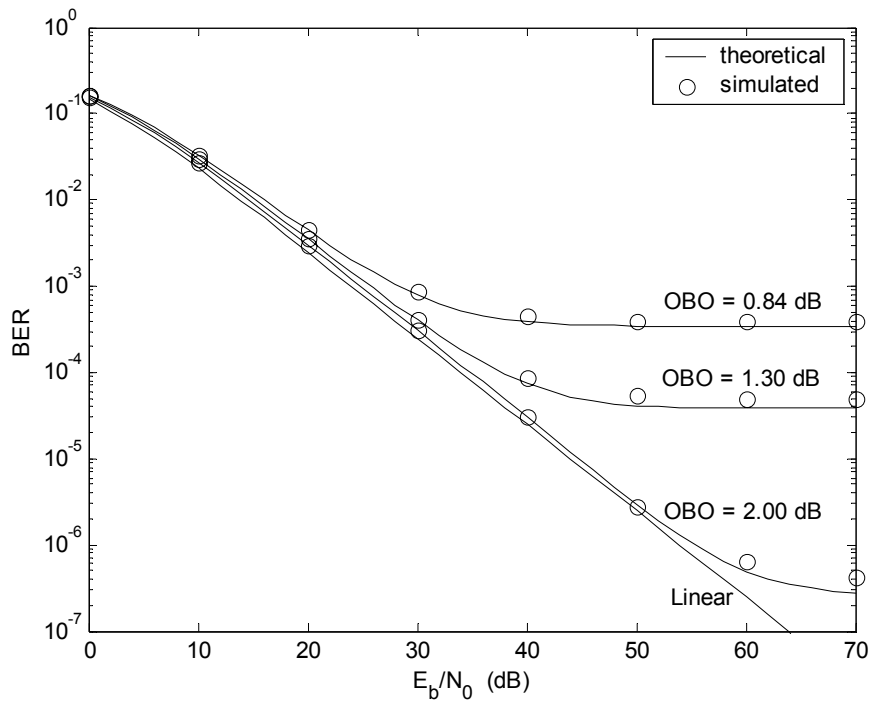


Fig. 39. Impact of the IMD on MC-DS-CDMA (WH codes, $K = G = 16$, no CFO).

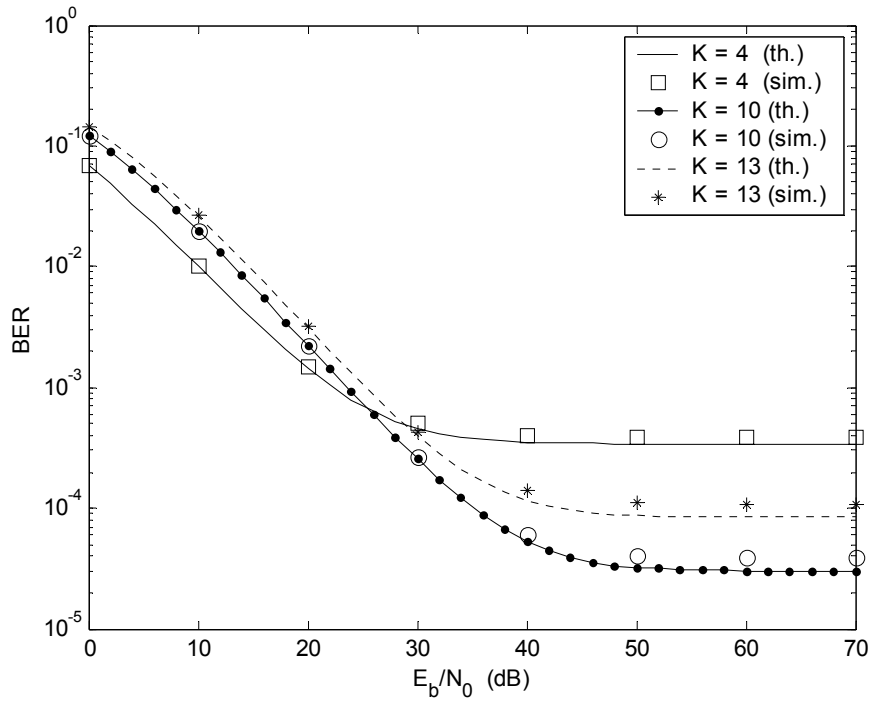


Fig. 40. Impact of K on MC-DS-CDMA (WH codes, $G = 16$, $OBO = 0.84$ dB, no CFO).

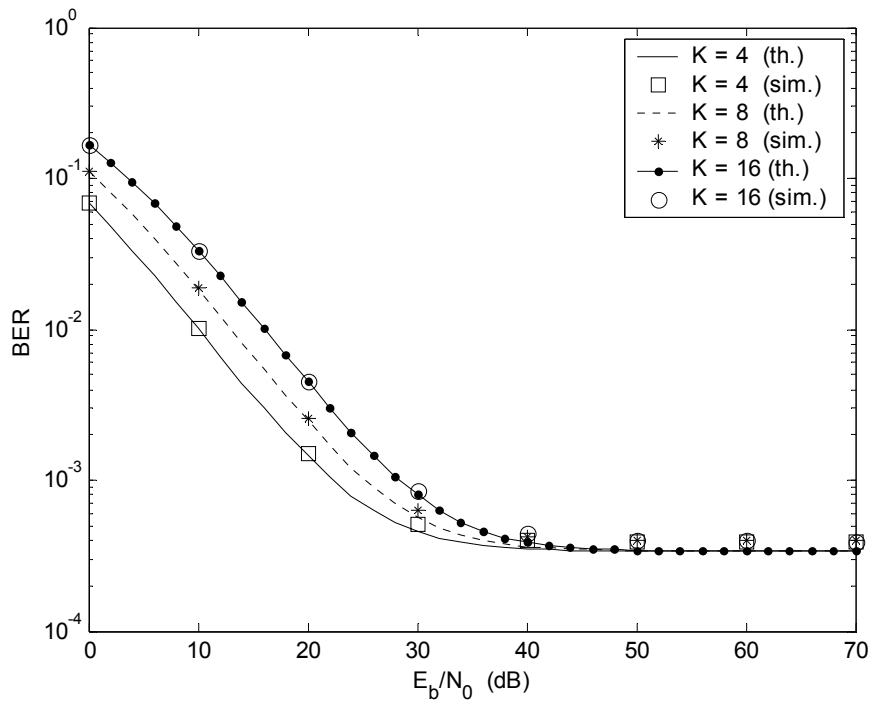


Fig. 41. Impact of K on MC-DS-CDMA (WH codes, $G = 16$, $OBO = 0.84$ dB, no CFO).

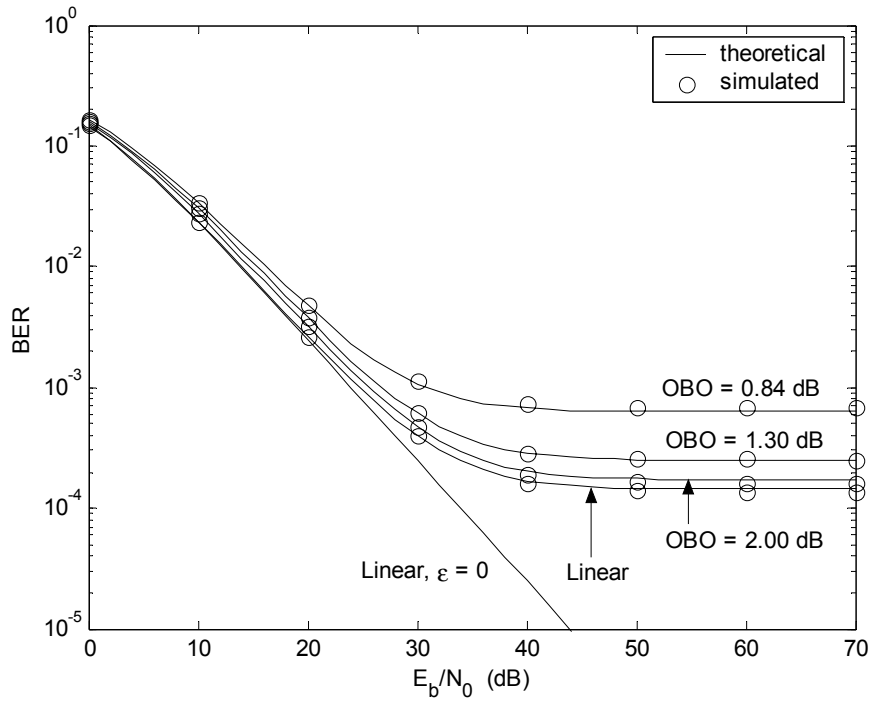


Fig. 42. BER of MC-DS-CDMA (WH codes, $K = G = 16$, $\epsilon = 0.02$).

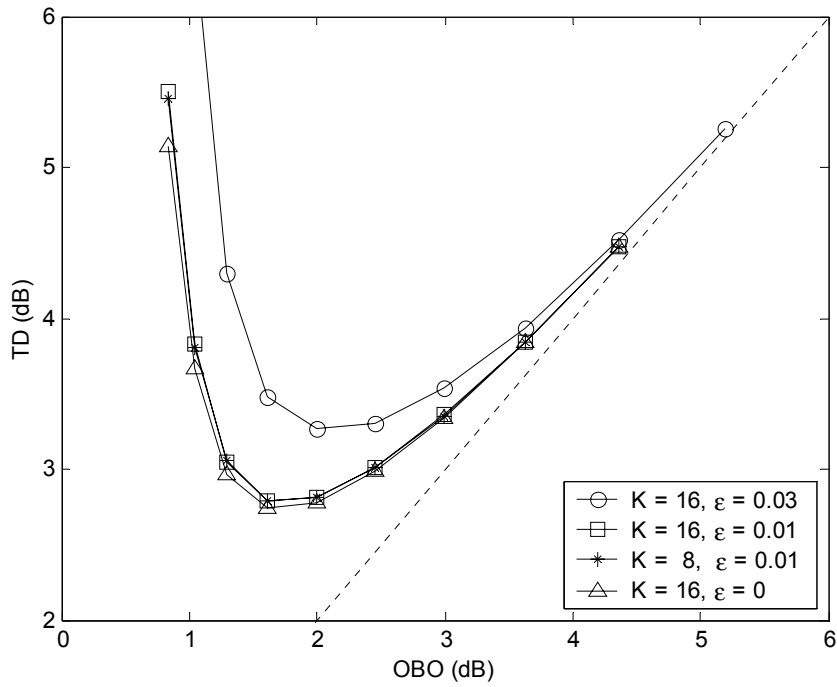


Fig. 43. TD in MC-DS-CDMA (WH codes, $G = 16$, $BER = 10^{-3}$).

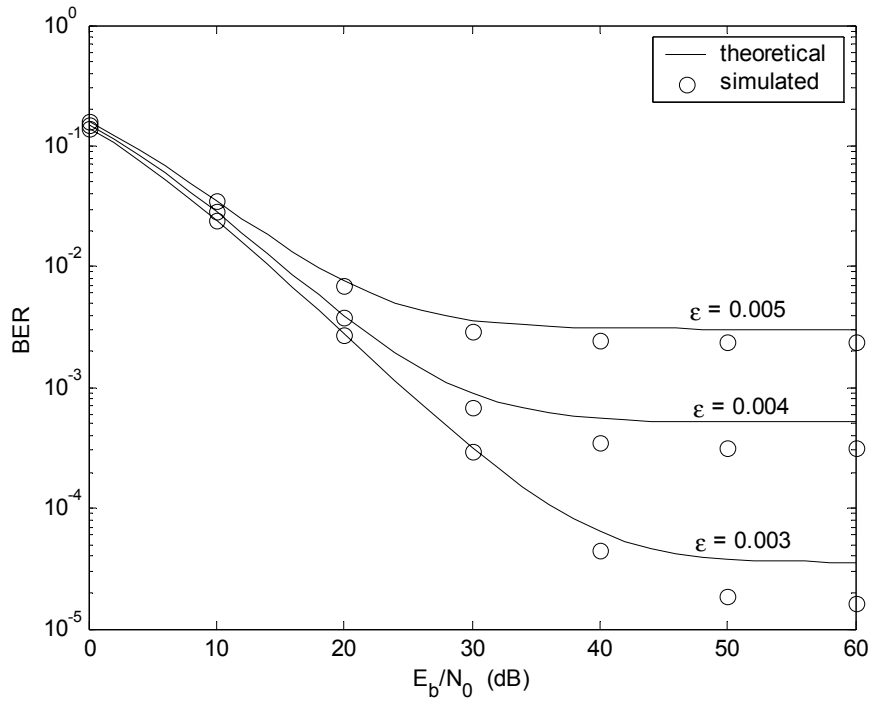


Fig. 44. BER in MC-DS-CDMA (Gold codes, $G = 31$, $K = 25$, no IMD).

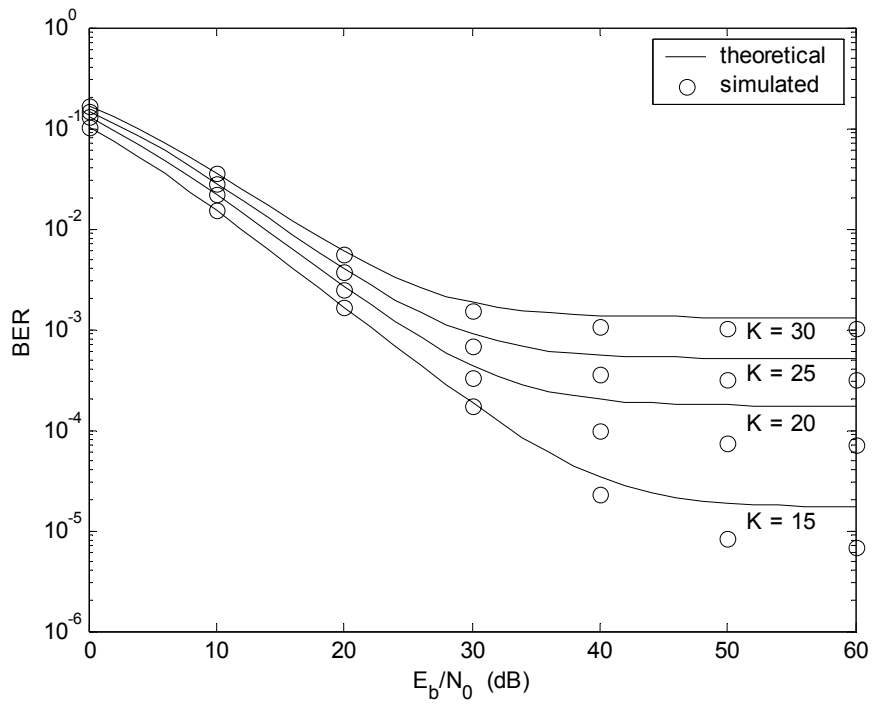


Fig. 45. BER in MC-DS-CDMA (Gold codes, $G = 31$, $\epsilon = 0.004$, no IMD).

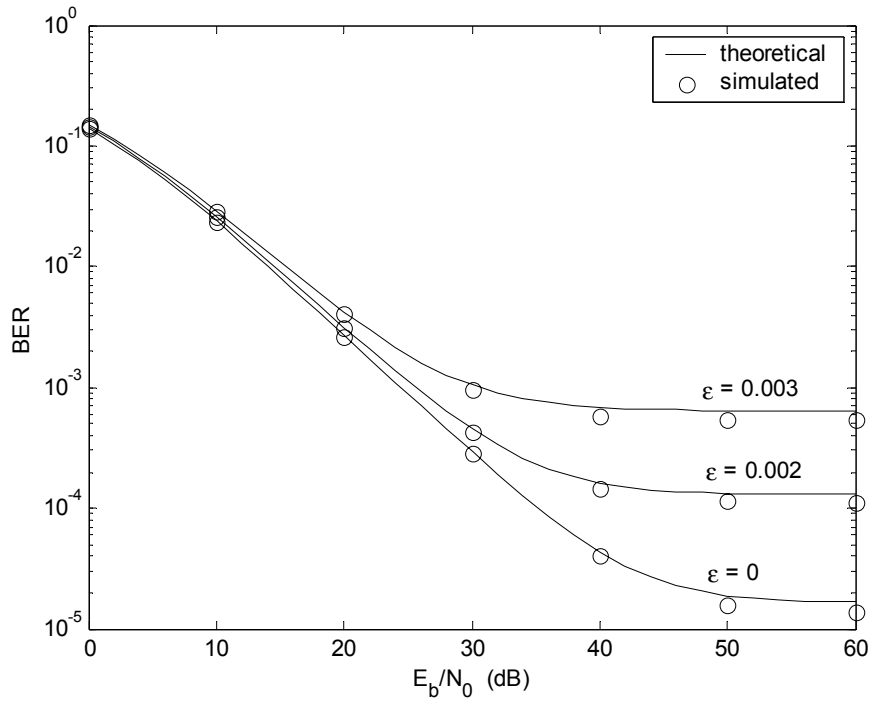


Fig. 46. BER in MC-DS-CDMA (Gold codes, $G = 31$, $K = 25$, OBO = 2.00 dB)

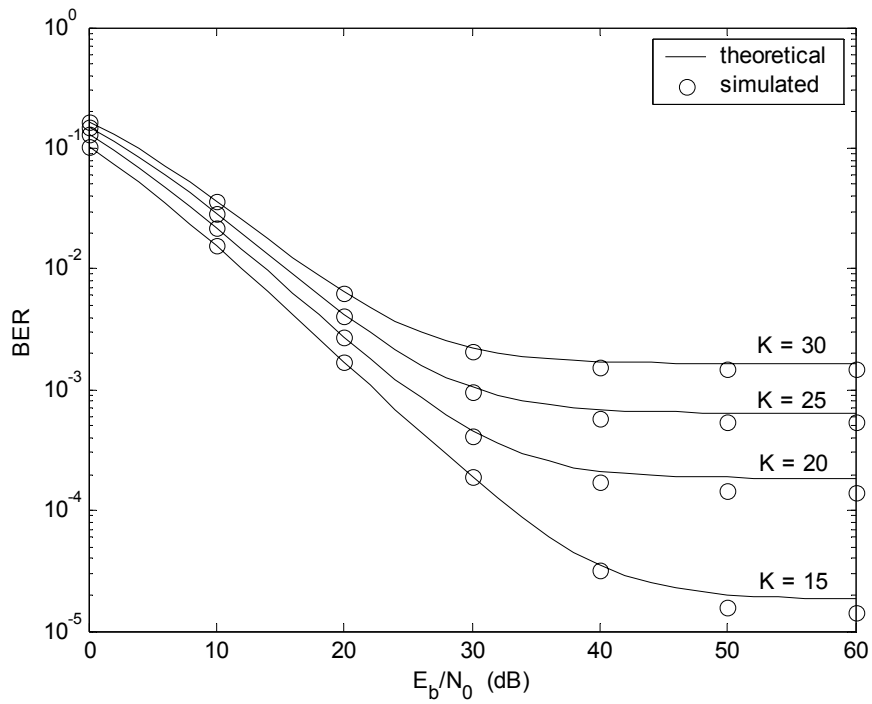


Fig. 47. BER in MC-DS-CDMA (Gold codes, $G = 31$, $\epsilon = 0.003$, OBO = 2.00 dB).

In a different simulation scenario, we assume that a rough estimate of the CFO-induced time varying phase-shift is available at the receiver (i.e., the Hypothesis H2 is true). In this case, since the MAI cannot be completely eliminated, we assume that the base station employs Gold codes of length $G=31$. Fig. 44 and Fig. 45 illustrate the BER performance for different values of the CFO ε and of the number of users K . It is evident that the BER analysis is quite accurate for $E_b/N_0 < 30$ dB, while a certain mismatch between theoretical and simulated BER exists at high SNR. This fact is due to the non-perfect Gaussian approximation of the MAI terms. However, the BER mismatch is smaller when also the NLA-induced distortions are present, as testified by Fig. 46 and Fig. 47 (OBO = 2.00 dB). Fig. 44 and Fig. 46 clearly show that, if only a rough phase estimate is available, the maximum tolerable CFO is rather small (e.g., $\varepsilon < 0.005$), because of the additional MAI. Therefore, the phase compensation step plays a crucial role on the BER performance of MC-DS-CDMA systems.

In the second group of simulations, we consider an OFDM system with $N=64$ subcarriers, with a subcarrier separation of $\Delta_f=1/T=312.5$ kHz, and with cyclic prefix of length $L=16$. We use the channel models B and D of the IEEE 802.11a WLAN standard [DABN]. In the models B and D, each time-domain tap suffers independent Rayleigh and Rician fading, respectively, with exponentially decaying power delay profile, and root mean square delay spread equal to 100 ns and 140 ns, respectively.

Fig. 48 exhibits the BER performance of the QPSK in the Rayleigh channel B, as a function of the received $E_b/N_0 = \sigma_\lambda^2 / (\sigma_{\text{AWGN}}^2 \log_2 M)$. It is evident that the theoretical analysis exactly predicts the simulated BER for different values of the normalized CFO ε . Such a good agreement clearly indicates that, differently from the AWGN case [KeHa], in frequency-selective scenarios the Gaussian approximation of the ICI leads to accurate results. The motivation of this accuracy can be easily explained. Indeed, when the interference is the sum of many variables, the approximation by a single Gaussian random variable gets worse at the tail of the Gaussian PDF, and consequently the approximated BER is not sufficiently accurate when the true BER is small (i.e., when the interference

power is small compared to the signal power). The mismatch between the approximated and the exact BER happens not only in AWGN channels, but also for the conditional BER $P_{\text{BE},n}(\lambda_n)$ in our scenario. However, in fading channels, the BER is obtained by averaging $P_{\text{BE},n}(\lambda_n)$ over the PDF of λ_n , and hence it is practically imposed by the values of $P_{\text{BE},n}(\lambda_n)$ that correspond to the small values of $|\lambda_n|$. For these values, the Gaussian approximation is very good, because $P_{\text{BE},n}(\lambda_n)$ is high (i.e., the interference power is significant with respect to the signal power), and therefore the obtained BER exactly matches with the true BER. This behavior is confirmed by the results of Fig. 49 and Fig. 50, which show the BER for the 16-QAM, and the BER of the QPSK versus the normalized CFO ε , respectively.

Fig. 48 and Fig. 49 also illustrate the BER performance obtained using the ICI approximation proposed in [ChHo]. Although the paper [ChHo] mainly deals with the effect of the channel estimation errors, it approximates all the ICI as a zero-mean Gaussian random variable with power independent of the fading gain. However, as we showed in the theoretical analysis, part of the ICI is proportional to the fading gain λ_n . Therefore, when $|\lambda_n|$ is low (high), the ICI power is smaller (larger) than the one assumed in [ChHo]. Since most of the errors are committed when $|\lambda_n|$ is low, it turns out that in [ChHo] the degradation due to the ICI is overestimated, as confirmed by the BER floors in Fig. 48 and Fig. 49.

Fig. 51 presents the BER when only $N - N_{\text{vs}} = 52$ out of $N = 64$ subcarriers are active [DABN], using the QPSK and the channel B. As a worst case for checking the Gaussian approximation, we consider the BER of the best subcarrier, because in this case the number of subcarriers that contribute to the ICI is the smallest one. Anyway, Fig. 51 clearly evidences that the approximation is very accurate in this context too.

Fig. 52 shows the BER performance in the presence of an IPA at the transmitter, when the normalized CFO is equal to $\varepsilon = 0.01$, using 16-QAM and the channel B. Since we are taking into account the presence of nonlinear distortions, we use the apparent E_b / N_0 . The results of Fig. 52 clearly indicate that the theoretical analysis is quite accurate also when both CFO and nonlinear distortions are present. Indeed, the Gaussian approximation of the

IMD noise is quite accurate for low OBO, i.e., when the IMD dominates the ICI. On the contrary, if the OBO is high, the Gaussian approximation of the IMD noise is not very accurate for $N = 64$ active subcarriers [NiJa]. However, at high OBO the IMD noise is dominated by the ICI, whose PDF is well approximated by a Gaussian function.

Fig. 53 and Fig. 54 illustrate the BER performance in the channel D with Rician factor $K_R = 10$, for QPSK and 16-QAM, respectively. In such a scenario, for high values of E_b / N_0 , the theoretical BER, which is obtained by Monte Carlo integration techniques, is less accurate than in the previous cases. The reason of this inaccuracy is the high Rician factor K_R , which produces a high value of the channel mean value λ_{LOS} . Consequently, the term $z_{\text{ICI,LOS},n}$ in (248) is the dominant one among the ICI terms in (247). Since $z_{\text{ICI,LOS},n}$ is similar to the ICI term in AWGN channels, we expect that the theoretical BER overestimates the true BER, as in AWGN channels [KeHa]. Nevertheless, as shown in Fig. 53 and Fig. 54, in Rician channels this mismatch is very small.

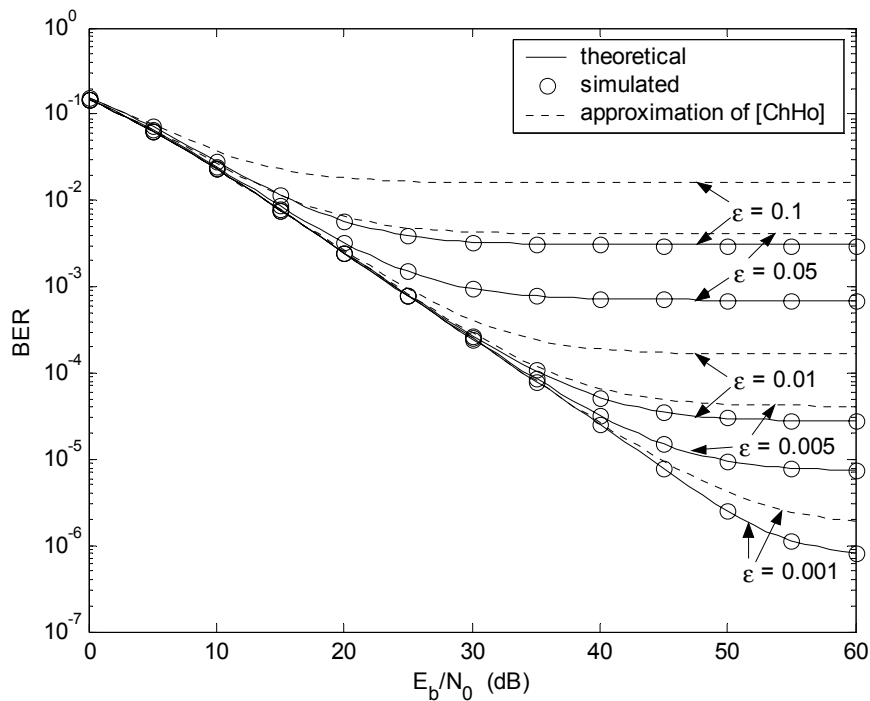


Fig. 48. BER versus E_b / N_0 in OFDM (QPSK, Rayleigh fading).

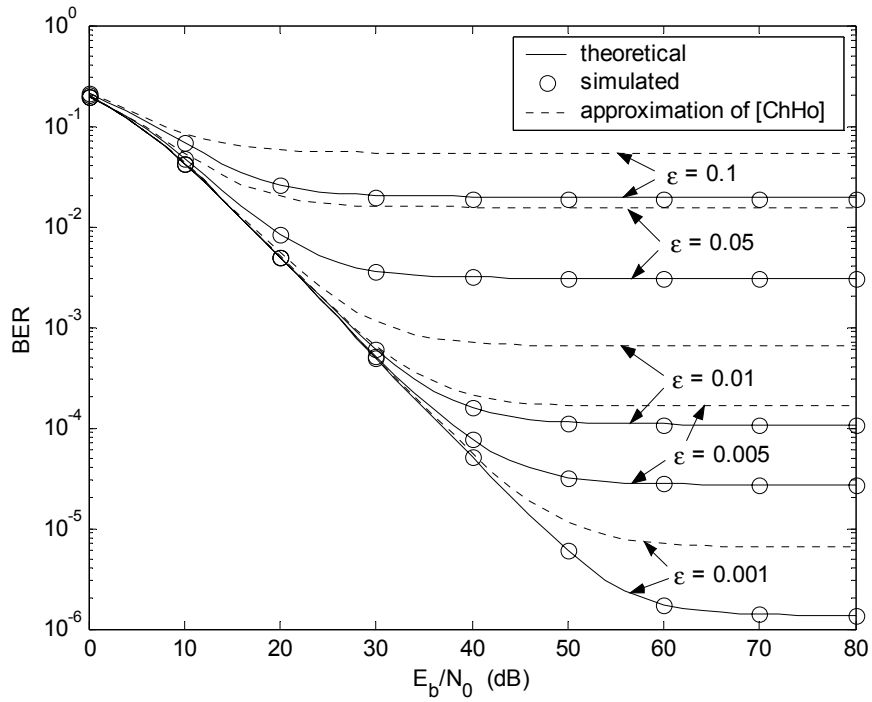


Fig. 49. BER versus E_b / N_0 in OFDM (16-QAM, Rayleigh fading).

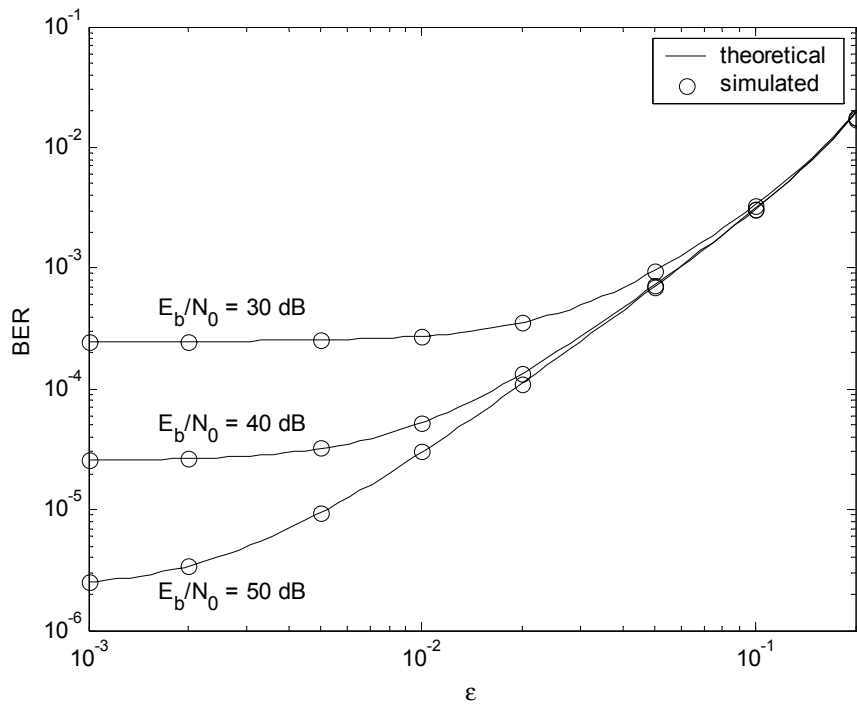


Fig. 50. BER versus ϵ in OFDM (QPSK, Rayleigh fading).

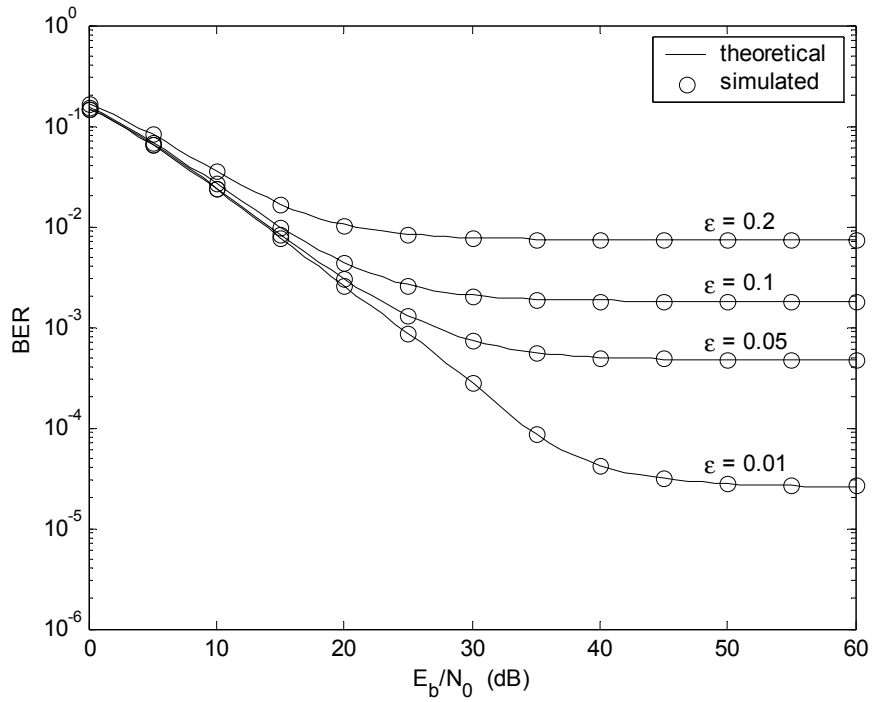


Fig. 51. BER in OFDM in the presence of guard bands (QPSK, Rayleigh fading).

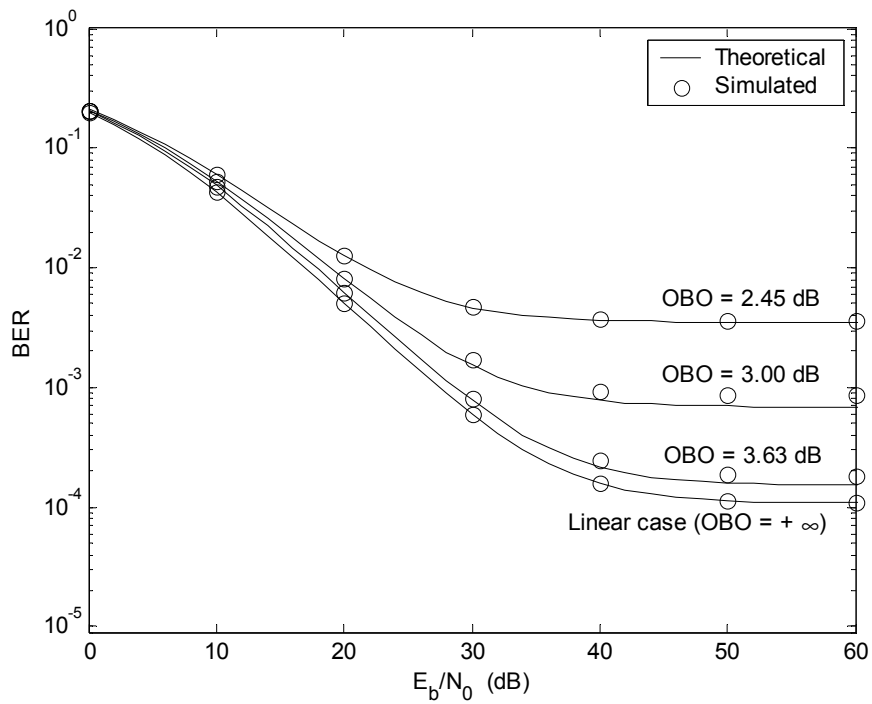


Fig. 52. BER versus E_b / N_0 in OFDM (16-QAM, Rayleigh fading, $\epsilon = 0.01$, IPA).

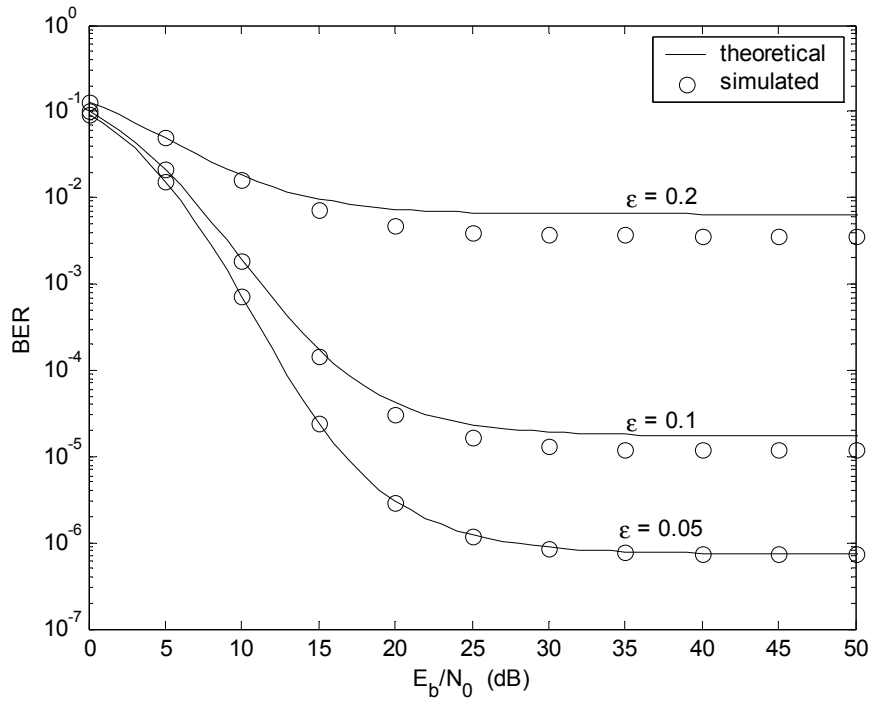


Fig. 53. BER versus E_b / N_0 in OFDM (QPSK, Rician fading).

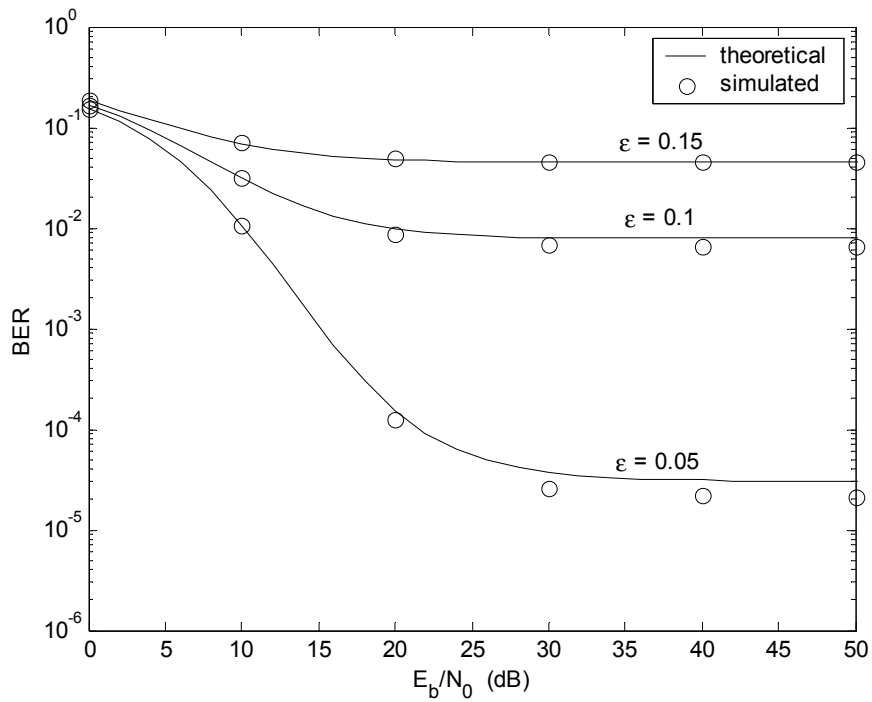


Fig. 54. BER versus E_b / N_0 in OFDM (16-QAM, Rician fading).

Finally, we want to point out that the Gaussian approximation of the ICI can be successfully applied not only in WLAN scenarios, but also in broadcasting environments. Indeed, the OFDM systems usually employed for broadcasting applications have thousands of active subcarriers [NePr], and therefore it is expected that the Gaussian approximation of the ICI will perform even better than in WLAN situations. Moreover, with thousands of active subcarriers, also the Gaussian approximation of the IMD noise is very accurate [BaCa] [NiJa], and therefore the proposed approach is even more reliable.

5. CONCLUSIONS

In this thesis, we have analyzed the BER performance of single-carrier and multicarrier DS-CDMA systems in the presence of distortions introduced by the transmitter and by the receiver. First, we have considered single-carrier DS-CDMA systems with short data blocks. In this case, the receiver cannot estimate the signal statistics accurately, causing significant performance degradation. Second, we have considered single-carrier DS-CDMA downlink signals transmitted by a nonlinear amplifier, which produces both in-band and out-of-band distortions. These distortions cause both BER degradation and spectral regrowth. Then, we have extended the previous analysis to multicarrier systems. Also the impairments due to the imperfect frequency synchronization at the receiver side have been taken into account. In the following, we give a detailed outline of the main results.

In Chapter 2, we have pointed out the estimation errors caused by the ill-conditioning of the covariance matrix of the received signal, and by a blind channel estimation technique, in single-carrier DS-CDMA systems. The effects of these errors on the BER performance degradation of the MMSE multiuser detector have been investigated by simulation in realistic scenarios. It has been shown that the channel estimation errors are predominant at low SNR, while the estimation errors of the inverse covariance matrix becomes remarkable at high SNR. Some techniques to counteract the covariance matrix ill-conditioning have been proposed. If accurate channel estimates for all the users are available at the receiver, as in the uplink, the covariance matrix can be conveniently estimated by employing such estimates, thereby improving the performance considerably. Moreover, a novel regularized MMSE detector for DS-CDMA downlink systems have been proposed. We have proven that the CMT approach reduces the eigenvalue spread of the covariance matrix. Two new tapering matrices have been introduced. We have shown that the CMT detector can outperform other regularized detectors.

In Chapter 3, we have presented an analytical framework to evaluate the SER performance of linear multiuser detectors for DS-CDMA downlink systems subject to the nonlinear distortions introduced by the transmitting HPA. We have derived closed form expressions for AWGN and flat Rayleigh fading channels, and we have proposed a semi-analytical SER evaluation in frequency-selective multipath fading channels. Results for QPSK mapping with square-root raised cosine pulse shaping waveforms have been presented, and the OBO that minimizes the system TD has been evaluated. Simulation results have shown that the analytical model is quite appropriate in a large number of scenarios. Therefore, the proposed approach represents a valuable tool to predict the SER performance in the presence of nonlinearities, with a dramatically reduced computation time with respect to simulations, which require signal interpolation.

In Chapter 4, we have evaluated the BER of MC-DS-CDMA downlink systems subject to both frequency synchronization errors and nonlinear distortions in frequency-selective Rayleigh fading channels. The BER analysis, which is quite accurate in many conditions, allows to identify the optimum OBO value of the HPA, depending on the amount of CFO. The analytical findings have also highlighted the importance of an accurate compensation for the CFO-induced phase-shift. The BER analysis has been extended to OFDM systems in frequency-selective Rayleigh fading channels. A semi-analytical BER prediction in Rician fading is also included.

5.1. FUTURE WORK

The analyses and techniques proposed in this thesis can be extended to different scenarios and conditions. As far as Chapter 2 is concerned, other channel estimation techniques than the subspace method could be employed to assess the performance of different regularized detectors. Moreover, further analytical investigations are required in order to obtain an automatic strategy to choose the optimum value for the regularization parameter of the CMT

detector. However, such a problem is not specific of the proposed technique, but is common to almost all the techniques proposed in the literature [Hans]. The development of novel regularization techniques that make the parameter choice easier is currently under investigation.

As far as Chapter 3 is concerned, the SER analysis can be extended to other multiuser detectors. In particular, the semi-analytical approach adopted in frequency-selective channels can also be employed to predict the SER of DS-CDMA receivers specially designed for the downlink [Klei]. The subject of future works may also include the design of nonlinear multiuser detectors that take into account the nonlinear distortions, as in [MeGe] and in [ReZh].

As regards Chapter 4, the BER analysis has been carried out for QAM, and it can be extended to PSK constellations, whose conditional BER is characterized by a sum of Q-shaped functions as in the QAM case [LLCL]. In addition, the BER performance of more complex multiuser detectors can be investigated. Future works may also focus on the effects of channel estimation errors [ChHo], and of channel coding [LXG][FaFe][NePr].

APPENDIX A

In order to prove the Theorem 2 of Section 2.4.2, we introduce the following theorem.

Theorem 3 (Eigenvalue majorization theorem): If \mathbf{R} is an $MN \times MN$ Hermitian matrix and \mathbf{T} is an $MN \times MN$ correlation matrix, then

$$\sum_{i=1}^n \lambda_i(\mathbf{R} \circ \mathbf{T}) \leq \sum_{i=1}^n \lambda_i(\mathbf{R}), \quad \forall n = 1, \dots, MN, \quad (257)$$

where $\lambda_i(\mathbf{R})$ is the i th eigenvalue of \mathbf{R} , with the eigenvalues ordered in decreasing order.

Proof: See [HoJo2].

By using Theorem 3 with $n = 1$, because of the eigenvalues ordering, we have

$$\lambda_{\max}(\mathbf{R} \circ \mathbf{T}) \leq \lambda_{\max}(\mathbf{R}), \quad (258)$$

where $\lambda_{\max}(\mathbf{R})$ is the largest eigenvalue of \mathbf{R} . Moreover, by Theorem 3 with $n = MN - 1$, and exploiting $\mathbf{I}_{MN} \circ \mathbf{T} = \mathbf{I}_{MN}$, we obtain

$$\sum_{i=1}^{MN-1} \lambda_i(\mathbf{R} \circ \mathbf{T}) \leq \sum_{i=1}^{MN-1} \lambda_i(\mathbf{R}), \quad (259)$$

$$\sum_{i=1}^{MN} \lambda_i(\mathbf{R} \circ \mathbf{T}) = \text{tr}(\mathbf{R} \circ \mathbf{T}) = \text{tr}(\mathbf{R}) = \sum_{i=1}^{MN} \lambda_i(\mathbf{R}), \quad (260)$$

respectively. Combining (259) and (260), it follows

$$\lambda_{\min}(\mathbf{R} \circ \mathbf{T}) \geq \lambda_{\min}(\mathbf{R}), \quad (261)$$

where $\lambda_{\min}(\mathbf{R})$ is the smallest eigenvalue of \mathbf{R} . From (258) and (261), we have

$$\chi(\mathbf{R} \circ \mathbf{T}) = \frac{\lambda_{\max}(\mathbf{R} \circ \mathbf{T})}{\lambda_{\min}(\mathbf{R} \circ \mathbf{T})} \leq \frac{\lambda_{\max}(\mathbf{R})}{\lambda_{\min}(\mathbf{R})} = \chi(\mathbf{R}), \quad (262)$$

which concludes the proof of Theorem 2.

APPENDIX B

In this appendix, we prove that the integral expressed by

$$I = \int_0^{+\infty} \alpha Q \left(\sqrt{\gamma \frac{r^2 \sigma_S^2}{r^2 \sigma_I^2 + \sigma_N^2}} \right) \frac{2r}{\Omega} e^{-r^2/\Omega} dr, \quad (263)$$

is equivalent to the series expansion expressed by

$$I = \frac{\alpha}{2} - \frac{\sqrt{2\gamma\Omega}\alpha}{4} \frac{\sigma_S}{\sigma_N} e^{-\frac{\gamma\sigma_S^2}{2\sigma_I^2}} \sum_{k=0}^{+\infty} \frac{1}{k!} \left(\frac{\gamma\sigma_S^2}{2\sigma_I^2} \right)^k {}_2F_0 \left(k + \frac{3}{2}, \frac{1}{2}; ; -\Omega \frac{\sigma_I^2}{\sigma_N^2} \right), \quad (264)$$

The parameters σ_S^2 , σ_I^2 , σ_N^2 , α , γ , and Ω are fixed and different from zero, while ${}_pF_q$ represents the generalized hypergeometric function [GrRy][AbSt]. The quantities σ_S^2 , σ_I^2 , σ_N^2 , can be interpreted as the useful signal power, the interference power, and the noise power, respectively. The integral I in (263)-(264) represents either the BER or the SER depending of the context.

Substituting $\beta^2 = r^2 / \Omega$, and setting

$$\mu^2 = \frac{\gamma\Omega\sigma_S^2}{\sigma_N^2}, \quad \nu^2 = \frac{\Omega\sigma_I^2}{\sigma_N^2}, \quad (265)$$

which can be considered as a scaled SNR and a scaled interference-to-noise ratio (INR), Expression (263) reduces to

$$I = \int_0^{+\infty} \alpha Q \left(\sqrt{\frac{\beta^2 \mu^2}{\beta^2 \nu^2 + 1}} \right) 2\beta e^{-\beta^2} d\beta. \quad (266)$$

Plugging $Q(x) = \frac{1}{2} \operatorname{erfc} \left(\frac{x}{\sqrt{2}} \right)$ in (266), and using $y = \frac{\beta\mu}{\sqrt{2+2\beta^2\nu^2}}$, we obtain

$$I = \alpha \int_0^{\mu/(\sqrt{2\nu})} \frac{2y\mu^2}{(\mu^2 - 2\nu^2 y^2)^2} e^{-\frac{2y^2}{\mu^2 - 2\nu^2 y^2}} \operatorname{erfc}(y) dy. \quad (267)$$

Integrating (267) by parts, it follows that

$$I = \frac{\alpha}{2} - \frac{\alpha}{\sqrt{\pi}} \int_0^{\mu/(\sqrt{2}\nu)} e^{-\frac{2y^2}{\mu^2 - 2\nu^2 y^2}} e^{-y^2} dy, \quad (268)$$

and substituting $t = \mu^2 - 2\nu^2 y^2$ in (268) it is easy to obtain

$$I = \frac{\alpha}{2} - \frac{\sqrt{2}\alpha}{4\sqrt{\pi\nu}} e^{\frac{2-\mu^2}{2\nu^2}} \int_0^{\mu^2} e^{-\frac{\mu^2}{\nu^2 t}} e^{\frac{t}{2\nu^2}} (\mu^2 - t)^{-1/2} dt. \quad (269)$$

By using the Taylor series expansion of $e^{t/(2\nu^2)}$, (269) becomes

$$I = \frac{\alpha}{2} - \frac{\sqrt{2}\alpha}{4\sqrt{\pi\nu}} e^{\frac{2-\mu^2}{2\nu^2}} \sum_{k=0}^{+\infty} \frac{1}{k!} \left(\frac{1}{2\nu^2}\right)^k \int_0^{\mu^2} e^{-\frac{\mu^2}{\nu^2 t}} t^k (\mu^2 - t)^{-1/2} dt. \quad (270)$$

The integral in (270) is in the same form of Equation 3.471.2 in [GrRy], hence we obtain

$$I = \frac{\alpha}{2} - \frac{\sqrt{2}\alpha}{4} \frac{\mu}{\nu} e^{\frac{1-\mu^2}{2\nu^2}} \sum_{k=0}^{+\infty} \frac{1}{k!} \left(\frac{\mu^2}{2\nu^3}\right)^k W_{-\frac{k+1}{2}, \frac{k+1}{2}} \left(\frac{1}{\nu^2}\right), \quad (271)$$

where $W_{-\frac{k+1}{2}, \frac{k+1}{2}}(\cdot)$ is the Whittaker W-function [AbSt] of order $-\frac{k+1}{2}, \frac{k+1}{2}$. By (265), the final result of the integral is

$$I = \frac{\alpha}{2} - \frac{\sqrt{2}\gamma\alpha}{4} \frac{\sigma_S}{\sigma_I} e^{\frac{\sigma_N^2 - \gamma\Omega\sigma_S^2}{2\Omega\sigma_I^2}} \sum_{k=0}^{+\infty} \frac{1}{k!} \left(\frac{\gamma}{2\sqrt{\Omega}} \frac{\sigma_S^2\sigma_N}{\sigma_I^3}\right)^k W_{-\frac{k+1}{2}, \frac{k+1}{2}} \left(\frac{\sigma_N^2}{\Omega\sigma_I^2}\right). \quad (272)$$

The solution (272) of the integral (263) can also be expressed as a function of the U hypergeometric function [AbSt] and of the generalized hypergeometric function ${}_2F_0(\cdot, \cdot; \cdot)$ [GrRy][AbSt] by means of Equation 13.1.33 and Equation 13.1.10 in [AbSt], which lead to the expression

$$I = \frac{\alpha}{2} - \frac{\sqrt{2}\gamma\alpha}{4\Omega} \frac{\sigma_S\sigma_N^2}{\sigma_I^3} e^{-\frac{\gamma\sigma_S^2}{2\sigma_I^2}} \sum_{k=0}^{+\infty} \frac{1}{k!} \left(\frac{\gamma}{2\Omega} \frac{\sigma_S^2\sigma_N^2}{\sigma_I^4}\right)^k U\left(k + \frac{3}{2}, k + 2, \frac{\sigma_N^2}{\Omega\sigma_I^2}\right), \quad (273)$$

and to Equation (264).

APPENDIX C

Obviously, for practical purposes, the evaluation of (264) in the Appendix B requires a truncation of the infinite series. As a consequence, it would be interesting to predict how many terms are necessary in order to obtain an accurate approximation of the exact result, and also which ones are the terms to consider. Since an analytical evaluation of the truncation error power seems to be difficult, we plot the term

$$t(k) = \frac{\sqrt{2\gamma\Omega}}{4} \frac{\sigma_S}{\sigma_N} e^{-\frac{\gamma\sigma_S^2}{2\sigma_I^2}} \frac{1}{k!} \left(\frac{\gamma\sigma_S^2}{2\sigma_I^2} \right)^k {}_2F_0 \left(k + \frac{3}{2}, \frac{1}{2}; ; -\Omega \frac{\sigma_I^2}{\sigma_N^2} \right) \quad (274)$$

that appears in (264) versus the summation index k , for different values of the parameters $\gamma\sigma_S^2/\sigma_I^2$ and $\gamma\Omega\sigma_S^2/\sigma_N^2$. These two parameters summarize the scaled version of the signal-to-interference ratio (SIR), and of the SNR, respectively.

Fig. 55, Fig. 56, and Fig. 57 show that the behavior of $t(k)$ is almost independent of the scaled SNR $\gamma\Omega\sigma_S^2/\sigma_N^2$, and it practically depends only on the scaled SIR $\gamma\sigma_S^2/\sigma_I^2$. Therefore, Fig. 57 can be used as a guide to select only the relevant terms of the series in (264). Interestingly, these relevant terms are adjacent, and therefore a good approximation of the exact value in (264) can be obtained as

$$I_{\text{approx}} = \frac{\alpha}{2} - \alpha \sum_{k=k_{\min}}^{k_{\max}} t(k) \quad (275)$$

by a convenient choice of k_{\min} and k_{\max} .

By using (275) instead of (264), we are able to reduce the computational complexity of the SER evaluation when $k_{\max} - k_{\min}$ is sufficiently low. In order to reduce such a complexity, while maintaining an adequate accuracy, the choice of the interval $[k_{\min}, k_{\max}]$ can exploit the two following observations, suggested by Fig. 57.

- For sufficiently high values of the scaled SIR $\gamma\sigma_s^2/\sigma_1^2$, the maximum of $t(k)$ is obtained when $k \approx \bar{k} = \left\lfloor \frac{\gamma\sigma_s^2}{2\sigma_1^2} \right\rfloor$;
- $t(k)$ has a parabolic-like shape in the logarithmic scale, and hence a Gaussian-like shape in the linear scale.

Consequently, if we choose to approximate $t(k)$ with the Gaussian function

$$G(k) = \frac{A}{\sqrt{2\pi}\sigma} e^{-\frac{(k-\eta)^2}{2\sigma^2}}, \quad (276)$$

we can approximate the series expansion $\sum_{k=0}^{\infty} t(k)$ by an integral expressed by $\int_0^{\infty} G(k)dk$ and, due to the positive value of η , we can evaluate the integral by means of the approximation

$$\int_0^{\infty} G(k)dk \approx \int_{\max\{0, \eta-3\sigma\}}^{\eta+3\sigma} G(k)dk \quad (277)$$

with a very small relative error. Therefore, thanks to the good matching of $G(k)$ with $t(k)$, we can conclude that the significant terms in (264) are the ones in the interval between $k_{\min} = \max\{0, \lfloor \eta - 3\sigma \rfloor\}$ and $k_{\max} = \lceil \eta + 3\sigma \rceil$, where $\eta = \bar{k}$.

In order to estimate the standard deviation σ to use in (276), we can exploit the following consideration. Since $I = \frac{\alpha}{2} - \alpha \sum_{k=0}^{+\infty} t(k)$ represent an error probability, for practical values of the error probability (i.e., below 0.1) we can assume $\sum_{k=0}^{+\infty} t(k) \approx \frac{1}{2}$, and therefore $A \approx 1/2$. Consequently, by imposing that $G(\eta) = G(\bar{k}) = t(\bar{k})$, we can estimate

$$\sigma \approx \frac{1}{2\sqrt{2\pi t(\bar{k})}}. \quad (278)$$

The accuracy of such an approximation is confirmed by Fig. 57, which outlines both the good accuracy of fitting $t(k)$ with $G(k)$, and the interval $[k_{\min}, k_{\max}]$ that is used in (275) to approximate (264).

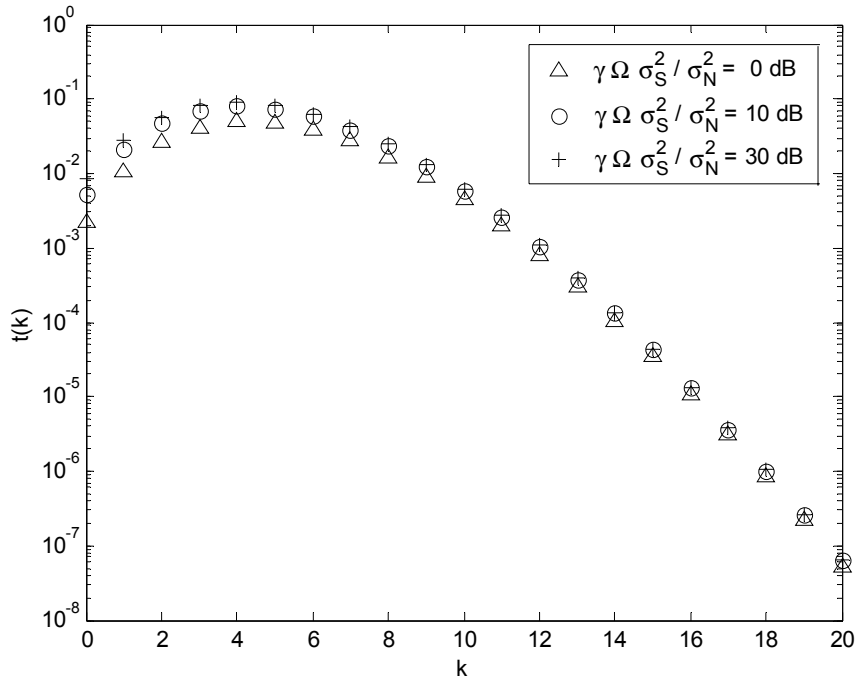


Fig. 55. Evaluation of $t(k)$ when $\gamma \sigma_S^2 / \sigma_I^2 = 10 \text{ dB}$.

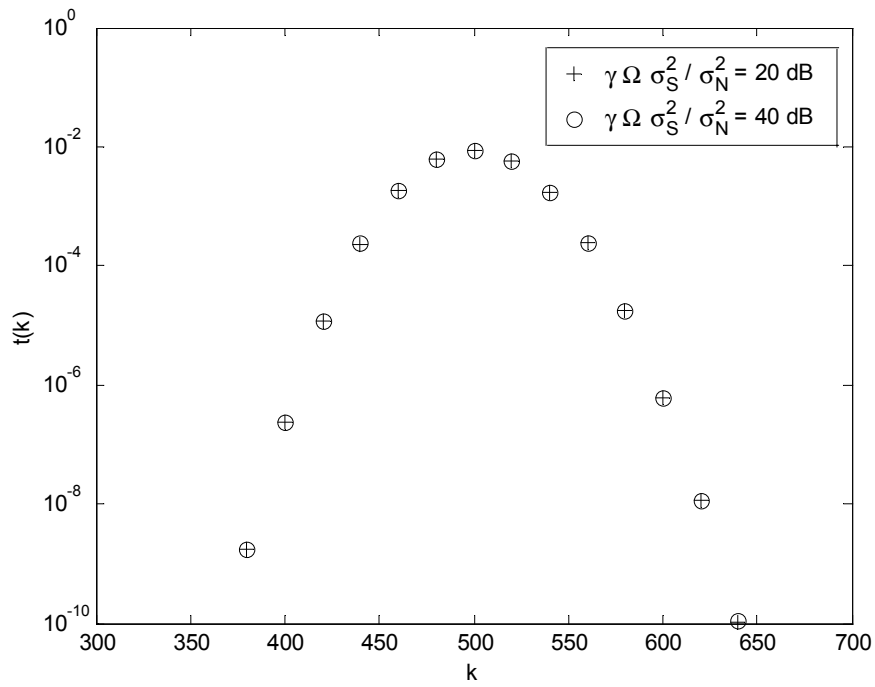


Fig. 56. Evaluation of $t(k)$ when $\gamma \sigma_S^2 / \sigma_I^2 = 30 \text{ dB}$.

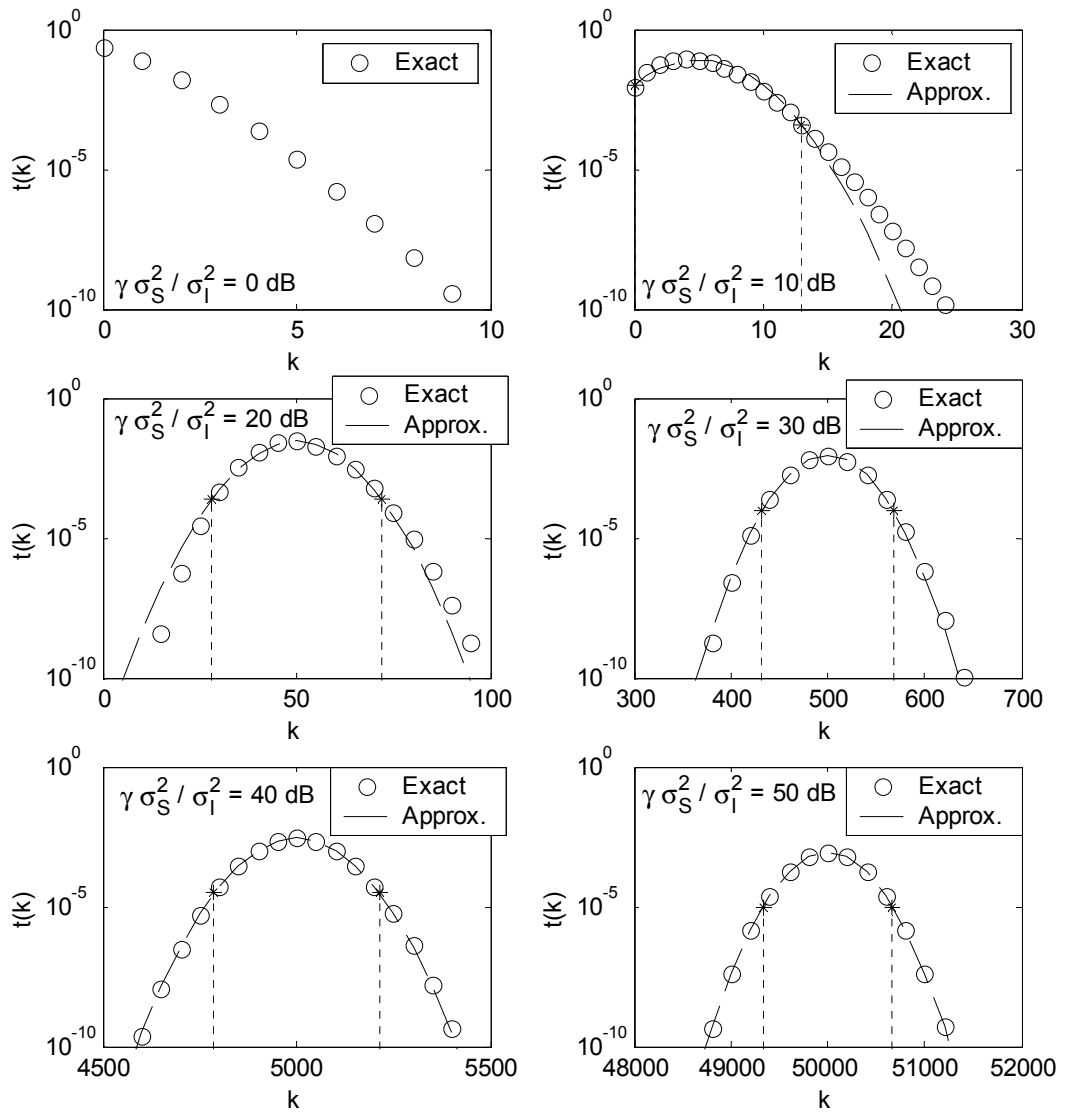


Fig. 57. Comparison between the exact $t(k)$ and the approximation $G(k)$.

The asterisks denote k_{\min} and k_{\max} . ($\gamma \Omega \sigma_S^2 / \sigma_N^2 = 30 \text{ dB}$.)

BIBLIOGRAPHY

- [AbSt] M. Abramowitz and I. Stegun, *Handbook of Mathematical Functions*, Dover Publications, 1970.
- [BaCa] P. Banelli and S. Cacopardi, "Theoretical analysis and performance of OFDM signals in nonlinear AWGN channels," *IEEE Trans. Commun.*, vol. 48, pp. 430-441, Mar. 2000.
- [BeAa] S. Bensley and B. Aazhang, "Subspace-based channel estimation for code division multiple access communication systems," *IEEE Trans. Commun.*, vol. 44, pp. 1009-1020, Aug. 1996.
- [BeKa] M. Benthin and K.-D. Kammeyer, "Influence of channel estimation on the performance of a coherent DS-CDMA system," *IEEE Trans. Veh. Technol.*, vol. 46, pp. 262-268, May 1997.
- [BPHN] H. Bölcskei, A.J. Paulraj, K.V.S. Hari, R.U. Nabar, and W.W. Lu, "Fixed broadband wireless access: state of the art, challenges, and future directions," *IEEE Commun. Mag.*, vol. 39, pp. 100-108, Jan. 2001.
- [BZM] Q. Bi, G.I. Zysman, and H. Menkes, "Wireless mobile communications at the start of the 21st century," *IEEE Commun. Mag.*, vol. 39, pp. 110-116, Jan. 2001.
- [Carl] B.D. Carlson, "Covariance matrix estimation errors and diagonal loading in adaptive arrays," *IEEE Trans. Aerosp. Electron. Syst.*, vol. 24, pp. 397-401, July 1988.
- [CDT] A. Conti, D. Dardari, and V. Tralli, "An analytical framework for CDMA systems with a nonlinear amplifier and AWGN," *IEEE Trans. Commun.*, vol. 50, pp. 1110-1120, Jul. 2002.
- [CGA] X. Cai, H. Ge, and A.N. Akansu, "Low-rank MMSE detector for synchronous DS-CDMA," *Proc. IEEE Asilomar Conf. Signals Systems Computers 1999*, pp. 940-944.
- [ChHo] H. Cheon and D. Hong, "Effect of channel estimation error in OFDM-based WLAN," *IEEE Commun. Lett.*, vol.6, pp. 190-192, May 2002.
- [ChYo] K. Cho and D. Yoon, "On the general BER expression of one- and two-dimensional amplitude modulations," *IEEE Trans. Commun.*, vol. 50, pp. 1074-1080, July 2002.
- [Cru] D.G.M. Cruickshank, "Suppression of multiple access interference in a DS-CDMA system using Wiener filtering and parallel cancellation," *IEE Proc.-Commun.*, vol. 143, pp. 226-230, Aug. 1996.
- [DABN] A. Doufexi, S. Armour, M. Butler, A. Nix, D. Bull, J. McGeehan, and P. Karlsson, "A comparison of the HIPERLAN/2 and IEEE 802.11a wireless LAN standards," *IEEE Commun. Mag.*, vol. 40, pp. 172-180, May 2002.

- [DaRo] W.B. Davenport and W.L. Root, *An Introduction to the Theory of Random Signals and Noise*, McGraw-Hill, 1958.
- [DaSo] V.M. DaSilva and E.S. Sousa, "Multicarrier orthogonal CDMA signals for quasi-synchronous communication systems," *IEEE J. Select. Areas Commun.*, vol. 12, pp. 842-852, June 1994.
- [DiJa] E.H. Dinan and B. Jabbari, "Spreading codes for direct sequence CDMA and wideband CDMA cellular networks," *IEEE Commun. Mag.*, vol. 36, pp. 48-54, Sept. 1998.
- [DTV] D. Dardari, V. Tralli, and A. Vaccari, "A theoretical characterization of nonlinear distortion effects in OFDM systems," *IEEE Trans. Commun.*, vol. 48, pp. 1755-1764, Oct. 2000.
- [ETSI] ETSI, "Selection procedures for the choice of radio transmission technologies of the UMTS," ETSI TR 101 112, Apr. 1998.
- [FaFe] K. Fazel and G.P. Fettweis, *Multi-Carrier Spread-Spectrum*, Kluwer Academic Publishers, 1997.
- [FaKa] K. Fazel and S. Kaiser, "Analysis of non-linear distortions on MC-CDMA," *Proc. IEEE Int. Conf. Commun. 1998*, pp. 1028-1034.
- [GHBK] D. Gesbert, L. Haumonte, H. Bölcskei, R. Krishnamoorthy, and A.J. Paulraj, "Technologies and performance for non-line-of-sight broadband wireless access networks," *IEEE Commun. Mag.*, vol. 40, pp. 86-95, Apr. 2002.
- [GoRe] J.S. Goldstein and I.S. Reed, "Reduced-rank adaptive filtering," *IEEE Trans. Signal Processing*, vol. 45, pp. 492-496, Feb. 2002.
- [GoVa] G.H. Golub and C.F. Van Loan, *Matrix Computations*, 3rd ed., Johns Hopkins Univ. Press, 1996.
- [GrRy] I.S. Gradshteyn, I.M. Ryzhik, *Table of Integrals, Series, and Products*, 5th ed., Academic Press, 1994.
- [GSSP] D. Gesbert, J. Sorelius, P. Stoica, and A. Paulraj, "Blind multiuser MMSE detector for CDMA signals in ISI channels," *IEEE Commun. Lett.*, vol. 3, pp. 233-235, Aug. 1999.
- [Guer] J.R. Guerci, "Theory and application of covariance matrix tapers for robust adaptive beamforming," *IEEE Trans. Signal Processing*, vol. 47, pp. 977-985, Apr. 1999.
- [GuMi] N. Guo and L.B. Milstein, "Uplink performance evaluation of multicode DS/CDMA systems in the presence of nonlinear distortions," *IEEE J. Select. Areas Commun.*, vol. 18, pp. 1418-1428, Aug. 2000.
- [Hans] P. C. Hansen, *Rank-Deficient and Discrete Ill-Posed Problems*, SIAM, 1998.
- [HaPr] S. Hara and R. Prasad, "Overview of multicarrier CDMA," *IEEE Commun. Mag.*, vol. 35, pp. 126-133, Dec. 1997.
- [Hayk] S. Haykin, *Adaptive Filter Theory*, 3rd ed., Prentice Hall, 1996.
- [HMY] M. Honig, U. Madhow, and S. Verdú, "Blind adaptive multiuser detection," *IEEE Trans. Inform. Theory*, vol. 41, pp. 944-960, July 1995.

- [HoGo] M.L. Honig and J.S. Goldstein, "Adaptive reduced-rank interference suppression based on the multistage Wiener filter," *IEEE Trans. Commun.*, vol. 50, pp. 986-994, June 2002.
- [HoJo1] R.A. Horn and C.R. Johnson, *Matrix Analysis*, Cambridge Univ. Press, 1990.
- [HoJo2] R.A. Horn and C.R. Johnson, *Topics in Matrix Analysis*, Cambridge Univ. Press, 1994.
- [HoTs] M. Honig and M.K. Tsatsanis, "Adaptive techniques for multiuser CDMA," *IEEE Signal Processing Mag.*, pp. 49-61, May 2000.
- [JoSt] J.H. Jong and W.E. Stark, "Performance analysis of coded multicarrier spread-spectrum systems in the presence of multipath fading and nonlinearities," *IEEE Trans. Commun.*, vol. 49, pp. 168-179, Jan. 2001.
- [JuLa] M. Juntti and M. Latva-aho, "Bit-error probability analysis of linear receivers for CDMA systems in frequency-selective fading channels," *IEEE Trans. Commun.*, vol. 47, pp. 1788-1791, Dec. 1999.
- [Kay] S.M. Kay, *Fundamentals of Statistical Signal Processing: Estimation Theory*, vol. 1, Prentice Hall, 1993.
- [KeHa] T. Keller and L. Hanzo, "Adaptive multicarrier modulation: a convenient framework for time-frequency processing in wireless communications," *IEEE Proc.*, vol. 88, pp. 611-640, May 2000.
- [KGE] A.R. Kaye, D.A. George, and M.J. Eric, "Analysis and compensation of bandpass nonlinearities for communications," *IEEE Trans. Commun.*, vol. 20, pp. 965-972, Oct. 1972.
- [Klei] A. Klein, "Data detection algorithms specially designed for the downlink of CDMA mobile radio systems," *Proc. IEEE Veh. Technol. Conf. 1997*, pp. 203-207.
- [KoMi] S. Kondo and L.B. Milstein, "Performance of multicarrier DS CDMA systems," *IEEE Trans. Commun.*, vol. 44, pp. 238-246, Feb. 1996.
- [KQMB] G.N. Karystinos, H. Qian, M.J. Medley, and S.N. Batalama, "Short data record adaptive filtering: the auxiliary-vector algorithm," *Digital Signal Processing*, vol. 12, pp. 193-222, July 2002.
- [Lau] V.K.N. Lau, "On the analysis of peak-to-average ratio (PAR) for IS95 and CDMA2000 systems," *IEEE Trans. Veh. Technol.*, vol. 49, pp. 2174-2188, Nov. 2000.
- [LeMi] J.S. Lee and L.E. Miller, "Analysis of peak-to-average power ratio for IS-95 and third generation CDMA forward link waveforms," *IEEE Trans. Veh. Technol.*, vol. 50, pp. 1004-1013, July 2001.
- [Lim] H.-B. Lim, "Beyond 3G: issues and challenges," *IEEE Potentials*, vol. 21, pp. 18-23, Oct./Nov. 2002.
- [LLCL] J. Lu, K.B. Letaief, J. Chuang, and M.L. Liou, "M-PSK and M-QAM BER computation using signal-space concepts," *IEEE Trans. Commun.*, vol. 47, pp. 181-184, Feb. 1999.
- [LWBÖ] D. Landström, S.K. Wilson, J.-J. van de Beek, P. Ödling, and P.O. Börjesson, "Symbol time offset estimation in coherent OFDM systems," *IEEE Trans. Commun.*, vol. 50, pp. 545-549, Apr. 2002.

- [LXG] Z. Liu, Y. Xin, and G.B. Giannakis, "Linear constellation precoding for OFDM with maximum multipath diversity and coding gains," *IEEE Trans. Commun.*, vol. 51, pp. 416-427, Mar. 2003.
- [Madh1] U. Madhow, "Blind adaptive interference suppression for direct-sequence CDMA," *IEEE Proc.*, vol. 86, pp. 2049-2069, Oct. 1998.
- [Madh2] U. Madhow, "Blind adaptive interference suppression for the near-far resistant acquisition and demodulation of direct-sequence CDMA signals," *IEEE Trans. Signal Processing*, vol.45, pp. 124-136, Jan. 1997.
- [Mail] R.J. Mailloux, "Covariance matrix augmentation to produce adaptive array pattern troughs," *IEE Electron. Lett.*, vol. 31, pp. 771-772, 11 May 1995.
- [MDCM] E. Moulines, P. Duhamel, J. Cardoso, and S. Mayrargue, "Subspace methods for blind identification of multichannel FIR channels," *IEEE Trans. Signal Processing*, vol. 43, pp. 526-525, Feb. 1995.
- [MeGe] G. Mei and E. Geraniotis, "Mitigation of nonlinear distortion in DS/CDMA systems," *Proc. IEEE Int. Symp. Personal, Indoor, Mobile Radio Commun. 2000*, pp. 266-270.
- [MHM] S.L. Miller, M.L. Honig, and L.B. Milstein, "Performance analysis of MMSE receivers for DS-CDMA in frequency-selective fading channels," *IEEE Trans. Commun.*, vol. 48, pp. 1919-1929, Nov. 2000.
- [Moos] P.H. Moose, "A technique for orthogonal frequency division multiplexing frequency offset correction," *IEEE Trans. Commun.*, vol. 42, pp. 2908-2914, Oct. 1994.
- [MTGB] X. Ma, C. Tepedelenlioğlu, G.B. Giannakis, and S. Barbarossa, "Non-data-aided carrier offset estimators for OFDM with null subcarriers: identifiability, algorithms, and performance," *IEEE J. Select. Areas Commun.*, vol. 19, pp. 2504-2515, Dec. 2001.
- [MZB] H. Minn, M. Zeng, and V.K. Bhargava, "On timing offset estimation for OFDM systems," *IEEE Commun. Lett.*, vol. 4, pp. 242-244, July 2000.
- [NePr] R. van Nee and R. Prasad, *OFDM for Wireless Multimedia Communications*, Artech House, 2000.
- [NiJa] H. Nikopour and S.H. Jamali, "Effects of Cartesian clipping noise on the performance of orthogonal frequency division multiplexing system: a theoretical approach," *Proc. IEEE Global Telecommun. Conf. 2002*, pp. 1254-1258.
- [Oclm] H. Ochiai and H. Imai, "On the distribution of the peak-to-average power ratio in OFDM signals," *IEEE Trans. Commun.*, vol. 49, pp. 282-289, Feb. 2001.
- [Pand] A. Pandharipande, "Principles of OFDM," *IEEE Potentials*, vol. 21, pp. 16-19, Apr./May 2002.
- [Papo] A. Papoulis, *Probability, Random Variables and Stochastic Processes*, 3rd ed., McGraw-Hill, 1991.

- [PBM] T. Pollet, M. van Bladel, and M. Moeneclaey, "BER sensitivity of OFDM systems to carrier frequency offset and Wiener phase noise," *IEEE Trans. Commun.*, vol. 43, pp. 191-193, Feb./Mar./Apr. 1995.
- [PoVe] H.V. Poor and S. Verdú, "Probability of error in MMSE multiuser detection," *IEEE Trans. Inform. Theory*, vol. 43, pp. 858-871, May 1997.
- [Proa] J.G. Proakis, *Digital Communications*, 3rd ed., McGraw-Hill, 1995.
- [PrOj] R. Prasad and T. Ojanperä, "An overview of CDMA evolution toward wideband CDMA," *IEEE Commun. Surveys & Tutorials*, 4th Quarter 1998. [Online]. Available: <http://www.comsoc.org/livepubs/surveys/public/4q98issue/prasad.html>
- [ReZh] A.J. Redfern and G.T. Zhou, "Blind zero forcing equalization of multichannel nonlinear CDMA systems," *IEEE Trans. Signal Processing*, vol. 49, pp. 2363-2371, Oct. 2001.
- [Rich] C.D. Richmond, "Derived PDF of maximum likelihood signal estimator which employs an estimated noise covariance," *IEEE Trans. Signal Processing*, vol. 44, pp. 305-315, Feb. 1996.
- [Rowe] H.E. Rowe, "Memoryless nonlinearities with Gaussian inputs: elementary results," *Bell Syst. Tech. J.*, vol. 61, pp. 1520-1523, Sept. 1982.
- [Sale] A.A.M. Saleh, "Frequency-independent and frequency-dependent nonlinear models of TWT amplifiers," *IEEE Trans. Commun.*, vol. 29, pp. 1715-1720, Nov. 1981.
- [SaTe] K. Sathanathan and C. Tellambura, "Probability of error calculation of OFDM systems with frequency offset," *IEEE Trans. Commun.*, vol. 49, pp. 1884-1888, Nov. 2001.
- [ScCo] T.M. Schmidl and D.C. Cox, "Robust frequency and timing synchronization for OFDM," *IEEE Trans. Commun.*, vol. 45, pp. 1613-1621, Dec. 1997.
- [SiAl] M.K. Simon and M.S. Alouini, *Digital Communication over Fading Channels: A Unified Approach to Performance Analysis*, Wiley, 2000.
- [SiMi] R. Singh and L.B. Milstein, "Interference suppression for DS/CDMA," *IEEE Trans. Commun.*, vol. 47, pp. 446-453, Mar. 1999.
- [Skla] B. Sklar, "Rayleigh fading channels in mobile digital communication systems part I: characterization," *IEEE Commun. Mag.*, vol. 35, pp. 90-100, July 1997.
- [SoNa] E.A. Sourour and M. Nakagawa, "Performance of orthogonal multicarrier CDMA in a multipath fading channel," *IEEE Trans. Commun.*, vol. 44, pp. 356-367, Mar. 1996.
- [StFe] B. Stantchev and G. Fettweis, "Time-variant distortions in OFDM," *IEEE Commun. Lett.*, vol. 4, pp. 312-314, Sept. 2000.
- [StMo] H. Steendam and M.E. Moeneclaey, "The sensitivity of downlink MC-DS-CDMA to carrier frequency offsets," *IEEE Commun. Lett.*, vol. 5, pp. 215-217, May 2001.
- [ToPe] L. Tong and S. Perreau, "Multichannel blind identification: from subspace to maximum likelihood methods," *IEEE Proc.*, vol. 86, pp. 1951-1968, Oct. 1998.
- [Verd] S. Verdú, *Multiuser Detection*, Cambridge Univ. Press, 1998.

- [WaGi] Z. Wang and G.B. Giannakis, "Wireless multicarrier communications: where Fourier meets Shannon," *IEEE Signal Processing Mag.*, vol. 17, pp. 29-48, May 2000.
- [WaPo] X. Wang and H. V. Poor, "Blind equalization and multiuser detection in dispersive CDMA channels," *IEEE Trans. Commun.*, vol. 46, pp. 91-103, Jan. 1998.
- [Xu1] Z. Xu, "On the second-order statistics of the weighted sample covariance matrix," *IEEE Trans. Signal Processing*, vol. 51, pp. 527-534, Feb. 2003.
- [Xu2] Z. Xu, "Perturbation analysis for subspace decomposition with applications in subspace-based algorithms," *IEEE Trans. Signal Processing*, vol. 50, pp. 2820-2830, Nov. 2002.
- [YaHa] L.-L. Yang and L. Hanzo, "Multicarrier DS-CDMA: a multiple access scheme for ubiquitous broadband wireless communications," *IEEE Commun. Mag.*, vol. 41, pp. 116-124, Sept. 2003.
- [YiNg] K.W. Yip and T.S. Ng, "Effects of carrier frequency accuracy on quasi-synchronous, multicarrier DS-CDMA communications using optimized sequences," *IEEE J. Select. Areas Commun.*, vol. 17, pp. 1915-1923, Nov. 1999.
- [Zatm] M. Zatman, "Production of adaptive array troughs by dispersion synthesis," *IEE Electron. Lett.*, vol. 31, pp. 2141-2142, 7 Dec. 1995.
- [ZhHä] Y. Zhao and S.G. Häggman, "BER analysis of OFDM communication systems with intercarrier interference," *Proc. IEEE Int. Conf. Commun. Technol. 1998*, vol. 2.
- [ZvBr] Z. Zvonar and D. Brady, "Linear multipath-decorrelating receivers for CDMA frequency-selective fading channels," *IEEE Trans. Commun.*, vol. 44, pp. 650-653, June 1996.